SSD

SCIENCE FOR A SUSTAINABLE DEVELOPMENT

ANTARCTIC SUBGLACIAL PROCESSES AND INTERACTIONS:

ROLE OF TRANSITION ZONES IN ICE SHEET STABILITY

"ASPI"

F. PATTYN, J.-L. TISON, P. HUYBRECHTS

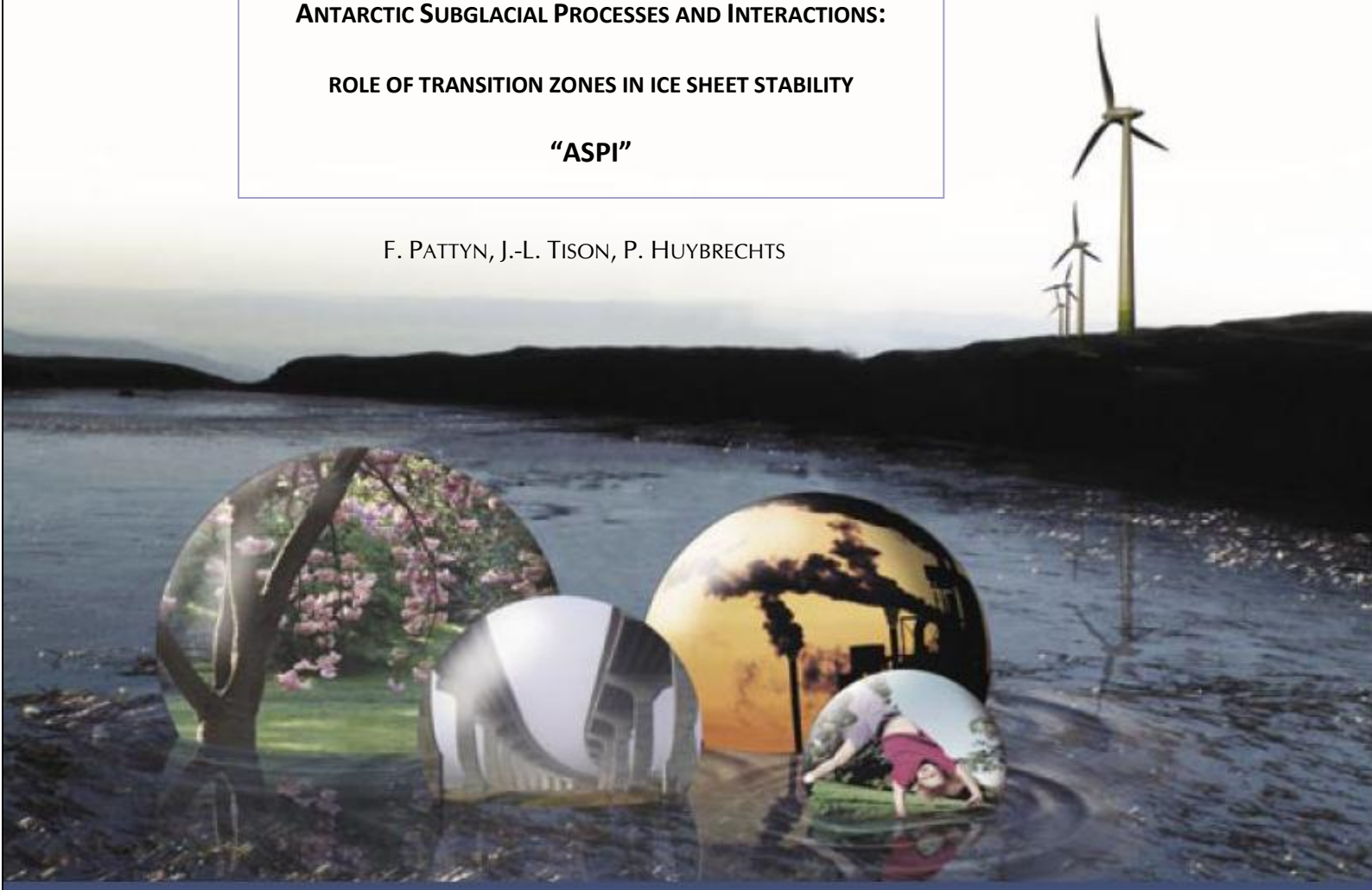

ENERGY

TRANSPORT AND MOBILITY

AGRO-FOOD

HEALTH AND ENVIRONMENT

CLIMATE

BIODIVERSITY

ATMOSPHERE AND TERRESTRIAL AND MARINE ECOSYSTEMS

TRANSVERSAL ACTIONS

.be

SCIENCE FOR A SUSTAINABLE DEVELOPMENT
(SSD)

Antarctica - Climate

FINAL REPORT

ANTARCTIC SUBGLACIAL PROCESSES AND INTERACTIONS: ROLE OF TRANSITION ZONES IN ICE SHEET STABILITY

"ASPI"

SD/CA/02

Promotors

Frank Pattyn, Jean-Louis Tison
Laboratoire de Glaciologie - ULB

Philippe Huybrechts
Earth System Sciences & Departement Geografie - VUB

Authors

Thierry Boereboom, Frank Pattyn, Laura Perichon, Jean-Philippe Rémy
Denis Samyn & Jean-Louis Tison (ULB)

Bert De Smedt, Philippe Huybrechts, Ann Huyghe, Oleg Rybak
Hans Van De Vyver (VUB)

ULB

Belgian Science Policy Office
belspo

Vrije Universiteit Brussel

D/2012/1191/5
Published in 2012 by the Belgian Science Policy
Avenue Louise 231
Louizalaan 231
B-1050 Brussels
Belgium
Tel: +32 (0)2 238 34 11 – Fax: +32 (0)2 230 59 12
http://www.belspo.be

Contact person: Maaike Vancauwenberghe
+32 (0)2 238 36 78

F. Pattyn, J.-L. Tison, P. Huybrechts, T. Boereboom, B. De Smedt, A. Huyghe, L. Perichon, J.-P. Rémy, O. Rybak, D. Samyn, H. Van de Vyver. **Antarctic Subglacial Processes and Interactions: role of transition zones in ice sheet stability (ASPI).** Final Report. Brussels : Belgian Science Policy 2012 – 103 p. (Research Programme Science for a Sustainable Development)

TABLE OF CONTENT

SUMMARY

Context

The objectives of ASPI met those of the third scientific support plan for a sustainable development (Global change, biodiversity and ecosystems) and the CliC (Climate and Cryosphere) project of the WCRP (World Climate Research Programme). ASPI forms part of international research programs such as the European Project on Ice Coring in Antarctica (EPICA), SCAR-SALE (Subglacial Antarctic Lake Environments, a core project of the Scientific Committee on Antarctic Research), and various ISMIP projects (Ice Sheet Model Intercomparison Project) sponsored by the Numerical Experimentation Group of WCRP/SCAR CliC. ASPI members were closely involved in the drafting of the IPCC Fourth Assessment report (AR4). Finally, the results from the paleoclimatic work are a direct contribution to SCAR-ACE (Antarctic Climate Evolution).

Objectives

The aim of ASPI (Antarctic Subglacial Processes and Interactions) is (i) to understand the interactions between the ice sheet and the subglacial environment and the processes that control the Antarctic ice sheet, and (ii) to quantitatively determine the stability of the ice sheet in a changing climate and the impact of climatic variations on the coastal ice sheet and vice versa.

A key factor in such quantification and impact assessment is the existence of transition zones within the ice sheet. Such transition zones are examples of specific boundary layers widely found in glaciology. Basically they are parts of the ice sheet that overlie basal transition zones where the flow is anomalous. Typical examples of such transition zones are the grounding lines, i.e. the interface between the ice sheet and an ice shelf, between an ice sheet and a subglacial lake, between an ice shelf and its pinning points as well as, more generally, between areas where the ice sheet switches from cold-based to warm-based conditions and vice versa. These transition zones are probably among the least understood elements of ice sheets, although they determine to a large extent the processes and dynamics of lateral expansion and retreat of ice sheets as well as the stability of marine ice sheets. Apart from their role in ice dynamics and ice sheet stability, processes and interactions within basal transition zones also hamper the interpretation of the paleoclimatic signal as recorded in deep ice cores. Basal deformation is responsible for disturbing this signal and understanding the processes at the base of ice sheets eventually enables such signal recovery. The subglacial environment opens up new frontiers in Antarctic explorations, as this dynamic and extreme interface still needs to be explored in terms of glaciological, geological, geochemical and biological research efforts.

Main conclusions

We analyzed the response of a marine ice sheet to different perturbations near the grounding line using a numerical ice sheet model that takes into account longitudinal stress coupling and grounding line migration. The model is based on an existing flowline model, but extended with a novel subgrid determination of the grounding line position and migration as a function of the size of the transition zone between the ice

sheet and the ice shelf. For instance, a wide transition zone is typical for an ice stream, a small transition zone typical in many areas around the East Antarctic ice sheet where the ice sheet rather suddenly changes into an ice shelf. Model results show that stress transmission or longitudinal coupling across the grounding line plays a decisive role. The grounding line migration is a function of the length scale over which the basal conditions change from frozen to the bed to floating, the “transition zone”. Perturbations at the grounding line, such as reduction in buttressing of the ice shelf, substantially thins the grounded ice sheet. Marine ice sheets with large transition zones - such as ice streams - seem highly sensitive to such perturbations, compared to ice sheets with small transition zones, such as an abrupt ice sheet/ice shelf junction.

A correct simulation of grounding line migration also requires an additional boundary condition on the ice flux across the grounding line, as recently pointed out in theoretical work from Christian Schoof. His boundary condition was subsequently embedded in numerical experiments in schematic 1D and 2D axisymmetric planform ice flow models that employed a fixed grid. The novel algorithm we devised was thoroughly tested to investigate theoretical requirements such as the reversibility of grounding line migration when subjected to accumulation and sea-level variations and the exact position of the grounding line as compared to analytical expressions. Our scheme was shown to behave well in the time domain and for fixed horizontal grid distances in the range between 2 and 40 km. Further numerical experiments tested heuristic representations for ice-sheet buttressing and for basal sliding. These refinements were implemented in a comprehensive 3D coupled ice-sheet/ice-shelf model of the whole Antarctic ice sheet.

Deformation experiments were conducted to shed more light on how marine ice accretion at the grounding line (and in other weak points of ice shelves) influences the flow properties of the ice sheet system in the transition zone. Therefore, a new analytical facility (pneumatically driven ice deformation unit) was designed, installed and tested at the ULB laboratory. Preliminary experiments clearly demonstrate the importance of such marine ice inclusions on the ice flow: marine ice is harder to deform than meteoric ice in a typical ice-shelf stress field (vertical uniaxial compression with lateral and longitudinal extension) and may therefore exert a stabilizing effect on the whole system. The importance of such result is in conjunction with results from inverse modelling of the transition zone. The latter technique allows for a determination of the ice viscosity properties and/or the basal characteristics in the transition zone, based on observed ice sheet configuration (ice thickness, surface topography) and observed surface velocities. Inverse modelling is therefore capable of determining the size of the transition zone, which is an important factor for predictive modelling. For instance, the application to Pine Island Glacier (WAIS) clearly allows us to determine to position of the onset of the ice stream as well as to delineate areas where stress coupling is essential.

But not only is the ocean influence an important boundary condition. Basal thermal conditions influence to a large extent the behaviour of the Antarctic ice sheet. Whenever the ice reaches pressure melting point, melt water is generated that may lead to enhanced ice flow. Also the presence of subglacial lakes is governed by the basal thermal conditions. Using a 3D thermomechanically-coupled ice sheet model, the influence of spatial variability of the geothermal heat flux on the basal

temperature regime of the Antarctic ice sheet was investigated. Results were compared with observations of known basal temperatures (e.g. ice core drill sites) as well as with the spatial distribution of subglacial lakes. This way it was possible to determine what dataset is more suitable for future model experiments and what basal conditions are more likely to reign underneath the Antarctic ice sheet. Using the most suitable representation of the geothermal heat flux, the same 3D model was furthermore used to reconstruct the current distribution of the age of Antarctic ice. Such qualitative simulations are extremely useful to guide potential deep drilling locations in the quest for ice older than 1 million years. Another model study that combined the large-scale 3D whole Antarctic ice sheet model with a fine scale higher-order model applied to eastern Dronning Maud Land assisted with the dating and interpretation of the EDML ice core drilled at Kohnen station. This work was performed within the framework of EPICA and combined in a unique way the expertise of the VUB modelling group with the ULB glaciology group.

Basal thermal conditions not only strongly control ice sheet flow; they also govern the nature of the interaction between the deep ice and the interface. In turn, this imposes potential restrictions on the validity of climatic and environmental reconstructions in the older ice. The research conducted in the ASPI framework has more specifically looked at the less understood case where melting occurs at the ice bedrock interface without detectable refreezing (EPICA Dome C). We have shown that, in that case, most of the paleoclimatic signatures in the ice are preserved, despite some local (scale of crystal sizes, decimetres) reworking of the chemical impurities under enhanced migration recrystallization at relatively high temperature and changing stress configuration near the bed. However, when noticeable (few hundred meters) bedrock topography changes exist, as in EDC, the time scale can be significantly altered, well above the basal ice (visible solid inclusions) sequence, therefore potentially limiting our exploration capabilities above the one million year range. Previous work of the team has shown that under large scale ice sheets (GRIP, Dye-3), strong mixing occurs between local pre-ice sheet and the active ice sheet ice, when the interface is below the pressure melting point. ASPI has undertaken the study of the basal ice layer of the medium scale (1000 m) Berkner Island ice cap. Results show that, although the bottom ice has clearly lost its paleoclimatic signature well above the visible debris-rich basal ice layer (biogenic impact), the transition is smooth for all the gas variables and shows no sign of mechanical mixing. This suggests that the ice is of much younger age and has not seen any significant displacement of the ice dome.

Subglacial lakes are yet another type of transition zones that are currently gaining attention. Recent observations demonstrate that subglacial lakes may drain and add significant amounts of basal water to the subglacial hydrological system. Hence, they have the potential of destabilising ice sheets through sudden lake outbursts, of which evidence exist along the coast of the East Antarctic ice sheet. In ASPI we investigate the effect of subglacial lake drainage on the stability of the ice sheet and especially how sensitive the subglacial lake system is towards drainage and flooding. Preliminary experiments show that only slight changes in surface topography might easily lead to partial drainage of such a lake.

Transition zones in the Antarctic ice sheets, whether it be grounding lines, subglacial lakes or the subglacial interface are key elements in the dynamic behaviour of the

Antarctic ice sheet and its stability. The ASPI project has considerably improved our understanding of the subglacial processes and interactions that occur at these interfaces. These seem even more important as a controlling factor than was previously thought of.

Contribution of the project in a context of scientific support to a sustainable development policy

The main contribution of the ASPI project to a sustainable development policy is that it has played a crucial role in keeping an original Belgian research capacity operational on both the national and international scale. The teams that participated in ASPI possess at the one hand a unique expertise in glaciological modelling, evident in their state-of-the-art ice flow models including one of the very few comprehensive 3D whole Antarctic ice sheet models available worldwide, and on the other hand a unique expertise in investigating basal ice properties and its paleoclimatic significance. Results and development work performed within this project therefore have found its way in international policy-oriented bodies (IPCC, SCAR, CliC, IPICS) and have set the stage for further participation of both the VUB and ULB modelling partners in EU FP7 research projects such as ice2sea (estimating the future contribution of continental ice to sea-level rise).

Keywords

Antarctica, ice sheet modelling, subglacial environment, ice core analysis, ice deformation

1. INTRODUCTION

Ice sheets are the major component of the Earth's cryosphere. They are now well recognized both as a crucial actor in the regulation of the Earth's climate and as a precious recorder of the climate of the past. Both of these aspects are considered in the ASPI project. On the dynamic side, the focus has been placed on reducing the uncertainties on the predictions of future sea level rise contribution from the potential destabilization of ice sheets, under a warming climate scenario. On the archive side, the motivation was to decipher to what extent the paleoclimatic record of the bottom part of deep ice cores can be trusted? Both objectives can be met by looking in more detail at what we refer to as "transition zones". These are examples of specific boundary layers widely found in glaciology. Basically they are parts of the ice sheet which overlie basal transition zones where the flow is anomalous. Typical examples of such transition zones are the grounding lines, i.e. the interface between the ice sheet and an ice shelf, between an ice sheet and a subglacial lake, between an ice shelf and its pinning points as well as, more globally, all the areas where the thermal regime of the ice sheet switches from cold-based to warm-based and vice-versa. These transition zones are probably among the least understood elements of ice sheets, although they determine to a large extent the processes and dynamics of lateral expansion and retreat of ice sheets as well as the stability of marine ice sheets. Apart from their role in ice dynamics and ice sheet stability, processes and interactions within basal transition zones also hamper the interpretation of the paleoclimatic signal as recorded in deep ice cores. Basal deformation is responsible for disturbing this signal and understanding the processes at the base of ice sheets potentially enables such signal recovery. The subglacial environment therefore opens up new frontiers in Antarctic explorations, as this dynamic and extreme interface still needs to be explored in terms of glaciological, geological, geochemical and biological research efforts.

Both of these major ASPI goals are standing at the forefront of the interrogations put forward by a number of climatically related international organizations. The recently published 4th assessment report of IPCC has already underlined major changes in the relative contributions to sea level rise, as compared to its previous version. Melting mountain glaciers, the most sensitive part of the Earth's cryosphere to climate variations, are now competing in nearly equal proportions with the thermal expansion of the ocean, which was previously the dominant factor. Various precise mass balance estimates of the Greenland ice sheet now all converge to net melting. In the Antarctic, the same estimates average around a neutral value. However, very recent satellite surveys and regional field observations already suggest that the IPCC AR4 is potentially underestimating important contributions from accelerating outlet glaciers, mainly in marine West Antarctica (the most studied example being probably the Pine Island Glacier area). This clearly reveals important limitations of present-day ice sheet models in reproducing the regional behaviour of the ice-sheet/ice shelf transition zones (grounding lines). On the continent too, recent scientific progress has suggested that the existence of a large number of interconnected subglacial lakes underneath the ice sheet might be responsible for its potential destabilization, because of the specific dynamic conditions existing in this other type of transition zone. These considerations have led the International Scientific Committee on Antarctic Research to set up a specific core project dedicated to the study of Subglacial Antarctic Lake Environments (SCAR-SALE), a community of field

glaciologists, biologists, geochemists and modellers, which has now extended its activities to the ice shelf grounding line problem. More specifically, the modelling activity developed in the context of the ASPI project is now a leading component of both the ISMIP-HOM and MISMIP projects of the Numerical Experimentation Group within WCRP/SCAR CliC.

Previous work on the physico-chemical and rheological properties of basal ice from deep ice cores in both hemispheres, in which the ASPI team has been a very active contributor, has underlined the fundamental role of the basal thermal regime on the processes occurring at the interface, and how these potentially interact with the chemical and mechanical properties of the ice above. This is a crucial issue for the scientific community focusing on the paleoclimatic information delivered by ice cores, since, because of the increasing layer compaction with depth, most of that information available timewise is stored within the deeper layers of ice sheets. Until now, the oldest ice considered as a climatically valid archive is about 800 ky old (the EPICA project), and located only a few hundred meters above the ice-bedrock interface. However, one of the main objectives of the international ice coring community, as summarized in the IPICS (International Partnerships in Ice Core Science) white papers, is to retrieve an Antarctic ice core which is at least 1.2 million years old (preferably 1.5 million). This is in order to document the environmental changes that accompanied the change from 40 kyr to 100 kyr cycles revealed by the oceanic records and use that information to better constrain the likely course our climate would take in the next few centuries to millennia in the absence of human interference. Clearly, a better knowledge of processes occurring at the ice-bedrock interface under thick ice sheets is fundamental to match the challenge.

In the next section of this final report, we show how the ASPI team has led its research to reach the objectives described above. On the ice sheet-ice shelf transition zone (grounding line), new algorithms have been developed and tested for grounding-line migration using both a higher-order flow line model (which takes into account longitudinal stresses) and considering a crucial boundary condition on the ice flux across the grounding line. The higher-order model approach is shown to be able to reproduce acceptable solutions for grounding line migration where “traditional” models using the Shallow Ice Approximation (SIA) do not succeed. But also the implementation of Schoof’s flux boundary condition in a SIA/SSA model is demonstrated to yield solutions that compare very well with analytical representations and moreover display the required reversibility characteristics as dictated by theory. These novel grounding line solutions have been implemented in a comprehensive 3D whole Antarctic ice sheet model and validation is currently in progress. The higher order model has also been implemented as an inverse model which allows derivation of information on basal processes and ice shelf viscosity from surface velocity fields.

Another potential improvement of ice shelf behaviour in transition zones is to take into account the considerable large scale heterogeneity of the ice itself, as demonstrated by numerous field observations. These indeed describe the presence in various places (transverse crevasses and rifts at the grounding line, junction between individual ice streams as they get afloat, frontal rifts) of large accumulations of marine ice formed as individual crystals in the ocean below as the result of ice-ocean interactions. In other places, the accumulation is dominated by a mixture of marine ice, sea ice, fallen blocks of meteoric ice and blown snow turned into firn,

which is referred to as the “ice mélange”. Modelling of these heterogeneities is a full project in itself, but the ASPI team has laid the first steps towards it, by studying the physico-chemical and rheological properties of both the marine ice and the “ice mélange”, and showing that the former is an order of magnitude “harder” than normal glacier ice in a typical ice shelf stress field.

In the subglacial lake transition domains, the impact of mass balance changes on potential lake water drainage is simulated and discussed. It is shown that the surface slope is the determining parameter, the flatter the surrounding area, the more stable the lakes. Only small mass balance perturbations are apparently necessary to lead to a sudden outburst. Finally, big lakes under thick ice in slow moving regions (such as lake Vostok) are expected to drain easily. In an attempt to further improve our knowledge on ice sheet dynamics above subglacial lakes, the first steps are also made towards coupling of the ice sheet model with a water circulation model in the lake.

The third studied “transition areas” are those dealing with the contrasts between cold-based and warm-based ice bedrock interfaces. The distribution of these are still extremely poorly known, essentially because of the lack of information on the intensity and spatial distribution of the geothermal heat flux under the Antarctic ice sheet. The ASPI team has used an existing 3-D thermomechanical ice sheet model to describe the sensitivity of the temperature distribution within the Antarctic ice sheet to the choice of the geothermal heat flux. More specifically, the distribution of areas at the pressure melting point obtained for the two existing geothermal heat flux data bases has been compared to the distribution of known existing subglacial lakes. In an extension of these three-dimensional experiments, the distribution of ice age is simulated based on the best choice of geothermal heat flux. This delineates those basal areas where old ice is likely to be present. Maps of the likely thickness of a basal ice layer of given age that contains a full glacial cycle of 100000 years are also presented. To link up with the EPICA Dronning Maud Land basal ice studies, a nested ice flow model for eastern Dronning Maud land was developed to date the ice core drilled at Kohnen Station. It is shown how the chronology of the lowermost 10% of the ice core is crucially affected by the badly constrained value of the geothermal heat flux. Based on these model studies, a number of scenarios are developed to better understand the history and chronology of the basal section of the EDML ice core.

Warm-based and cold-based interfaces are likely to result in contrasted interaction processes with the ice above. We have documented these contrasts in various environments during the ASPI project. At EPICA Dome C and EPICA Dronning Maud Land, the interface is at the pressure melting point. Investigating the bottom 60 meters of the deep ice at EPICA Dome C, where only melting and no refreezing occurs, shows that the ice properties are not significantly altered (apart from localized reworking), but that the time scale can be seriously distorted by the change of stress configuration (stretching of the bottom layers), thereby also degrading the archive. At EPICA Dronning Maud Land, where the basal ice still needs to be investigated, the study of the subglacial refrozen water sheds light on the origin and properties of the subglacial waters. At Berkner Island we have been able to document the processes occurring under an ice cap of medium thickness, where the interface is therefore below the pressure melting point. There, as in other cold-based sites, we show that

the paleoclimatic signal is lost well above the debris-rich basal ice. However, the smooth shape of the different profiles suggests no major reworking through mixing (as seen in the other cold based sites), but rather interactions with the underlying substrate in the early stages of the ice dome build-up.

2. METHODOLOGY AND RESULTS

2.1. Grounding lines and ice sheet modelling

2.1.1. A new algorithm for grounding line migration in ice sheet models

Marine ice sheets rest on a bed that lies well below sea level and the drainage of the ice sheet (necessary to balance the ice accumulation) takes place through surrounding ice shelves. Marine ice sheet stability is believed to be controlled by dynamics of the grounding line, i.e. the junction between the grounded ice sheet and the floating ice shelf. The WAIS has therefore received particular attention because it has been the most dynamic part of the Antarctic ice sheet in the recent geological past, and because most of it is grounded below sea level - a situation that, according to early models, could lead to flow instabilities and rapid ice discharge into the ocean when the surrounding ice shelves would weaken. Such instability is governed by the physical interaction between ice streams and shelves, more precisely the feedback between grounding lines and ice flux. The potential of the WAIS to collapse in response to future climate change is still a subject of debate and controversy. If the entire WAIS would collapse, global sea level would rise by 5 to 6 m. It has been suggested that present observed rapid thinning of the WAIS is due to increased melting under ice shelves caused by a gradual ocean warming (Shepherd et al., 2004). Payne et al. (2004) showed that such melting could lead to an acceleration of grounded ice flow.

Grounding line migration is a key element in assessing the stability of marine ice sheets, and the WAIS in particular. We believe that stress transfer or longitudinal stress coupling across the grounding line plays a decisive role herein and is determined by the length of the transition zone between ice sheet and ice shelf. Such transition can be small, i.e. an abrupt change from ice sheet to ice shelf, or large when an ice stream makes the linkage between both systems. Several theories exist with respect to the behaviour of marine ice sheets, in which some even neglect the presence of an ice shelf. For this project we analyzed the response of a marine ice sheet to different perturbations near the grounding line using a numerical ice sheet model that takes into account longitudinal stress coupling and grounding line migration. The model is based on the flowline models developed by Pattyn (2002), but extended with a novel subgrid determination of the grounding line position and migration as a function of the size of the transition zone between the ice sheet and the ice shelf (Pattyn et al., 2006). Consider the function based on flotation criterion (with h ice thickness, z_{sl} sea level and ρ_i and ρ_w the density of ice and sea water, respectively:

$$f = \frac{(z_{sl} - b)\rho_w}{\rho_i h} \qquad (1)$$

It follows that $f = 1$ at the grounding line, $f < 1$ in the grounded ice sheet, and $f > 1$ in the ice shelf. The exact position of the grounding line x_g (km) is then defined by linear interpolation between the last grounded and the first floating grid point:

$$x_g = \frac{1 - f_j + \nabla f \, x_j}{\nabla f} \qquad (2)$$

where $\nabla f = \left(f_{j+1} - f_j\right)/\Delta x$. This scheme has the advantage that it can be easily translated to the plane. The difference between the ice sheet and shelf arises because the shelf is floating and because it experiences vanishing tangential traction on the bottom as well as the upper surface (Hindmarsh, 1993). The length of the transition zone is then determined by the distance over which this vanishing traction occurs. Vanishing traction towards the grounding line is introduced through a friction parameter β^2 that relates the basal velocity to the basal drag, $\tau_b = u_b \beta^2$. For $\beta^2 = 0$, basal drag equals zero (no traction) which is a situation similar to an ice shelf; for $\beta^2 = +\infty$, the basal velocity equals zero (ice frozen to the bedrock) which is valid for the ice sheet; for $0 < \beta^2 < +\infty$ a transition zone exists. We shall not consider the physical mechanisms that are responsible for the reduction in traction (i.e. sliding) but suppose basal friction to be of the general form: $\beta^2 = \exp\left[\beta_0\left(x_g - x\right)\right]$, where β_0 controls the length of the transition zone. The exponential form of the basal friction stems from an analysis of the longitudinal profile of PIG (Pattyn et al, 2006). Linking the subgrid determination of the position of the grounding line directly with the stress field within the ice sheet is a novel approach. There is no need to *a priori* prescribe what ice sheet, ice stream or ice shelf is and the use of these relationships is independent of the chosen grid size, which make the basal conditions independent of grid size as well. Values of β_0 and their relation to observed Antarctic transition zones can be found in Table 1 in Pattyn et al (2006). The size of the transition zone will also have an impact on the resulting ice sheet / ice shelf profile: the more concave shape is due to a wider transition zone, as can be observed in ice streams as well (Figure 1).

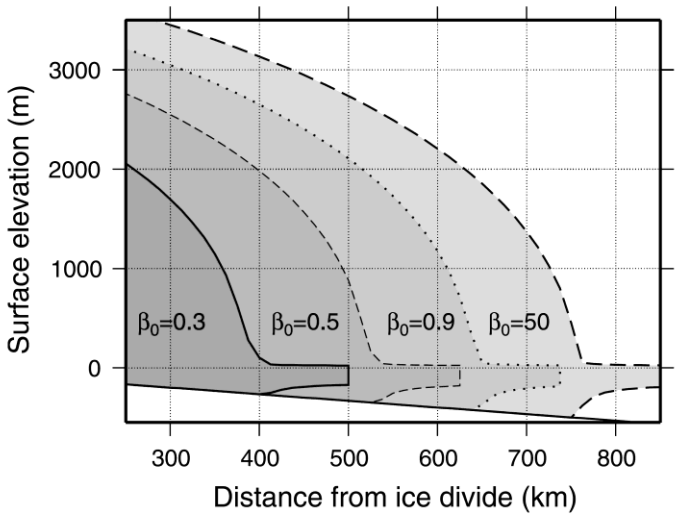

Figure 1: Equilibrium profiles of a marine ice sheet on a sloping bedrock for different sizes of the transition zone between the ice sheet and the ice shelf. All experiments started from a fixed grounding line at x = 750 km.

Experiments were carried out for different sizes of transition zones, which has a major impact on the shape of the longitudinal profile of the ice sheet/ice shelf system: the shape of the transition becomes more concave when the transition zone is wide, a typical feature for the ice stream/ice shelf transition. Our basic sensitivity analysis has shown that grounding line advance and retreat is a function of transition zone characteristics. The retreat is minimal for small transition zones, and the grounding line remains more or less where it is. However, the reversibility of the process increases with the length of the transition zone. These results corroborate the neutral equilibrium hypothesis of Hindmarsh (1993), i.e., that for a small transition zone multiple equilibria may exist, therefore not necessarily exhibiting reversibility. For larger transition zones the grounding line returns to its initial position, which shows the reversibility of the process, similar to the behaviour of moving grid models (Vieli and Payne, 2005). Thus, according to our model results, grounding line migration for small transition zones exhibits hysteresis, while for larger transition zones the migration process is reversible. Stress transmission or longitudinal coupling across the grounding line plays also a decisive role. The grounding line migration is a function of the length scale over which the basal conditions change from frozen to the bed to floating, the “transition zone”. We have demonstrated that thinning of the ice shelf due to bottom melting has a negligible effect on the grounded ice mass, at least when other parameters do not come into play. Only perturbations at the grounding line or reduction in buttressing of the ice shelf substantially thins the grounded ice sheet. Inclusion of lateral drag does not alter these results qualitatively. Marine ice sheets with large transition zones - such as ice streams - seem highly sensitive to such perturbations, compared to ice sheets with small transition zones, such as an abrupt ice sheet/ice shelf junction. Ice streams are therefore more sensitive to changes at the grounding line and form therefore a potential positive contribution to future sea-level rise. This is illustrated in Figure 2.

2.1.2. Validating stress coupling across the grounding line

Although predictions of sea-level rise due to global warming have become more precise over the last decade, as highlighted by the recent report from the Intergovernmental Panel on Climate Change (IPCC), the contribution that could arise from rapidly changing flow in ice sheets, especially in Greenland and Antarctica, remains excluded (Vaughan and Arthern, 2007). Furthermore, it is apparent that the late 20th- and early 21st-century ice sheets at least are dominated by regional behaviours that are not captured in the models on which IPCC predictions have depended (Shepherd and Wingham, 2007). The viscous flow of ice is rather well understood on a theoretical level, but the difficulties in modelling the ice sheet system arises from the specification of stress boundary conditions at the base and the seaward margin. Here, several stress components come into play in regions of high variability in basal topography and/or basal slipperiness.

Despite the lack of comprehensive predictive ice-sheet modelling, the ice-sheet modelling community has evolved considerably over the last decade. Increasing computational power has led to the development of more complex ice sheet models, with varying degrees in approximations to the Stokes system. Although only few models solve the full Stokes problem in three dimensions, there is a need for validating these so-called higher-order models (i.e. models that incorporate further mechanical effects, principally longitudinal stress gradients) as analytical solutions are not always available. Such a benchmark exercise was done with large-scale ice sheet models in the 1990s

(e.g. Huybrechts et al., 1996). Similar benchmark experiments are carried out now and validated by >22 numerical ice-sheet models of varying degrees of complexity (Pattyn et al., 2008). Besides benchmarking, the experiments also allowed to discern under which conditions the approximations to the Stokes system are viable and whether numerical issues play a role in the result.

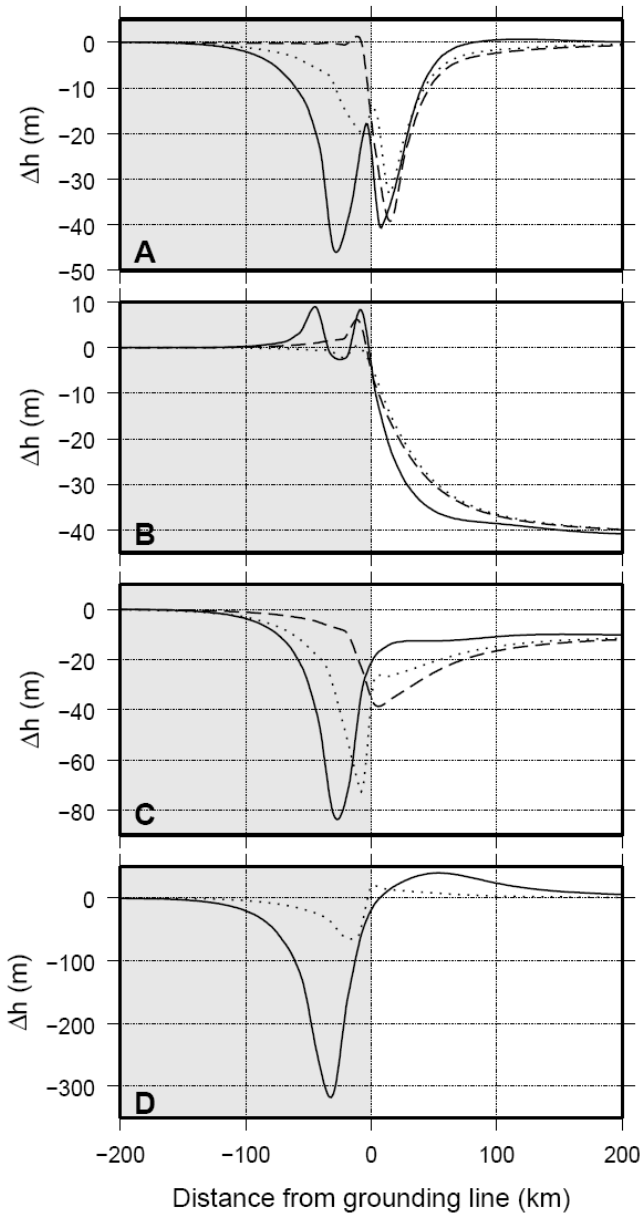

Figure 2: Ice sheet response near the grounding line to perturbation for β_0 = 50 (dashed line), 0.9 (dotted line) and 0.3 (solid line) after 100 year. (A) Melting of 1 m/a at the grounding line; (B) Melting of 0.5 m/a along the whole length of the ice shelf; (C) Reduced ice shelf buttressing (see text for details); (D) Decrease in β_0, from β_0 = 0.9 to 0.7 and from β_0 = 0.3 to 0.2. The grounded ice part is shaded.

The approach followed by Schoof (2007a, 2007b) makes it possible to test models, and any new model that is going to be built should be conform theoretical results. For instance, Schoof (2007b) found that marine ice sheets may undergo dramatic and irreversible changes - hysteresis - under changes in physical properties (sliding, ice

viscosity) or external forcing (accumulation rates, sea levels). The basic questions that arise from these papers and earlier work are the following:

- Do marine ice sheets have one or more distinct equilibrium shapes, or do they not exhibit `neutral equilibrium': will a perturbation in grounding line position away from steady state result in the grounding line either returning to the (stable) steady state position or migrating away from the (unstable) steady state position to a stable steady state?
- Do stable steady states have to have their grounding lines in a region of downward-sloping bed?
- How do equilibria depend on bed geometry and the physics of sliding at the bed, ice viscosity and gravitational forces as well accumulation rates?
- Is hysteresis under changes in forcing and internal physical properties possible when the bed is overdeepened?
- To what extent is high grid resolution, especially near the grounding line, necessary to obtain reliable results? Is this particularly important when modelling transients?

Experiments with the above described flowline model have been carried out to test the hypothesis of stable grounding line equilibria on a downward sloping bed as well as on an overdeepened bed that should exhibit hysteresis (combination of stable and unstable equilibria). This also allows us to test whether the stress balance matters in the transition zone or not (i.e. can we just use the shallow-ice approximation (SIA) to solve the stress field upstream of the grounding line or do we explicitly have to take into account longitudinal stress gradients?). The impact of higher-order stress gradients is shown in Figure 3, which displays the evolution of steady state grounding line positions for different values of the ice flow factor A. Starting from an initial ice sheet configuration the parameter A was changed and the ice sheet/ice shelf system evolved until a new steady state was reached. For decreasing values of A, the grounding line moves forward (as depicted by the blue dots in Figure 3). However, using a SIA model – shallow ice approximation – increasing values of A do not lead to a grounding line retreat and the grounding line remains more or less at its initial position (Figure 3a). Using the higher-order model with the grounding line interpolation scheme as described above, leads to a reversible grounding line migration (Figure 3b), conform the theoretical considerations described by Schoof (2007b).

Building further on these studies, we have tested various approaches to implement a new scheme for grounding-line migration in three dimensions. This new scheme incorporates the Schoof boundary conditions and will ultimately combine a high-resolution fixed grid with a higher order stress solution in the transition zone using a nested modelling approach similar to the one adopted recently for dating and interpreting the EPICA Dronning Maud Land ice core (Huybrechts et al., 2007).

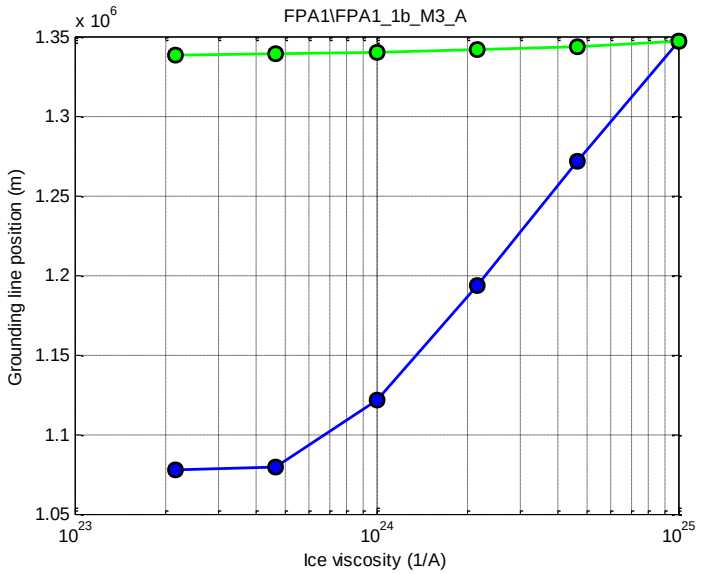

Figure 3a: Steady state grounding line positions for different values of the ice flow parameter A. The blue curve shows the evolution of stepwise decreasing values of A. the green curve the reverse evolution. Results are shown for a SIA model with coupled ice shelf model.

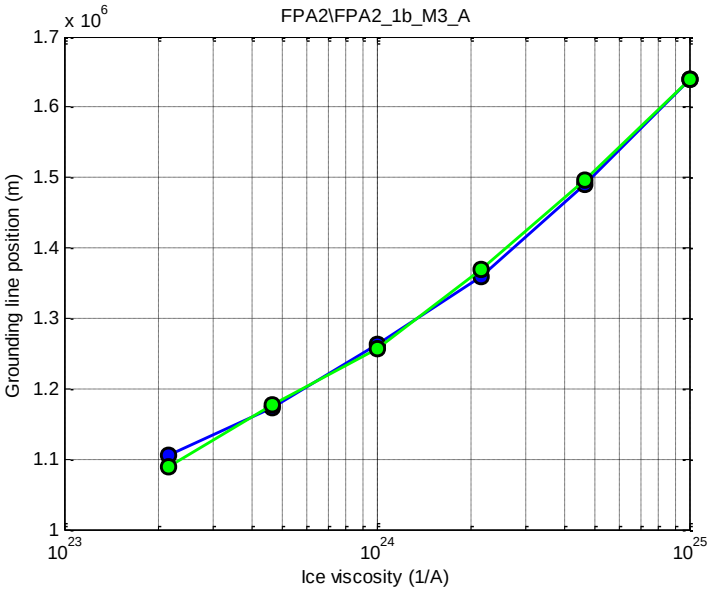

Figure 3b: as Figure 3a, but with the higher-order model. Note that increasing and decreasing values of A result in similar steady state ice sheet configurations with the grounding line at more or less the same position.

2.1.3. Implementation of grounding line migration in a 3D ice sheet model

Migration of the grounding of the Antarctic ice sheet is a process (or a complex of interrelated physical processes), which is not well understood and therefore not adequately reproduced in present-day ice-sheet numerical models. The mechanical problem has long been stated from the fundamentally different stress balance in floating and grounded ice. While the grounded ice is dominated by vertical shear, ice-shelf flow is a buoyancy-driven flow dominated by longitudinal stretching and lateral shearing (e.g. Van der Veen, 1999). This implies a transition zone across the grounding zone which

dimensions are crucially controlled by the importance of basal sliding in the adjacent ice sheet (e.g. Mayer and Huybrechts, 1999; Pattyn et al., 2006). So far grounding line migration in existing 3-D Antarctic ice sheet models is only implemented in the models of Ritz et al. (2001), Huybrechts (1992, 2002) and Pollard and DeConto (2009). In the first two models, the position of the grounding-line is diagnosed from a floatation criterion. Ritz et al. (2001) introduced the concept of a 'dragging ice shelf' to incorporate ice-stream dynamics, which is particularly important for the Siple Coast area of the West Antarctic ice sheet. In their model, inland ice is differentiated from an ice-stream zone by the magnitude of basal drag. This is based on the observation that ice-stream zones are characterized by low surface slopes, and thus low driving stresses, but have fast sliding. Ritz et al. (2001) treat these zones as semi-grounded ice shelves, and replace the shallow-ice approximation by a set of equations for ice-shelf flow to which basal drag is added. In the Huybrechts models two sets of equations are solved independently for grounded and floating ice. The transition zone at the grounding line is assumed to consist of one grid point only, located directly adjacent to the ice shelf. Here, longitudinal stresses are taken into account in the effective stress term of the flow law, which additional stress terms are found by iteratively solving three coupled equations for depth-averaged horizontal stress deviators. Gross model behaviour of both models turns out to be quite similar, except that the Grenoble model has a lower surface slope near the grounding line in West Antarctica and that the break in the slope occurs further upstream at the place where the dragging ice shelf joins the inland ice subject to the shallow-ice approximation. One consequence is that grounding-line retreat in the Ritz et al. (2001) model occurs more readily in response to rising sea levels. In the Pollard and DeConto (2009) model, migration of the grounding line under varying environmental conditions is simulated using a boundary condition for ice flux across the grounding line, as was suggested by Schoof (2007b) for a 1D model. The algorithm they implemented to treat the grounding line is considered below in more detail.

The grounding line problem is crucial for understanding the dynamics of ice sheets, but the controlling quantitative dynamics of marine ice sheets remain unknown (Hindmarsh, 2006). The study of possible fast responses of marine ice sheets requires a new generation of ice-sheet models. This also applies to the reconstruction of the dynamics of ice sheets in the past because present-day ice sheet models fail to reproduce adequately the processes of the Antarctic ice sheet during the last deglaciation. One of the elements to be essentially improved is grounding line migration (Little et al., 2007). One of the possible approaches within a finite difference model is the application of adaptive meshes (Goldberg and Holland, 2007). This is a promising but numerically complicated and computationally expensive technique. It fits into the task formulated by Lipscomb et al. (2008) to obtain an accurate and numerically robust treatment of grounding line migration on a fixed grid.

Almost a decade after the EISMINT experiments (Huybrechts et al., 1998), Vieli and Payne (2005) reconsidered a comparative study of the ability of numerical ice sheet models to simulate grounding line migration. They found that the dynamics of the grounding line are mainly controlled by the discretization scheme used and that the physics (such as longitudinal coupling) incorporated into a particular model appears to have only secondary importance. Moreover, moving grid models perform fundamentally different from fixed grid models, the latter allowing for larger changes in response to an imposed forcing. Another thing, which became very clear already from the EISMINT

tests, is that grid resolution of the transition zone is also of crucial importance in any properly functioning scheme.

The problem of grounding line treatment suffers from the lack of a general theoretical background. Recently, an attempt was made by Schoof (2006, 2007a, b) to fill this gap. In Schoof (2006), an approach is suggested to incorporate in a sophisticated way the dynamics of narrow marginal ice streams into an overall dynamical picture of an ice sheet. Schoof (2007a) applied boundary layer theory in order to obtain analytical approximations for the ice flux in the transition zone. In Schoof (2007b), which is of particular interest for our study, three different models are employed based on a moving grid. Grid refinement in the transition zone is again identified as a critical component to obtain reliable numerical results. Mathematically spoken, the models solve a free boundary value problem, which means that the moving boundary is also part of the problem. Schoof remarks that parabolic free boundary value problems, such as the Stefan problem, require two boundary conditions. This is in contrast to the moving grid models of Hindmarsh (1996), Hindmarsh and Le Meur (2001) and Vieli and Payne (2005) who use only one boundary condition. Based on this observation, and on a suggestion for the second boundary condition, Schoof (2007b) uses an analytical approximation to describe steady states, stability and hysteresis. His work supports several earlier theories predicting instability, cf. Weertman (1974). According to Schoof (2007b), the boundary condition in his "Type B" model on ice flux across the grounding line is:

$$Q_g = \left[\frac{\overline{A}(\rho_i g)^{n+1}(1-\rho_i/\rho_w)^n}{4^n C} \right]^{\frac{1}{m+1}} \theta^{\frac{n}{m+1}} h_g^{\frac{m+n+3}{m+1}} \quad , \qquad (3)$$

where $\overline{A}$ is the depth average parameter in Glen's flow law, *C* is the basal sliding parameter, *g* the acceleration of gravity, and n the exponent of the flow law, with m=1/n. The second term on the right hand side is responsible for the buttressing effect, $0 \le \theta \le 1$, though it is not explicitly defined. Obviously, the grounding line position is determined in (3) only by ice-sheet geometry, ice softness and the sliding law.

Based on the work by Schoof, Pollard and DeConto (2007) embedded a relation for the flux across the grounding line in a higher-order model, but using an equidistant 10 km numerical grid. This approach produced very similar results to another experiment, in which a very fine 0.1 km grid was used around the grounding line, but not the boundary condition on the grounding line flux. From these experiments, it may be concluded that the reasons for unrealistic behaviour produced by earlier models (such as those included in EISMINT) at the transition zone is not the resolution problem itself, but some parallel effect. Large grid sizes cause an inaccurate flux at the grounding line, which can only be overcome by using a numerically-demanding high resolution grid or by imposing the flux itself. Later on a similar approach was implemented by Pollard and DeConto (2009) for treating grounding line in a 3D model of the Antarctic ice sheet.

Based on the theoretical findings of Schoof (2007b) and suggestions by Pollard and DeConto (2007, 2009) we elaborated a novel algorithm and computer routine for implementing grounding line migration into a coupled ice-sheet/ice shelf model. This algorithm was first tested for 1D and 2D horizontal plane simplified ice sheet models. We first of all implemented the grounding line migration algorithm (GLMA) in a

slightly modified version of the 1D EISMINT grounding line intercomparison tests (Huybrechts et al, 1998). Ice flow in the grounded domain follows the Shallow Ice Approximation (SIA) approach. In the ice shelf domain ice flow is found from the solution of a coupled set of non-linear elliptic equations. A staggered grid is employed to calculate velocities in the ice shelf. The model is isothermal and employs a constant accumulation rate. Basal sliding velocity is proportional to the basal shear stress. In the model, the exact position of the grounding line is undefined. It is supposed to be located between the last grounded grid point and the first ice shelf grid point, corresponding to a transition zone. The exact position of the grounding line is found from the linear approximation given in eq. (2). This immediately gives ice thickness at the grounding line, which is the 1st boundary condition according to Schoof (2007b). Schoof (2007b) showed that application of the 2nd boundary condition (on mass flux through the grounding line, eq. 3) makes the grounding line migrate freely in case the horizontal coordinate is stretched (i.e. moves with the grounding line) and grid refinement takes place around the grounding line.

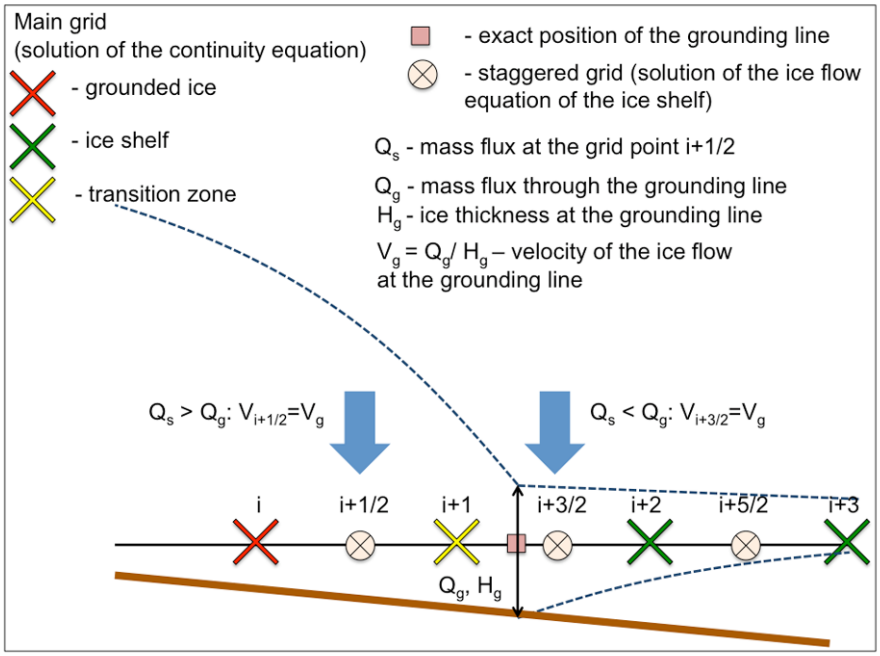

Figure 4: Implementation of the Schoof boundary condition in a 1D ice sheet/ice shelf model. In case the analytically derived flux across the actual (i.e. linearly approximated) grounding line position Q_g from eq. (3) is greater than the modelled ice flux through the modelled grounding line (point i+1/2), a velocity $V_g = Q_g / h_g$ is imposed on the staggered grid point i+1/2, which corresponds to the modelled grounding line. Otherwise V_g is imposed on the grid point i+3/2 downstream from the grounding line point.

Pollard and DeConto (2007, 2009) studied the behaviour of the grounded line in a series of numerical experiments with a 1D ice flow model where the horizontal coordinate was not stretching. They found that in case the grid resolution is coarser than ~0.1 km, the model failed to reproduce migration of the grounding line. In order to circumvent the use of a fine resolution around the grounding line, they suggested following a certain heuristic rule. In case the analytically derived flux across the *actual* (i.e. linearly approximated) grounding line Q_g from eq (3) is greater than the

modelled ice flux through the modelled grounding line, a velocity $V_g = Q_g / h_g$ is imposed on the staggered grid point that corresponds to the *modelled* grounding line. Otherwise V_g is imposed on the grid point downstream from the grounding line point (see sketch in Figure 4). Implementation of this simple rule creates a violation of the mass flux at the model grid point. Actually, this violation turns out to be a driving force of advance and retreat of the grounding line.

To investigate the applicability of the Schoof boundary condition on the mass flux of regularly-spaced grids with resolutions in the range 2-40 km we implemented the rule of Pollard and DeConto (2007, 2009) into our model. We performed a series of EISMINT tests aiming at simulating the movement of the grounding line (Huybrechts et al., 1997). Two types of tests were involved:

1. H-test. An initial ice sheet in a steady state is forced by sea-level lowering of 125 m. After the ice sheet has adjusted to a new steady state it is forced by a sea level rise of 125 m. Initial and final positions of the grounded line are compared.
2. A-test. An initial ice sheet in a steady state is forced by an accumulation increase from 0.3 m/yr to 0.5 m/yr. After the ice sheet has adjusted to a new steady state it is again forced by a decreasing accumulation rate from 0.5 back to 0.3 m/yr. Initial and final positions of the grounded line are compared.

The theoretical steady-state positions of the grounding line are found as intersections of the net accumulation rate with the curves of the mass flux across the grounding line, which follow from eq. 3 (Figure 5, upper panel). As an initial state (ice thickness, velocity) we used output of the original EISMINT model result (i.e. without boundary condition on the flux across the grounding line) integrated to its steady state. Starting from this initial state the ice sheet was evolved to a new steady state corresponding to the undisturbed conditions in our H- and A-tests. Further on, we performed the H- and A-tests for the range of $\overline{A}$ and C values in which the grounding line returned to a position close to the initial one to within ~1 grid size distance. Shown in Figure 5 (middle panel) are modelled mass fluxes calculated in every grid point as $F = \left|\bar{V}\right| h$, where $\bar{V}$ is the vertically averaged velocity of the ice flow. One can see apparent deviations of ice fluxes at the modelled grounding line, which however disappear further downstream. Note that the deviation of the flux during the phase when the ice sheet advances is greater (and this was the case in all our tests) than in the retreat phase. Evolution of the grounding line position, of the ice thickness at the grounding line and of the ice flux across the grounding line is shown in Figure 6.

After a series of preliminary testing we found how to reduce the magnitude of the flux violation at the grounded line. Instead of imposing V_g, a reduced difference $\left(V_g - V_{i+1/2}\right)/n$ or $\left(V_g - V_{i+3/2}\right)/n$ must be imposed at the relevant grid point. During the "advance" phase of the ice sheet the greater the n the smaller is the flux violation.

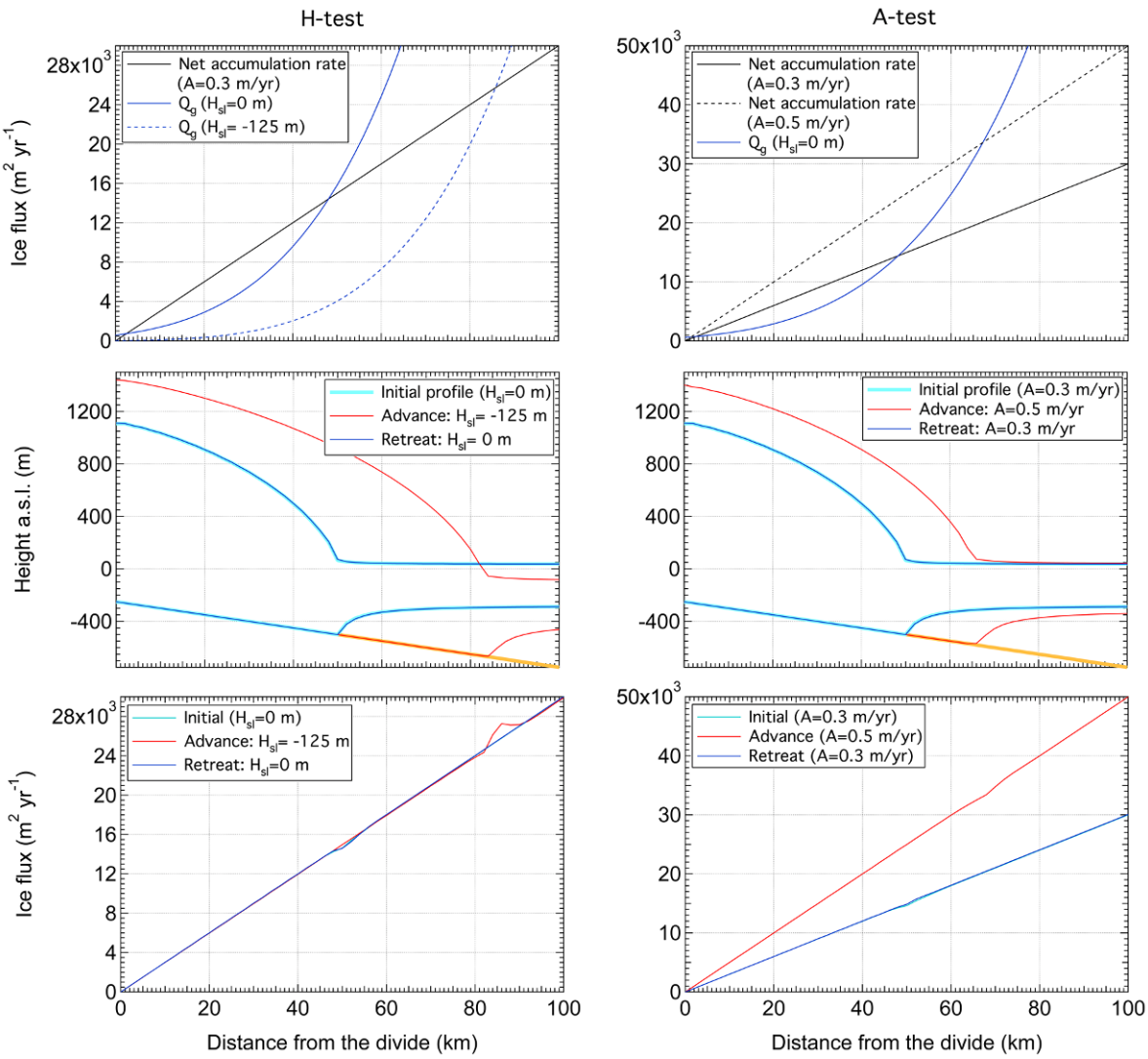

Figure 5: Results of the H-test (left column) and A-test (right column) within an EISMINT type ice sheet/ice shelf model with $\bar{A}$=1.68405×10^{-18} yr^{-1} Pa^{-3} and C=2×10^{-16} N^{-3}y^{-1}m^{7}: theoretical position of the grounding line (upper row), ice sheet profile (middle row), ice fluxes (lower row). The accuracy of the "advance-retreat" cycle in both tests is smaller than the grid size (2 km).

During the retreat phase a larger *n* prevents the grounding line to move properly, and *n*=2 was found to be a good compromise.

It is not possible to get rid of the flux violation totally in models with a coarse grid. This is explained by the mere fact that the analytical flux, which only depends on the ice sheet / ice shelf geometry and bed geometry (if buttressing is not taken into account) determines the flow velocity. This velocity is imposed to one or another grid point around the grounding line and does not agree with the SIA velocity. It merely sets the boundary value for the ice-shelf velocity, and the continuity of the flux is thus violated at the grounding line. Since velocities in the grounded domain are defined locally, the mechanism of transfer of a flux violation is absent. Further adjustment of the ice sheet geometry to changed mass fluxes on the lateral border is performed through the change of ice thickness under the influence of a changed mass flux. One can see this adjustment process in Figure 6. Small oscillations in all three (interdependent) variables show a jump-like change of the model fluxes approaching

the analytical one in a certain point. After the value of the analytical value is achieved the analytical velocity is imposed at the grid point downstream of the grounding line (in case of grounding line retreat) or upstream of the grounding line (in case of grounding line advance). Thus a new flux imbalance is created. During the final stage when the grounding line approaches a position where the flux through the grounding line must be theoretically equal to the net accumulation rate, this imbalance becomes smaller and smaller. In the end, solving the ice flow equation in the ice shelf causes the modelled ice flux to slightly oscillate around the theoretical value causing tiny retreats and advances of the grounding line. This in turn causes tiny oscillations in ice geometry, etc. Note that the phase of the flux imbalance at the last stage, when the final possible position of the model grounded line is achieved, is random. The model simply switches the value of the flux (hence ice flow velocity as well) between higher or lower values.

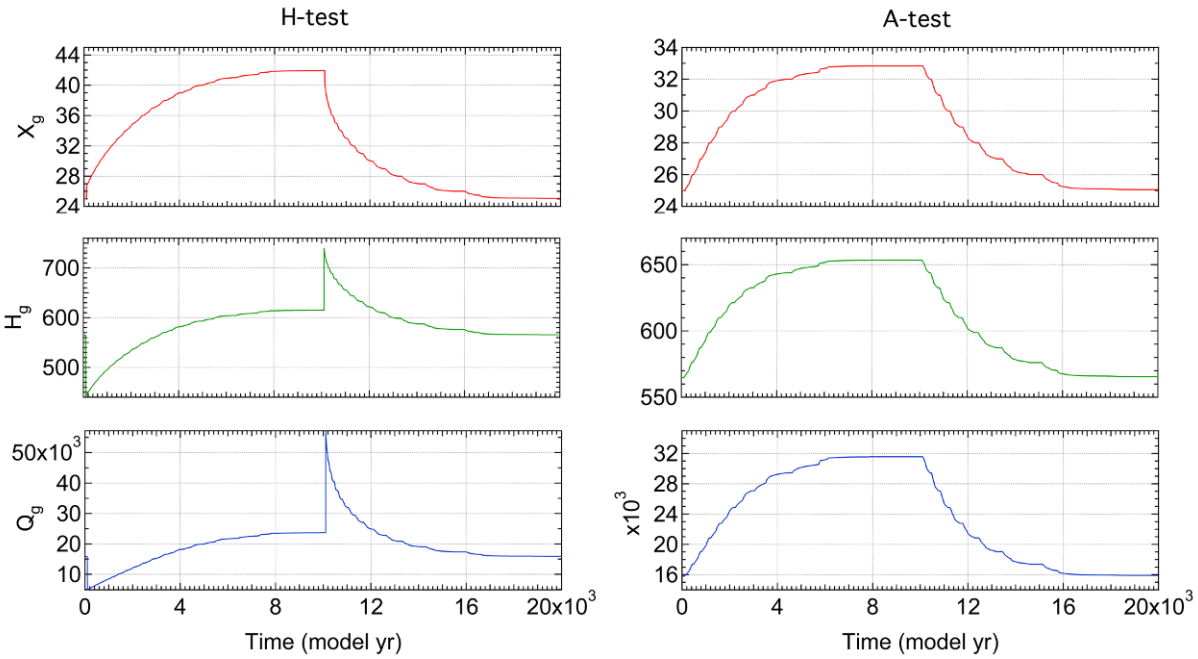

Figure 6: Results of the H-test (left column) and A-test (right column) with settings as in Figure 5: positions of the grounding line (upper row), ice thickness at the grounding line (middle row) and ice flux across the grounding line (lower row).

It is therefore clear that the accuracy with which the grounded line will come back to the position that preceded the perturbation will depend on the grid size. The accuracy of the "advance-retreat" cycle with a grid size of 2 km is smaller than one spatial step. With the increase of the spatial step the accuracy drops in absolute and relative values. For spatial resolutions in the range of 10-40 km the error of the return position with respect to the start point is ~1-1.5 times the spatial step (see Figure 7). Still this result is much better than was obtained by this type of models in the EISMINT tests with no boundary conditions on the flux through the grounding line. This accuracy is also conserved when the simple bed profile is replaced by the bed profile used by Schoof (2007b) in his numerical experiments as well as in one of the MISMIP tests. After having been perturbed by a sea-level drop the grounding line advances to a limiting value suggested by the theory, and after sea-level goes up again to its present value, the grounding line retreats to a position to within one grid size distance of the initial one.

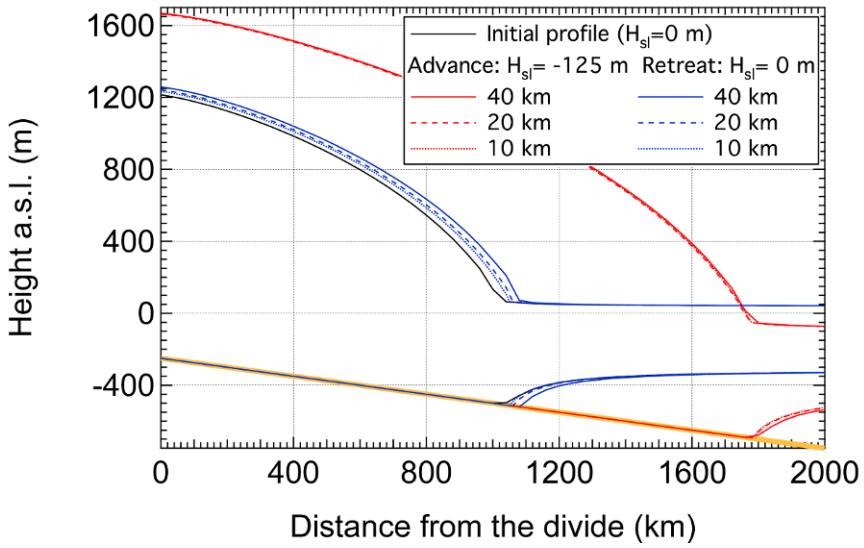

Figure 7: Results of the H-test with the EISMINT type ice sheet/ice shelf model with $\overline{A}=1\times10^{-18}$ yr^{-1} Pa^{-3} and C=2×10^{-16} N^{-3}y^{-1}m^{7}: effect of spatial resolution: ice sheet profile (a) and corresponding ice fluxes (b) for grids with resolutions of 40 km, 20 km, and 10 km. The error of the return position with respect to the start point is within ~1-1.5 times the spatial step.

Basal melting being applied to the ice shelf causes it to thin and induces retreat of the ice front when ice thickness goes to zero. In our experiments, however, that had no effect on the grounding line position (Figure 8). This result contradicts the conclusions of some previous studies. For example, Payne et al. (2004) showed that such melting could lead to an acceleration of grounded ice flow. In the model study of Walker et al. (2008), the grounding line retreated with increased basal melting. The mechanism by which ice sheet melting influences the position of the grounding line is probably not well captured by the type of model we employ here, since there is no direct melting of ice at the grounding line. One the other hand, the grounded ice does not "feel" what happens in the ice-sheet domain, since there is no transfer of the longitudinal stresses into the grounded domain, as occurs in the higher order models employed by Walker et al. (2008).

In the real world this mechanism is probably crucial for the description of ice dynamics. In particular this is important for understanding the present-day dynamics of the WAIS. For instance, it has been suggested that the presently observed rapid thinning of the WAIS is due to increased melting under the ice shelves caused by a gradual ocean warming (Shepherd et al., 2004).

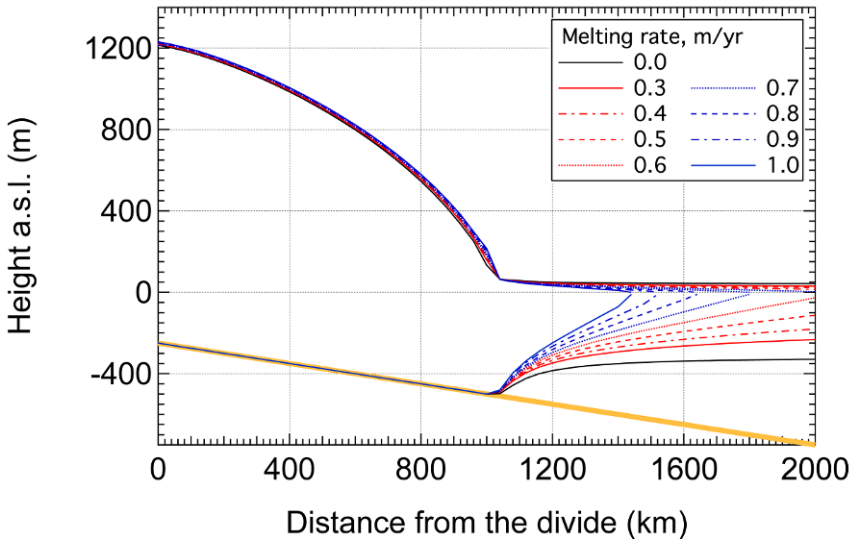

Figure 8: Results of the numerical experiments with varying basal melting under the ice shelf with the EISMINT type ice sheet/ice shelf model with settings as in Figure 7. Increase of basal melting has no effect on the grounding line position.

The mechanism that should theoretically oppose basal melting is buttressing. Though the term responsible for buttressing is present in eq. 3, it is not explicitly defined. To account for the mechanism of buttressing Pollard and DeConto (2009) considered $\theta = \tau_{kk} / \tau_0$, where:

$$\tau_{kk} = -2\overline{A}^{-1/n} h_g \left| \frac{\partial u_k}{\partial k} \right|^{1/n-1} \frac{\partial u_k}{\partial k} \tag{4}$$

is the longitudinal stress across the grounding line from the shelf-flow equation and:

$$\tau_0 = \frac{1}{2} \rho_i g h_g^2 \left(1 - \frac{\rho_i}{\rho_w} \right) \tag{5}$$

is the same quantity as τ_{kk} in the absence of any buttressing. We tested the effect of buttressing on the grounding line position by simply decreasing θ from 1 (no buttressing) to 0.6 (medium buttressing). By doing this we decrease the flux across the grounding line, which naturally causes the ice sheet to grow and expand (Figure 9). Similarly, it can be interpreted that a decrease of buttressing (increase of θ) makes the ice sheet shrink and the grounding line retreat. This somewhat illustrative example clearly demonstrates the role of buttressing in the dynamics of a marine ice sheet. Of course, in the above example θ is introduced as a parameter. In case of a 2D or 3D model this is hardly possible. According to Schoof (2007b) θ must be determined through momentum conservation in the ice shelf, which in turn depends on the evolving three-dimensional geometry of the ice shelf.

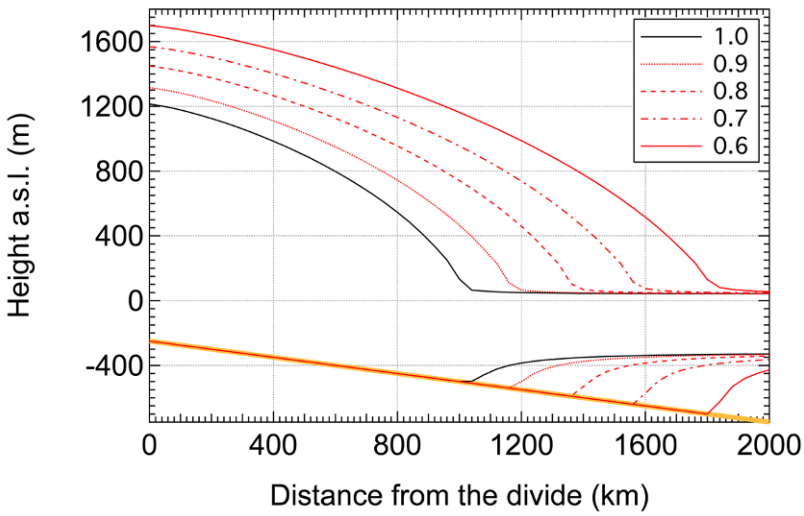

Figure 9: Results of the numerical experiments with varying buttressing with the EISMINT type ice sheet/ice shelf model with settings as in Figure 7. The ice sheet profiles correspond to values of θ as given in the legend. A decrease of θ, which corresponds to an increase of buttressing forces the grounding line to advance to a new stable position. Conversely, a decrease of buttressing (increase of θ) forces the grounding line to retreat.

Eq. 3 was established for the case of a 1D ice model. There is no general theory for the case of 2D flow, where the mass flux across (i.e. perpendicular to) the grounding line is accompanied by a mass flux along the grounding line. In spite of the 1D nature of eq. 3, Pollard and DeConto implemented the Schoof boundary condition (eq. 3) with a strong assumption. They neglected the gradients of the ice velocity parallel to the grounding line, which were considered to cause only small second-order effects in typical 2-D flows (Pollard and DeConto, 2009, with reference to a personal communication by Schoof). They assumed the grounding line to be a “continuous series of perpendicular segments” (Pollard ant DeConto, 2009, suppl. material) in the *x* and *y* directions. The same heuristic rule was implemented to capture grounding line movement as in the 1D case.

In our experiments, we followed the basic ideas of Pollard and DeConto (2009) and also use a staggered grid for the calculation of velocity components in the ice shelf (this type of staggered grid is known as a type C grid according to the Arakawa classification). We implemented a slight modification to their heuristic rule as we did in the 1D case (see above). A sketch demonstrating the implementation of the method is shown in Figure 10. As well as in the 1D case the analytically derived velocities are imposed on the grid point upstream or downstream of the actual grounding line depending on the value of the analytical mass flux compared to the modelled one.

To check the performance of the grounding line migration in a 2D case we carried out H-tests similar to the 1D case. The bed had a conical form obtained by rotating the 1D bed profile around its vertical axis. The same applied to the initial ice thickness and ice velocity in the ice shelf. One of the test examples is shown in Figure 11 for a 33×33 grid with a coarse spatial resolution of 125 km. From this initial state the ice sheet evolves to a steady-state. After a sea-level drop by 125 m it expands to a new steady state. After the increase of the sea level to the initial value the ice sheet

contracts to a state close to the initial one. This test demonstrates that the model is able to reproduce grounding line advance and retreat in the 2D case. The difference of the grounding line position before and after perturbation is far smaller than 1 gridpoint distance.

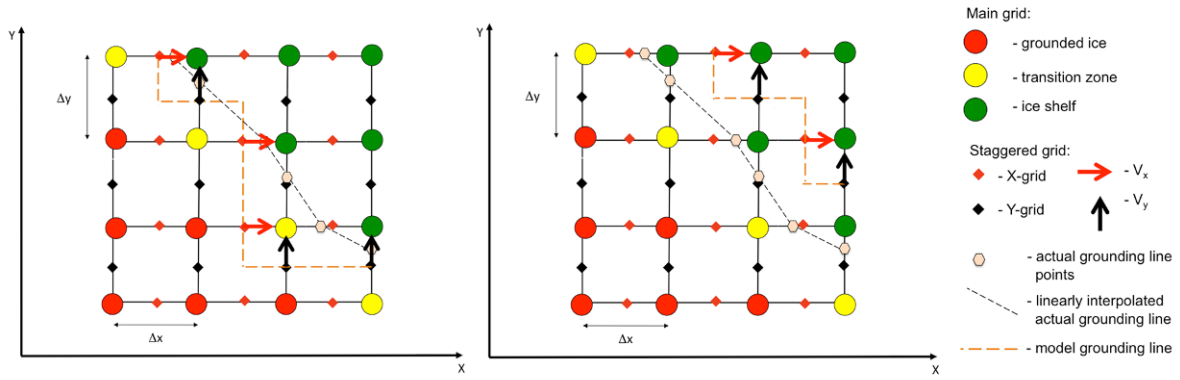

Figure 10: Implementation of the Schoof boundary condition in a 2D ice sheet/ice shelf model. Velocity components in the ice shelf are calculated on a staggered grid. As in the 1D case analytically derived velocities are imposed on the grid point upstream (left panel) or downstream of the actual grounding line (right panel) depending on the value of the analytical mass flux compared to the modelled one.

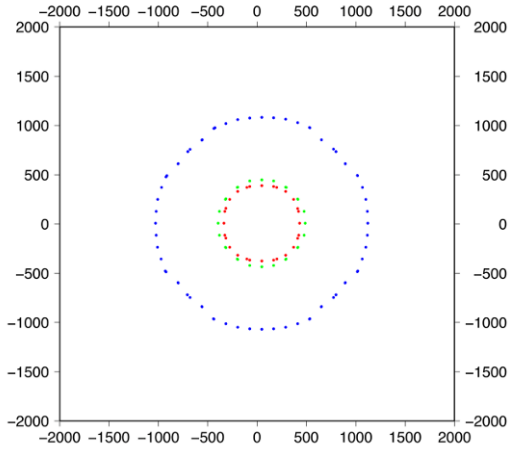

Figure 11: Results of the H-test with the 2D ice sheet/ice shelf model with $\overline{A}=1\times10^{-18}$ yr^{-1} Pa^{-3}, $C=2\times10^{-16}$ N^{-3}y^{-1}m^{7} and a spatial resolution 125 km. Initial positions of the grounding line are shown by red dots (H_{sl}= 0 m), positions at the end of the advance phase (H_{sl}=-125 m) with blue dots, and positions at the end of the retreat phase (H_{sl}= 0 m) with green dots. Apparently at the end of the retreat phase the grounding line migrates again to a position close to the initial one.

Summarizing the results of our tests we can conclude:

- When an internal boundary condition for the ice flux at the grounding line is imposed, 1D and 2D models are able to capture migration of the grounding line. In both the 1D and 2D experiments the perturbed grounding line came back to the unperturbed state to within an accuracy not exceeding ~1.5 times the spatial step. Still we have to point out that there is no general theory to derive the flux across the grounding line for the 2D case.
- The implementation of a boundary condition for the ice flux across the grounding line in a model with fixed mesh increases the computational cost of the model. Strictly speaking the steady state position of the grounding line can never be found on a coarse grid. Computations end in very small oscillations

of the flux at the *modelled* grounding line around the theoretical boundary value. Changing the boundary condition on every time step affects the number of iterations for the solution of the ice flow equation(s) in the ice shelf.

- In the 2D case the ice flux along the grounding line is neglected. Treating the grounding line as a set of perpendicular segments and neglecting gradients of the ice velocity along the grounding line causes perturbations in the migration of the grounding line.
- In the 3D case the problem becomes more complicated because of the effects of temperature change in the vertical. In particular, temperature changes non-linearly with depth, so minor variations cause a significant change of $\overline{A}$ in eq. 3 thus changing boundary conditions for the ice flux and as a result causing the grounding line to move. Another problem is the fast horizontal temperature change across the grounding line. This change adds uncertainty in $\overline{A}$. This uncertainty increases with increasing spatial resolution of the model.

2.1.4. Impact of grounding line evolution

It is generally expected that the amount of basal sliding plays a crucial role in the evolution of the Antarctic ice sheet. In the three-dimensional thermomechanical ice-sheet model (Huybrechts, 2002) basal sliding is restricted to basal areas which are within 1°C of the pressure melting point. Basal sliding is considered to be of Weertman-type, relating basal sliding to basal shear stress to the third power and inversely proportional to the reduced normal load due to the pressure of subglacial water. In a first series of experiments, we tested the influence of the multiplier in the basal sliding law while keeping the value of the exponent unchanged. Changing the basal sliding parameter by an order of magnitude is found to have a critical impact on the simulated evolution over the last 30000 years (Figure 12). Considering a basal sliding parameter 10 times lower than in the reference experiment, all other things being equal, increases overall ice volume by 15% and moreover impedes grounding-line retreat in response to postglacial rising sea levels. The main reason is a steeper and thicker margin, especially in West Antarctica, which directly impacts on the height of buoyancy of the inland ice. Conversely, increasing the basal sliding parameter by a factor of 10 considerably thins the overall ice sheet and results in a smaller grounded ice sheet area. It can be concluded that the strength of basal sliding crucially impacts on the process of grounding-line retreat.

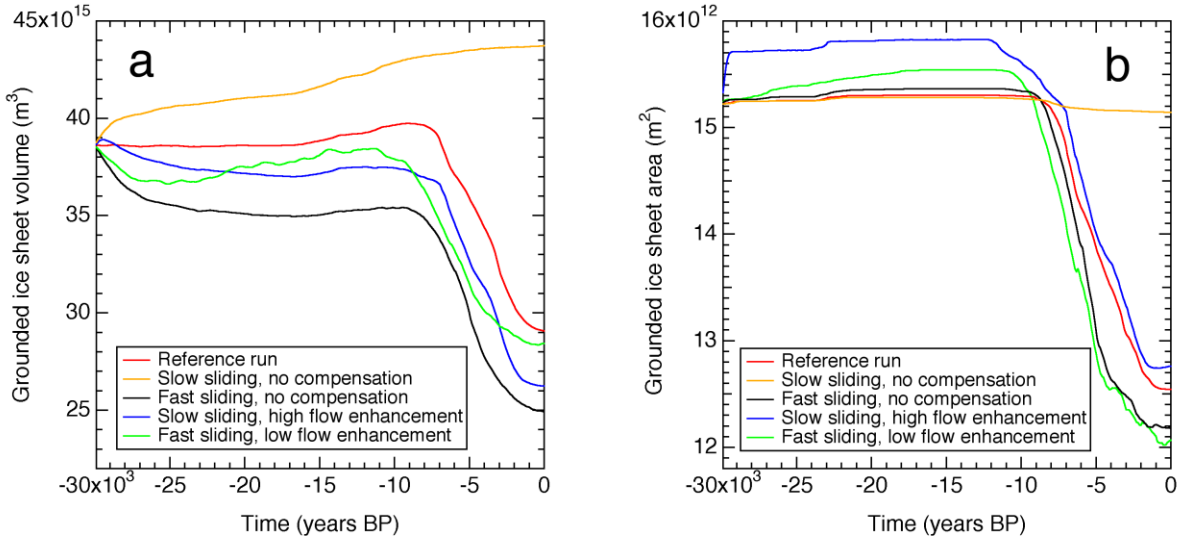

Figure 12: Evolution of the Antarctic ice sheet over the last 30000 years in experiments with varying amounts of basal sliding that is/ or not compensated by commensurate changes in the rate factor for ice deformation. (a) Grounded ice sheet volume; (b) grounded ice sheet area.

To compensate for the overall volume change from changes in basal sliding, one can modify the stiffness of the ice, and hence, the rate factor for ice deformation in Glen's flow law. In the slow sliding case, a five-fold flow enhancement yields a rather similar ice volume and ice sheet area as in the reference run, and again produces grounding-line retreat in West-Antarctica. Fast sliding can be compensated by a flow enhancement with a factor 0.1 (making the ice 10 times harder), again producing a larger overall ice volume. As can be seen on Figure 13, this results in quite different surface geometries. In the fast sliding case one remarks a clear thinning for wet-based parts of the East Antarctic ice sheet and a thickening in those central dome locations frozen to bedrock. The effect is also clearly visible in West Antarctica, where the high-sliding case produces a surface elevation profile closer to observations than in the reference run. It must be noted, however, that owing to the long Antarctic response times, the geometries in these preliminary sensitivity tests have not yet fully adjusted to the parameter changes at 30 kyr BP, and are therefore out of equilibrium not only with the environmental forcing, but also with the internal model physics. We infer from these experiments the need to further investigate the effect of the sliding law exponent and the physical mechanisms controlling the sliding law multiplier, such as basal roughness and basal water depth.

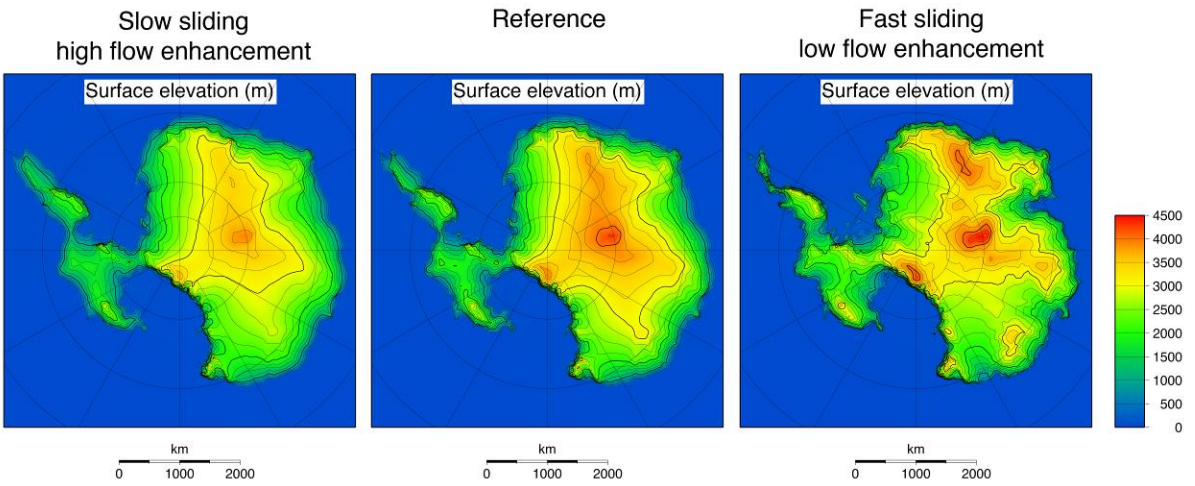

Figure 13: Present-day modelled Antarctic ice sheet geometry in three experiments which varied the basal sliding parameter by an order of magnitude with respect to the reference run (middle panel). At the left is the resulting ice-sheet elevation with a ten-fold reduction of the sliding parameter, compensated by a five-fold increase of the rate factor for ice deformation. At the right is the result of an experiment with a ten-fold increase in the basal sliding parameter together with a ten-fold reduction of the rate factor.

2.2. Marine ice properties and its influence on ice shelf flow

2.2.1. Technological advances

2.2.1.1. Set up and testing of a new pneumatic ice deformation apparatus

To ensure fast and low-cost build-up of the new ice deformation unit to be implemented in the ULB Glaciology Laboratory, we opted for a compression rig operated by pneumatic drives. The design of the whole system has been completed with the advice from engineers from *Festo*, a Belgian company specialized in industrial pneumatic systems. The shell of the rig was built by *Lichtert Industries*, an independent Belgian workshop, and the pneumatic compression system was assembled and embedded in the shell by *Festo*. There has already been several months of delay in the assemblage of the machine due to the novel aspect of the design (in the few other laboratories that use ice deformation rigs the load is usually provided in a direct way, i.e. purely mechanically, i.e. by weights and proper adaptable levers) and also due to security issues (mostly as a result of the high impact potential of the driving units).

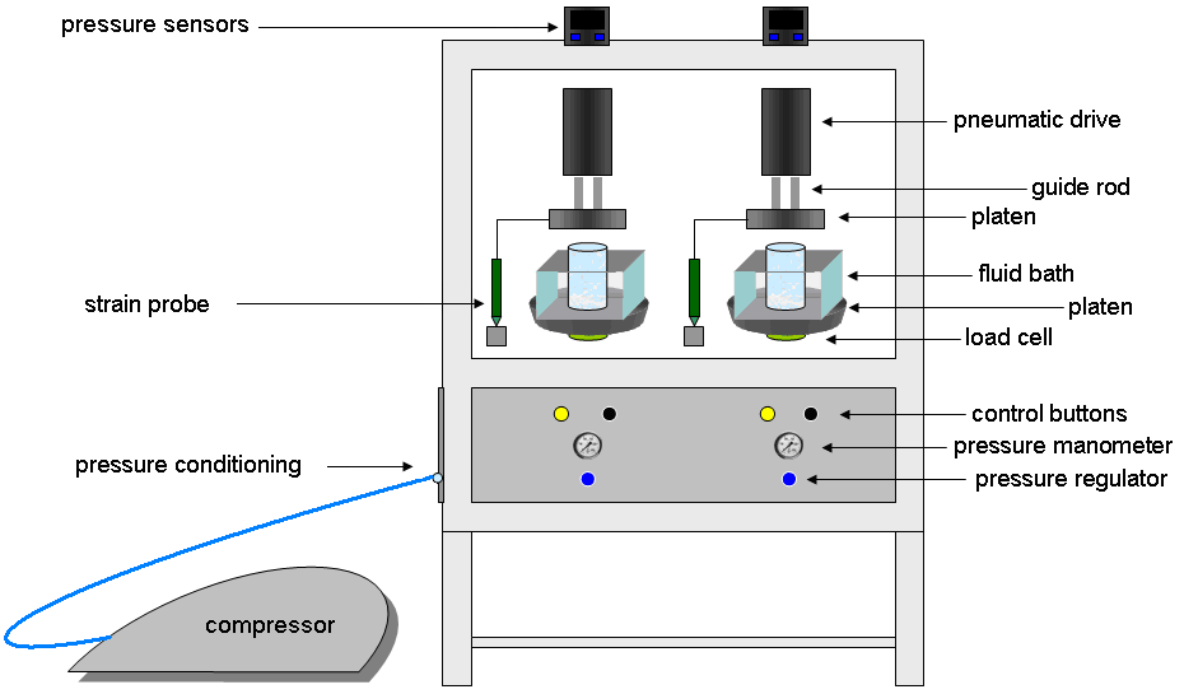

Figure 14 : Diagram of the pneumatic compression rig at the ULB-Glaciology Lab

The compression rig (Figure 14) allows for two independent, simultaneous strain experiments. It has been designed to perform uniaxial compression tests at constant load and under unconfined conditions. It is however pre-equipped for use with rotational shear configuration in the future. Load is provided by pneumatic drives with integrated guide rods. Operating pressure ranges from about 0.5 to 10 bars. The pressure is applied into the pistons' room through a gas supply line. Compensators are placed at the beginning of the feeding line. This circuit is closed so that the compensators regulate the pressure in the circuit itself. The laboratory has installed taps on the line to isolate these two compensators in case of necessity. In addition, pressure sensors have been installed in the piston rooms to measure the gas pressure continuously. Currently, the system is actuated by an air compressor; which applies a constant pressure in the room of the rig.

Initially, the deformation rig has been set up in a cold room in order to optimally regulate the experimental conditions. It turned out that the low operating temperature was actually hindering the movements of the rigs pistons. This resulted in jumps in the strain curves that were recorded under a given constant applied stress. Two different kinds of jumps were indentified: those due to the defrost cycles of the cold room (black circles) and those associated with too high friction forces in the rigs pistons' jackets (black arrows), as shown in Figure 15.

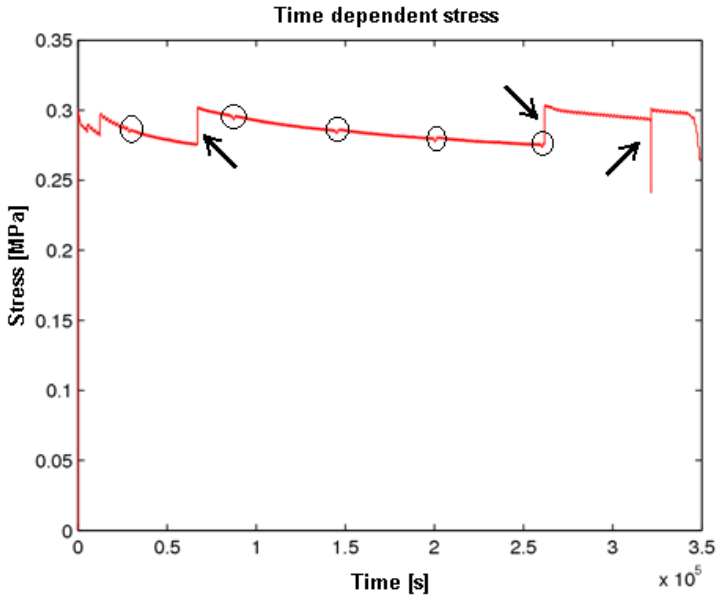

Figure 15: Stress curve recorded for a sample of artificial ice with the deformation rig operated in the cold room. The observed jumps are artefacts resulting from too high a friction on the pistons' jackets (black arrows) and from the defrost cycle of the cold room (black circles).

The deformation rig was therefore taken out of the cold room, set up at ambient temperature and isolated to minimize temperature and humidity fluctuations in the surrounding air. To maintain the ice at low and constant temperature, the samples are immersed in a liquid bath connected to an external refrigeration system. Silicone oil of low viscosity and low volatility is used as a cooling liquid in the bath, which has the advantage to protect the ice from ablation, to be highly stable at experimental conditions and to help keeping the ice temperature constant, a drastic pre-requisite for good quality data. During the experiments, the vertical movement of the piston is measured by displacement sensors. These sensors are linked to the top arm of the press by metal rods. They are inserted at an angle of 45°. The applied force is measured by force sensors located below the sample stage.

The press is currently equipped with three displacement sensors, one with a displacement range of 2mm (uncertainty of 0.1% of its travel, i.e. 0.002mm) and two with a range of 5mm (uncertainty of about 0.2%, i.e.0.005mm). The force sensors are below the sample stage and are all identical. Their uncertainty is approximately 0.1N. All these sensors are connected to a common data logger and a computer set up as a fast rate digital acquisition system. Ice deformation is indeed measured by displacement sensors with digital signal output. Several digital probes can be used together in any combination by means of a network system connected to a PC via USB. Compression load is monitored by analogue load cells that are connected to the digital network through analogue input modules. Precision temperature probes are similarly connected to the network. Readings from the various sensors have been designed to be acquired directly into an Excel™ spreadsheet, which conveniently prevents the use of specialized and expensive data acquisition software. The digital network allows monitoring an experiment in process from remote places, a feature which may be convenient as strain experiments may last up to several weeks or months. This original digital network represents another novel step in the field of ice deformation.

Calibration

As in any other system, the deformation rig introduces a certain intrinsic distortion behaviour which is due to its imperfection, and some external parameters. In our case, there is for example the deformation of the displacement sensor and/or of the piston itself. To quantify this in a comprehensive manner and thereby calibrate the press, a test on a steel cylinder has been performed. Deformations obtained by this test are the addition of two parts: the deformation of the engine, always present, and the deformation of the steel cylinder. From that, it is possible to evaluate the intrinsic error due to the machine itself.

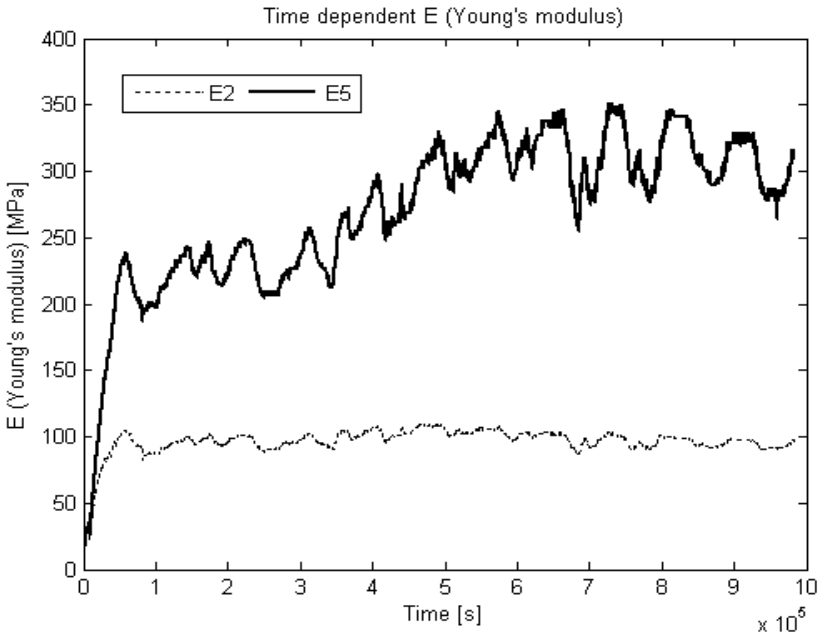

Figure 16: Time dependent calculated Young modulus E during the strain experiment on a steel cylinder. A time average is performed to calculate the value of E for each sensor.

The approach used is to hypothesize that the piston has an elastic behaviour, which is a good approximation as the system is composed of aluminium and steel. According to Hook's law ($\varepsilon = \sigma / E$), when we know the Young's modulus (E, MPa) and the applied stress σ, it is easy to determine the strain ε due to the metal. σ and ε were measured during the experiment and a time variable E was deduced, as shown in Figure 16. This value was then time averaged to determine the Young module for each sensor. Mean values of 97MPa and 270MPa are found for the sensors of 2mm and 5mm respectively. In future experimental protocols, the errors originating from the press will now on be subtracted from the values obtained by the data acquisition system.

This test can also be used to determine the intrinsic uncertainty of the machine. At very low pressures (about 0.5 bars), the error on the force sensor of the piston reaches 20%. In fact in this pressure range the friction forces along the piston rods are of the same order of magnitude as the pressure induced forces applied on the sample. To solve this problem, one must either increase the working pressure, or change the geometry of the piston chamber. As a first step, we have chosen to work at high pressure. In the future, we plan to convert the piston chamber to work with lower stress and get closer to the best natural conditions, *i.e.* closer to atmospheric

pressure. At a working pressure of 3.5 Bars, the error reduces to 3.5%. Note that these remaining errors are also partly due to the compensator that feeds continually the chamber of the piston with gas to counterbalance the loss of pressure in the pressure gauges (loss which allows greater accuracy in the pressure in the room).

Segmentation error

During the first tests on ice, we were able to determine the value of the error on the applied force on the ice. At first glance, this error is about 6 to 7% for a pressure close to 3.5 bars. Note that the error is larger for ice than for steel because of its higher deformability. Steel is stiffer than ice: it deforms slower and the piston remains more stable.

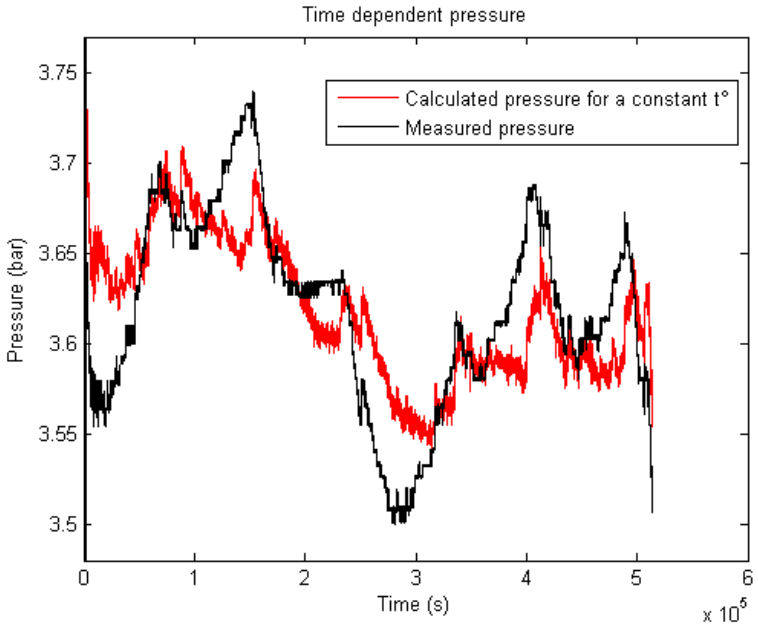

Figure 17: Applied pressure during a stress experiment on natural ice. The red curve is the calculated pressure for a constant temperature in the experimental room.

It was found that there was an inverse linear relation between measured pressure and measured ambient temperature. Using this relation, we determined a calculated pressure for a constant temperature in the room, as shown in Figure 17 (red curve). After analysis, it was found that over 30% of this error is due to the change in temperature in the room (which is independent of any temperature change in the cryostat, in which the sample is immersed). It is therefore essential to control ambient air to minimize maximum deviations of the temperature. Works is currently underway to address this issue (use of a dedicated air conditioned laboratory).

Artificial ice

For the first ice test, we attempted to create artificial ice to avoid wasting natural ice samples. As a first step, tests were simply made on frozen tap water. The strain evolution did not show very satisfactory results since all the impurities present in water (including limestone) prevented grains moving as they should have. Too high stresses were necessary to obtain the desired strain, probably because of the large crystal sizes. Although these tests are still not perfect model system of ice deformation, they however proved that the system works. For a stress of 13 bars at -

4°C, we obtained a vertical deformation of the ice cylinder of more than 3% in less than 24 hours. From the strain as a function of time, it was possible to determine the strain rate and trace the curve of strain rate versus total strain, a diagram commonly used to characterize the various steps of the deformation process (Figure 18).

From this curve, it is possible to determine the viscosity of ice, but as stated above, this ice being formed simply from tap water; impurities and limestone are influencing this value. Moreover, since it is close to a single crystal of ice, the viscosity obtained was higher than the viscosity of natural ice (factor of order 10).

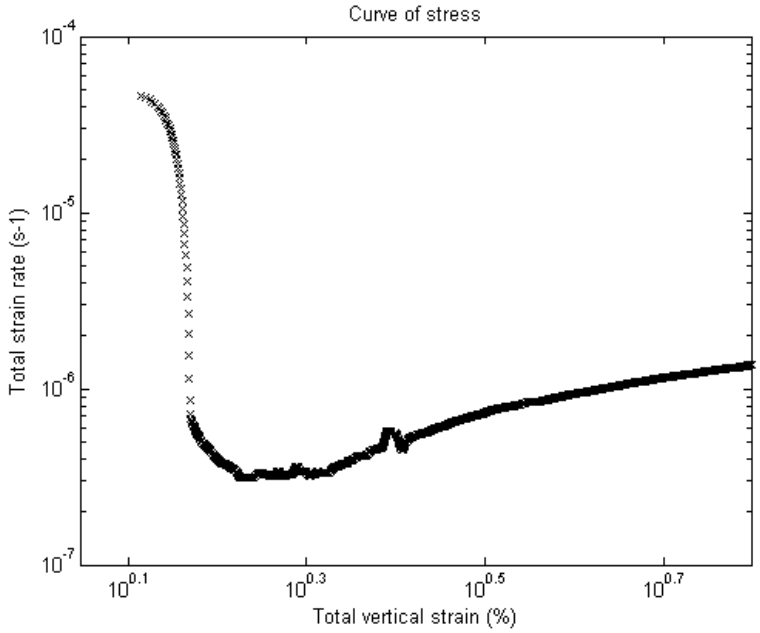

Figure 18: Strain rate as a function strain curve during a strain experiment of an artificial ice cylinder.

Subsequently, following the procedure of Jacka et al. (1984), we made several attempts to produce artificial granular ice without impurities. The results were however not yet satisfactory. Several steps of the protocol are still under study , such as the time of freezing after compression, the amount of water at 0°C to accept in the mix pre-consolidation, the obligation to store (or no)t the ice before the deformation, etc. The objective here is to produce artificial ice with a relatively predictable ice texture (grain size) and ice chemistry, to constrain the individual effect of each of these variables on the ice viscosity deduced from the deformation experiments.

Natural ice

The samples chosen for this analysis come from the alpine Glacier de Tsanfleuron (Switzerland) and were retrieved in October 2007. The first sample was collected from the accumulation zone of the glacier. Using Timco et al. (1996) to determine its density, we found that the sample is at the limit of ice and firn. The density (870.1 ± 8.2 kg/m³) indicates that this sample is in the fourth phase of the transformation of ice, which means that the ice incorporates a lot of bubbles as enclose sealed air pockets.

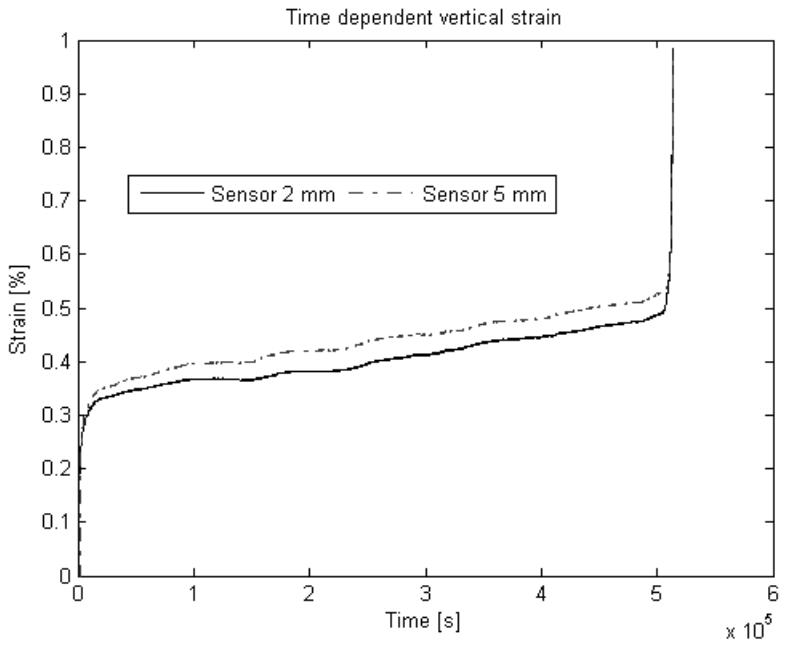

Figure 19: Strain curve recorded on natural ice. The discrepancy between the readings of the two sensors comes from the fact that they are not exactly parallel one with each other.

After 6 days of compression in constant stress at 3.6 bar (±0.12) and -10°C, we reached 1% of vertical strain. In Figure 19 we can see that the end of secondary creep (secondary creep = a plateau in the strain curve; since the deformation takes place at nearly constant and minimal rate) is characterized by a fairly significant acceleration of the deformation. We also note that the end of secondary creep occurs at around 0.5% deformation.

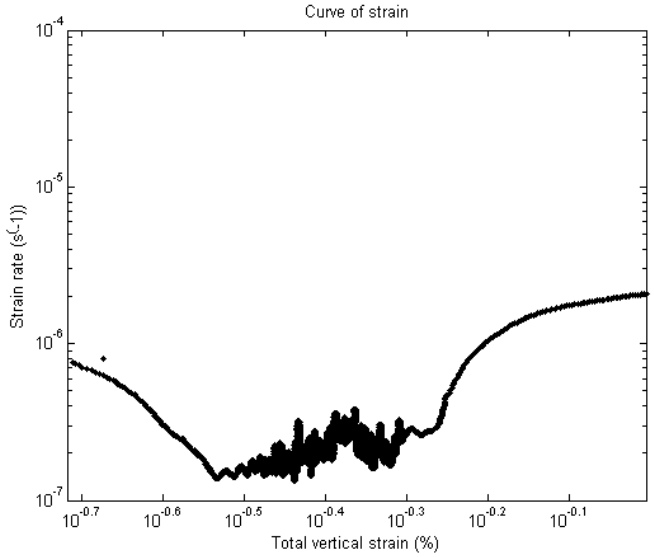

Figure 20: Strain rate curve obtained from the strain curve shown in Figure19.

We can then draw the strain rate vs. total strain curve (Figure 20) for this deformation experiment, which allows us to determine the viscosity. According to Glen's law:

$$\dot{\varepsilon} = A\,\tau^{n} \qquad (6)$$

We obtain for the fluidity A a value of $7.394.10^{-17}$ [$s^{-1}(kPa)^{-3}$] around -10 ° C, for this alpine ice containing a lot of bubbles. This is by a factor of 5 to 10 higher than the range of values given by Paterson (1994) for natural ice at the same temperature, but we have to remember that our sample is still at the end of the firnification process.

2.2.1.2. Set up of an Automated Ice Fabric Analyzer (AIFA)

An Automated Ice Fabric Analyzer makes it possible to study ice textures and fabrics from the whole polycrystal to the sub-millimetric scale in a fully automatic way. It is therefore theoretically much more reliable, has a much higher resolution (pixel information) allowing the study of internal deformation structures of a single crystal and considerably less time consuming and more comfortable to use than the traditional manual c-axes determination procedure (Langway, 1958). Such a device, hereafter G50, has been delivered by the Australian designer D. Russell-Head (DRH) in May 2007. Although it has been around for nearly two decades, this type of equipment is still in a prototype phase.

The ULB G50 works with two types of experimental settings: one with a reduction tube, providing relatively fast scanning of the thin section at a large angle of view, and another (without the reduction tube) providing slower scanning but at finer resolution. This device is also suitable for studying other uniaxial materials like quartz or apatite.

The analyzer is made of 4 different parts, from bottom to top:

a) The light source and polarization system: it is located in the lower part of the hardware casing and made of two polarizing filters, a set of 8 white LEDs positioned symmetrically in a circle at equal inter-distances and at a given angle on the vertical, a set of RGB LEDs positioned on a vertical axis. A 2cm diameter glass plate allows the light to enter the ice thin section above
b) A mobile stand 100x100mm, on which the thin section is laid. In order to cover all the thin section area, the stand is piloted by a pulley system driven by two electrical motors controlled by a computer via USB connection
c) The optical system is made of:
    1. Objective lens Nikon 50 mm f1.2
    2. Imaging lens Nikon 85 f2
    3. Reduction tube: it consists of a reduction lens and a « flat image » in fibreglass. The role of the latter is to capture the oblique light rays from the imaging lens below and redirect those vertically before getting into the reduction lens
d) The sensor which transfers the images to the computer via a firewire connection

The software of the G50 instrument fully automates the analysis, thanks to a set of algorithms simultaneously controlling the polarizers' rotation, the move of the mobile stand, the image acquisition and the record of pixels orientation values. At the end of the procedure (about one hour) the software generates a suite of colour coded images corresponding to the various orientation angles of the polarizers. Each image is in fact a tile of several photographs (10x10mm). A raw data file is also generated with the pixels orientation values.

We use the Matlab software "Texture Toolbox" developed by G. Durand and co-workers (LGGE-Grenoble). It allows extracting the plot of the individual c-axes and a suite of statistical treatment (e.g. eigenvectors, density plots, concentration indices...) from the raw data files. The Texture ToolBox and its users' guide are available at http://www-lgge.obs.ujf-grenoble.fr/~durand/toolbox_micro/micro_main.html.

2.2.2. Analytical and experimental work

2.2.2.1. Marine ice and "ice mélange" properties

Specific ice shelf deformation processes at ice streams boundaries (Nansen Ice Shelf, Terra Nova Bay)

Ice textures and fabrics from the Nansen Ice Shelf (74°51'32"S; 162°41'17"E), initially described by Khazendar et al. (2001), have been resampled locally to study strong deformation features with the help of the Danish Automatic Ice Fabric Analyzer (Figure 21). As depth increases, the crystal texture gets less homogeneous, while the crystal mean equivalent diameter, the concentration index and the first eigenvector value all slightly increase. Clear folding structures concurrently develop within the marine ice. Considerations from the local ice shelf geometry setting, the c-axes orientation and the crystal elongation clearly indicate the development of longitudinal compressional folding, an unusual situation for ice shelves where only vertical compression is usually considered. This, together with the development of well oriented fabrics, suggests a totally different stress/strain anisotropy that has never been considered before in ice shelf modelling. It underlines the potential necessity for considering longitudinal stresses in future ice shelf modelling efforts too. It also suggests that future deformation tests should also look at sideways compressive stress, especially since the c-axes distribution is highly anisotropic and susceptible to react differentially to the orientation of the applied stress field.

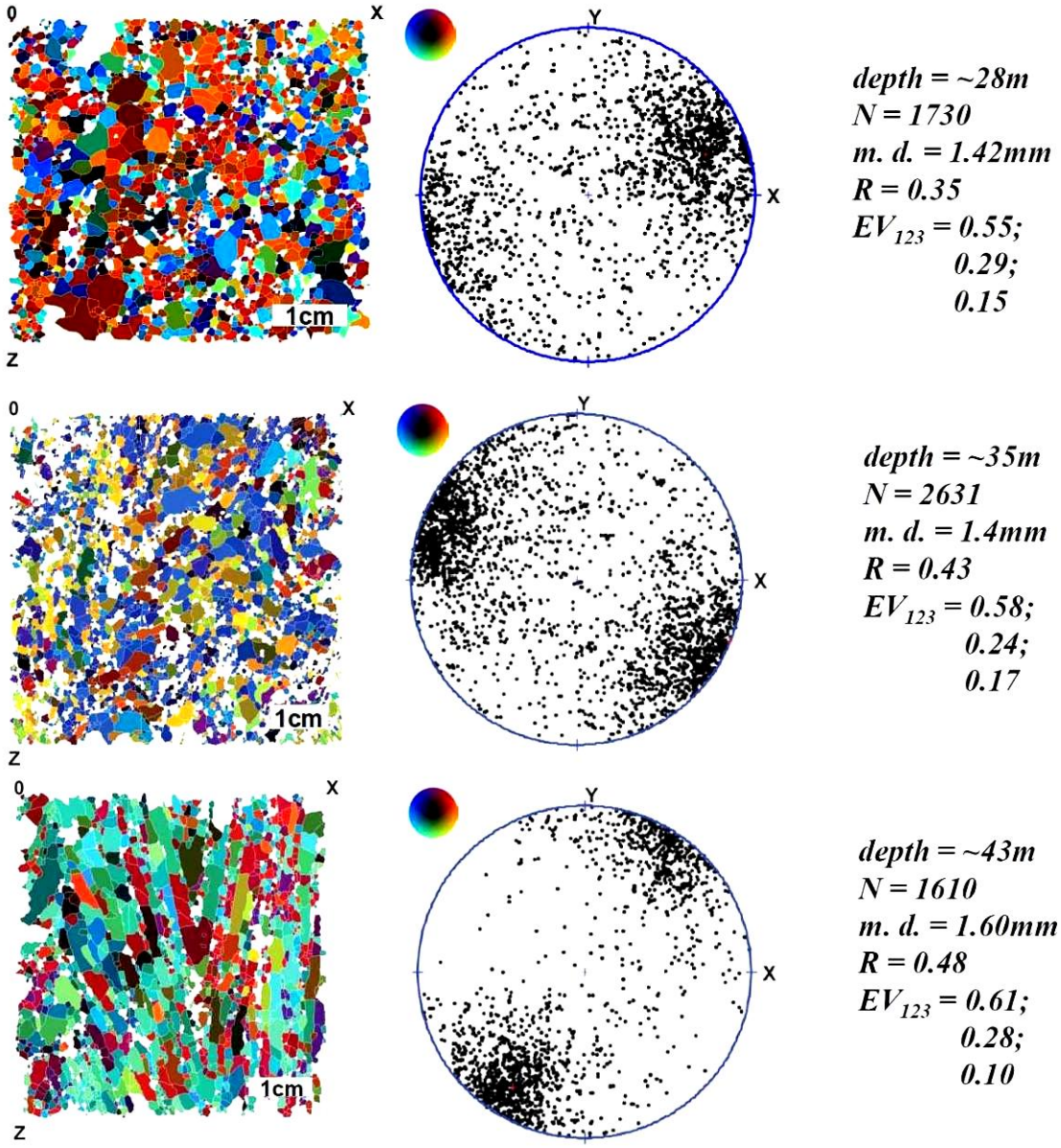

Figure 21 : Textural and structural characteristics of three samples located at increasing depth along the NIS1 marine ice core (Nansen Ice Shelf, Terra Nova Bay, Antarctica). The polarized thin sections (left) are shown in the vertical (x-z) plane and the c-axes distribution in the horizontal plane (x-y). It is not possible to reconcile the azimuthal angle between the three samples. Color codes are from the Textural toolbox and associated to the position on the lower hemisphere of the Schmidt equal area projection (see color scale in caption circle). N is the number of crystals measured; m.d. the mean diameter; R the degree of c-axes concentration, EV_{123} the three Eigen-vectors. See text for details.

"Ice mélange" properties in frontal rifts at Brunt Ice Shelf (Antarctic Peninsula)

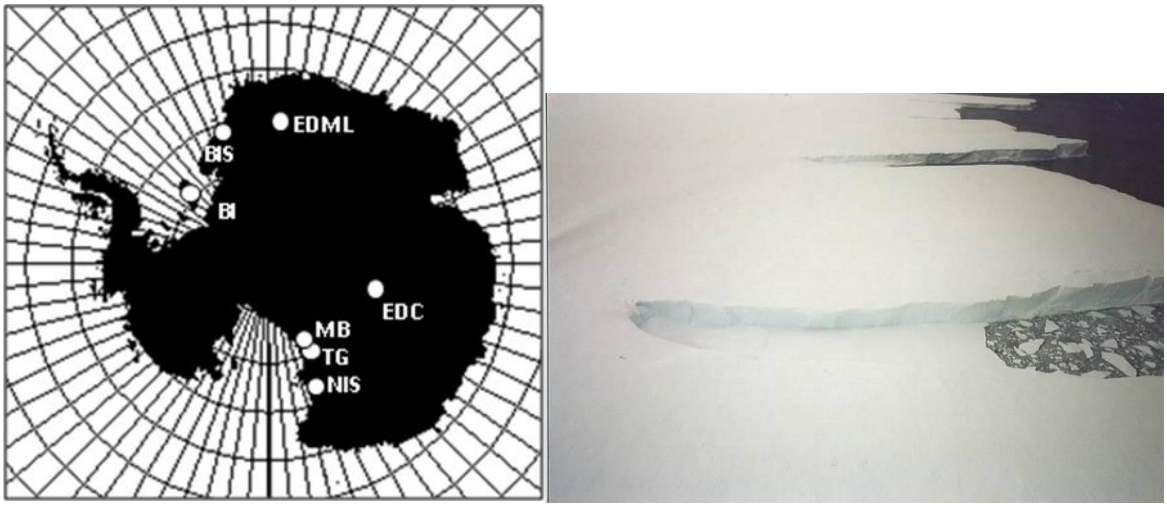

Figure 22 : (left) Location of sampling sites in Antarctica : NIS : Nansen Ice Shelf, BIS : Brunt Ice Shelf, BI: Berkner Island, MB : Minna Bluff, TG : Taylor Glacier ; EDC: EPICA Dome C, EDML: EPICA Dronning Maud Land; (right) Aerial photograph of the samples rift at the front of the Brunt Ice Shelf (BIS)

During the 2004-2005 Antarctic summer cruise of the RV Bransfield (British Antarctic Survey – Dr. A. Jenkins/ A. Khazendar, UK), we had the opportunity to sample the "ice mélange" forming in marginal rifts at the front of the Brunt Ice Shelf (Figure 22 - 75°00'S, 25°00 W). The drill site was located partly on a snow ramp connecting the bottom of the rift to the ice shelf front. A 22 meters core has then been collected. It consisted of an upper firn section of about 12 meters thickness, underlain by 10m of solid ice.

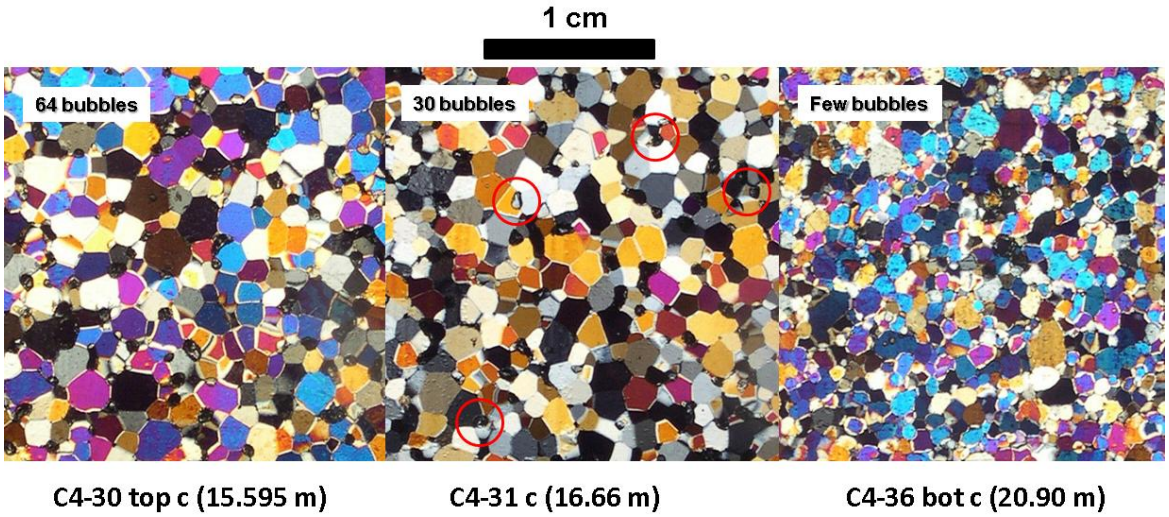

Figure 23: Some textural properties along the Brunt Ice Shelf ice core. Red circle indicate suspected bubble fill-in with new crystals. See text for details.

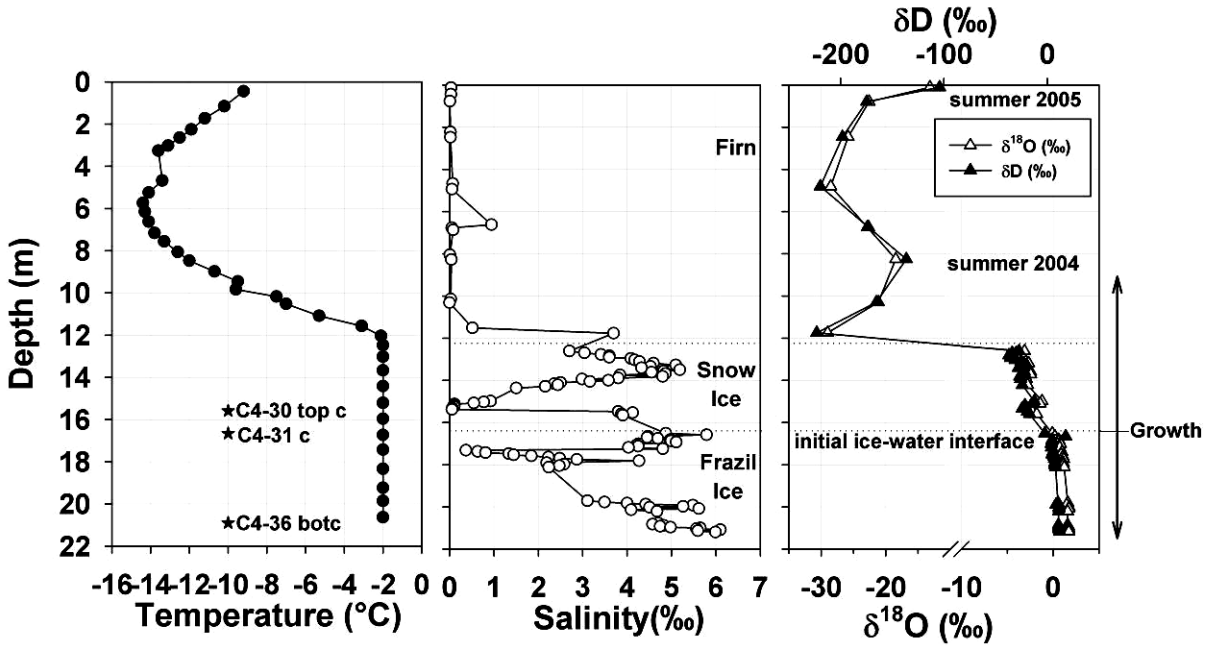

Figure 24: Temperature, Bulk salinity, $\delta^{18}O$ and δD profiles in the Brunt Ice Shelf ice core.

Thin sections have been prepared along the whole 22 meters of the ice core. A few samples are shown in Figure 23. Figure 24 shows the profiles of Temperature (±0.1°C, measured "in situ" inserting a thermistor probe within the ice core immediately after retrieval), bulk salinity (±0.1‰, measured with a conductivity meter calibrated with standard sea water), $\delta^{18}O$ (±0.05‰) and δD (±0.5‰) for the same core.

The whole core is 100% made of granular ice, with relatively homogeneous grain size (few millimetres), and a slightly lower mean grain size in the lower section. In the upper part, crystals are clearly polygonal in shape while they are more rounded in the lower section. Also, the number of bubble inclusions clearly decreases with depth (see Figure 23). The profiles of Figure 24 support a two to three layers structure. Below the 8-10 meters where seasonal fluctuations are expected to be seen, the temperature steadily goes down to the sea water melting point (-1.9°C), where it stabilizes in the lower sections (below 12 meters depth), clearly showing interaction with sea water in a recently accreted bottom layer. Bulk salinity shows the same strong contrast between the upper part with negligible values and the lower section (below 12 meters) where the salinity strongly fluctuates between 0 and more than 6 ‰. The stable isotopes profiles and the co-isotopic plot of Figure 25, allow us to refine the interpretation, defining three different units: the top part (0-12 meters) shows very negative values, which is to be expected for firn (meteoric ice). Interestingly, a cyclic variation between roughly -13‰ and -30‰ in $\delta^{18}O$ is seen, which suggest that the snow-firn cover of the access ramp as only been around for two winters (-30‰) and two summers (-20 to -13 ‰). A second section (from roughly 12 to 17 meters) shows all the characteristics of what is known as "snow ice" in the sea ice world, i.e. the lower part of the snow cover sinking into sea water under its own weight and therefore showing layers of high salinity, and an isotopic signal which is intermediate between pure meteoric ice and refrozen sea water. Note that, in this section, the isotopic signal steadily increases with depth, while the bulk salinity does the reverse and goes down to negligible values again. Finally, the bottom 2.5 meter

section is characterized by positive isotopic values, typical of pure sea water freezing, with only a slight increase downwards. Here salinity steadily increases again, up to values higher than 6 ‰. The co-isotopic diagram of Figure 25 nicely illustrates this gradual mixing between a meteoric end term and a pure refrozen sea water end term.

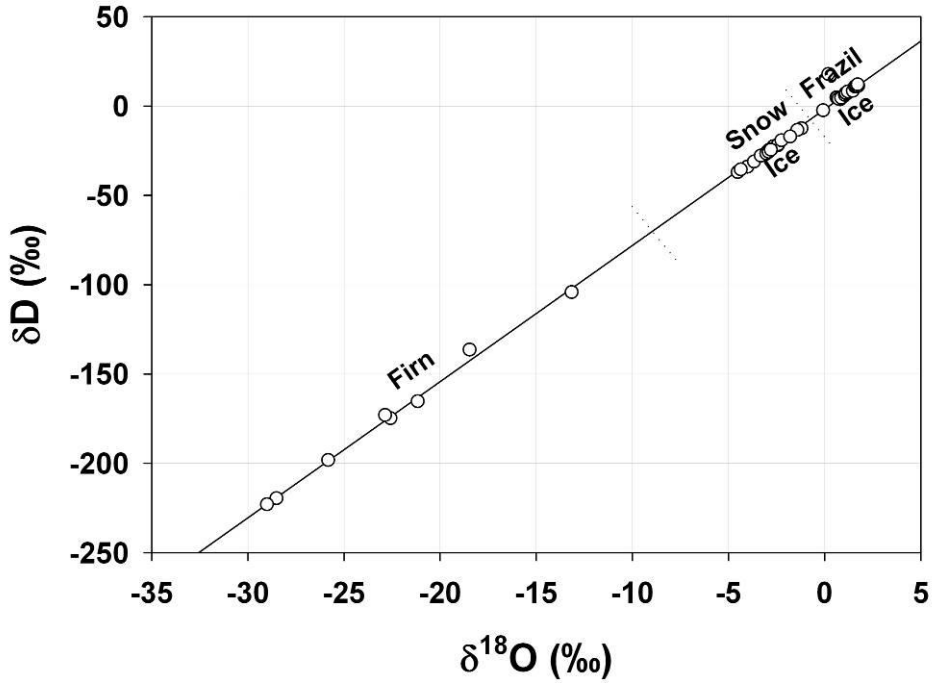

Figure 25: Co-isotopic characteristics of the “ice mélange” in the Brunt ice core.

These observations allow us to propose a growth scenario for the “ice mélange” within the marginal rifts of the Brunt ice shelf. The three main sections recognized represent respectively, from top to bottom: firn, snow ice and frazil sea ice or marine ice accreting at the front of the ice shelf. The initial air-water/ice interface has to be located at the limit between snow ice and frazil ice, i.e. at about 16.2 meters depth (Figure 24). The ice cover must have been initiated as a surface frazil ice layer, probably partly mixed with blown snow inputs from the ice shelf front. The ice sheet has then grown both upwards as “snow ice” and firn and downwards as frazil sea ice or marine ice. It is difficult to decide if this bottom section is sea ice (grown at the ice ocean interface) or marine ice (grown in the water column and then accreted at the bottom of an existing ice sheet). Typical bulk salinities for marine ice accreted under ice shelves are usually reported within the 0.03 to 0.3 ‰ range (e.g. Tison et al. 1993, Khazendar et al., 2001, Tison et al., 2001, Moore et al., 1994, Tison, 2002). However, when it accretes under the landfast sea ice fringing ice shelf fronts, where consolidation rates are much faster, marine ice can show bulk salinity ranges similar to those of sea ice (Tison et al., 1998, Tison et al. 2002). It is interesting, in this regard, to compare the behaviour of the stable isotopes and bulk salinity profiles in the two lower sections. In both cases, salinity fluctuations are much larger than isotopic fluctuations. This is because changes in the salinity signal are mainly associated to changes within the intergranular liquid layer (brines), while most of the isotopic signal is stored within the ice crystals (Tison et al. 2001, Tison, 2002). Interestingly enough the bulk salinity-stable isotopes relationship globally goes opposite ways in snow ice (section 2) and in sea/marine ice (section 3) giving us some hints on the consolidation process. In snow ice the salinity strongly decreases

with depth, while the stable isotopes steadily increase. This is what should be expected if the signals reflect the impact of the freezing rate on both signals: as the freezing rate of the interstitial sea water having initially invaded the snow decreases, salts are more efficiently rejected from the ice and heavy isotopes preferentially incorporated into the newly formed interstitial ice. Moreover, brine desalinization processes will help lowering the salinity signal, until we reach the lower boundary at the snow ice-frazil ice interface, where salinity increases again.

In the lower section, salinity decreases first for about a meter, which again would be expected for the effect of a decreasing freezing rate during consolidation of the initial frazil ice cover, but then the salinity globally increases again for the last three meters, while the stable isotopes only slightly increasing. This is unexpected for sea ice, where the so called “C-shaped” profile (e.g. Weeks and Ackley, 1986, Eicken, 1992, Eicken, 1998) only shows a potential increase of salinity in the bottommost skeletal layer (10-15 cm). Note also that an accumulation of more than 3 meters of frazil sea ice is rather unusual and probably restricted to deformed ice on the outer rim of large scale polynyas, and not in sheltered rifts. We therefore favour a marine ice origin for this lower section of the Brunt ice core. In that case, the steady increase of both the salinity and the stable isotopes could reflect a compaction process of the loose frazil as a result of the increasing buoyancy force, due to the large accumulation of frazil ice crystal sedimenting upwards from the water column (Eicken et al., 1994). Note that this process could well be intermittent, as suggested by the few excursions of the salinity profile towards higher salinities. The Brunt ice shelf ice core certainly provides us with an ideal source of material to test the specific rheological properties of the “ice mélange”, and this is ongoing work downstream of this project.

Marine ice formation at the lateral margin of McMurdo Ice Shelf (Minna Bluff, Antarctica) and interactions with moraine deposits

Preliminary co-isotopic (δD-δ^{18}O) results have been obtained from various sampling sites at Minna Bluff (McMurdo Ice Shelf, Antarctica, Figure 22), in collaboration with Prof. S. Fitzsimmons (University of Dunedin, New Zealand). Samples from firn, marine ice, debris-rich ice and melt ponds were pre-processed at Scott Base facility, on return from the field, and were analysed at University of Alberta, Canada, by Prof. M. Sharp. On a co-isotopic diagram, all samples (N=38) align with a good fit (>0.994) on a slope of 8.41, which is compatible with a “Local Meteoric Slope”, although this could also potentially reflect some mixing processes (Figure 26). Indeed, end members on this slope are the firn samples (most depleted in heavy isotopes) and the marine ice samples (forming a cluster of positive values, a few per mil above SMOW composition). The composition of debris-rich ice samples, which were retrieved at the contact between the ice shelf and shore moraines, is trending toward that of marine ice, whereas the composition of the melt ponds is scattered between the firn and the debris-laden samples. This setting reflects some recycling between the various reservoirs on site. Mixing ratio calculations between firn and marine ice suggest a contribution of firn to~70% of the melt ponds composition. A preliminary interpretative scenario would be that meltwater from hanging glaciers at Minna Bluff produces melt ponds in topographic depressions which can eventually drain to the shore vicinity. Transgression phases of the ice shelf would then allow forming push-up moraines on shore, thereby mixing debris-rich ice from the base of the ice shelf, of partially marine ice origin, with local melt ponds. This scenario is supported by marine organism

skeletons found within debris-rich ice, shore moraines and melt ponds. Deformation studies on these marine ice samples, with a potentially large range of debris content and salinities, will provide us with another ideal tool to study the control of solid and dissolved inclusions in marine ice on its rheological properties.

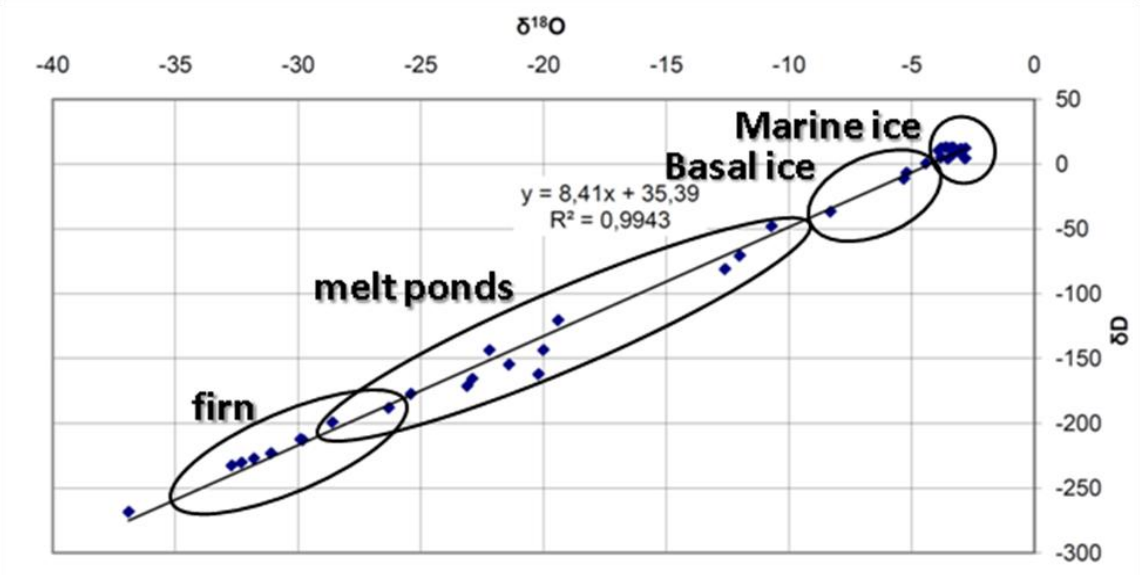

Figure 26: co-isotopic properties of various ice types at the Minna Bluff sampling site. See text for details.

2.2.2.2. Deformation experiments on marine ice from the Nansen Ice Shelf

Three creep experiments have been performed on marine ice samples retrieved from the Nansen Ice Shelf (Terra Nova Bay, Antarctica - Khazendar, 2000; Khazendar et al., 2001; Tison et al., 2001). These experiments have been conducted on a mechanical deformation rig in the cold rooms of the LGGE (Grenoble - France) in the framework of our collaboration with P. Duval and M. Montagnat., following the procedure described in the related literature (e.g. Duval, 1976).

Sample Code	Salinity (‰)	$\delta^{18}O$	Depth (m)	Mean crystal size (cm)
NIS2-112b	0.043	2.0 ± 0.2	43.30	0.15
NIS1-59a firn	0.095	2.0 ± 0.2	22.00	0.14
NIS2-72c	0.038	2.0 ± 0.2	27.80	0.25

Table I: physico-chemical properties of the deformed samples

Table I shows the main physico-chemical characteristics of the samples selected. Salinity and isotopic values are typical of marine ice and all samples are devoid of bubbles. However, although we aimed at samples as homogeneous as possible, salinity and mean crystal size varied by a factor of 2. Fabrics (c-axes) and crystals shapes were also selected to be as isotropic as possible, although, as shown on Figure 21 (top), this eventually appeared not to be the case, even when no apparent fold structure was seen within the samples.

The three samples were deformed under unconfined vertical compression along the axis of the core, i.e. in conformity with the usual stress field in an ice shelf, away from the margins. Table 2 summarizes the parameters of the creep experiments and Figure 27 shows an example of acquisition curve.

# sample	Time (days)	Applied normal stress (Mpa)	Octahedral shear stress (Mpa)	Temperature (°C)	$\dot{\varepsilon}_{min}$ (s^{-1})
NIS2-112b	2	0.2	0.094	-10.8 ± 0.1	Not reached
NIS2-112b	13	0.5	0.236	-10.8 ± 0.1	2.4 E-9
NIS1-59a	16	0.5	0.236	-10.8 ± 0.1	1.6 E-9
NIS1-59a	3	0.7	0.330	-10.8 ± 0.1	3.4 E-9
NIS2-72c	9	0.5	0.236	-10.8 ± 0.1	3.3 E-9
NIS2-72c	3	0.7	0.330	-10.8 ± 0.1	1.0 E-8
NIS2-72c	1	0.9	0.424	-10.8 ± 0.1	3.08 E-8

Table II: creep experiments parameters (ε min = Minimal strain rate)

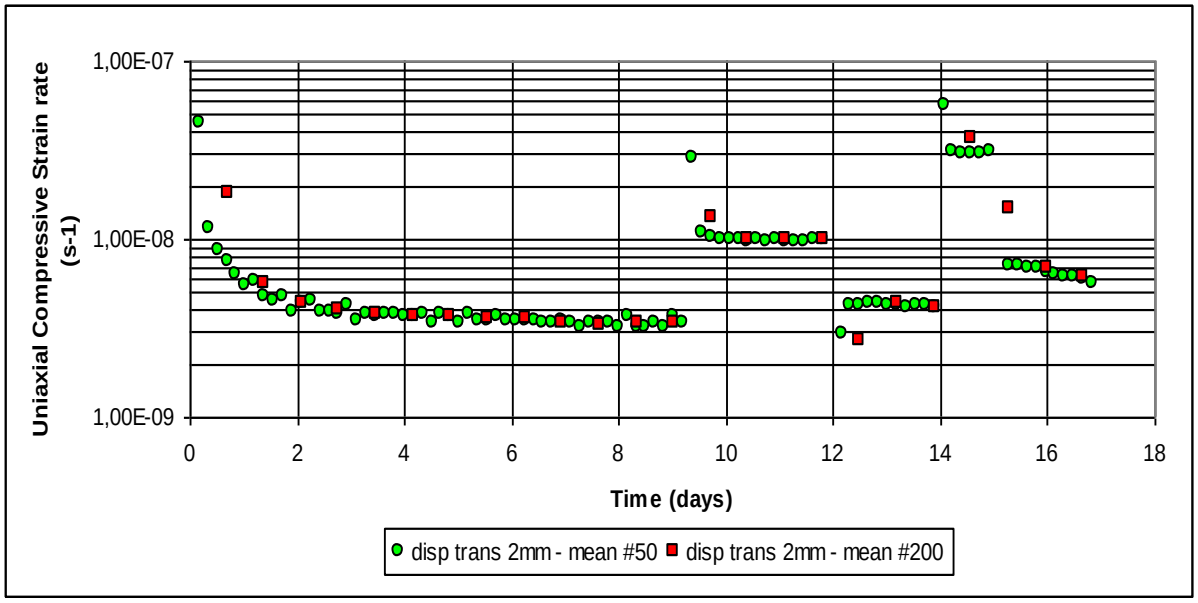

Figure 27: Example of acquisition curve for the deformation of a marine ice sample (NIS2 72c). The raw displacement measurements have been converted into an uniaxial compressive strain rate and plotted against time. The driving stress has been increased twice in the course of this experiment. “disp trans 2mm” stands for “displacement transducer with a course of 2 millimetre”. Green dots correspond to means calculated with integration values of 50. Red dots correspond to means calculated with integration values of 200.

The samples were strained at a temperature set to -10.8 °C, for periods of two to three weeks. Usually an initial stress of 0.5 MPa (5 bars, corresponding to an octahedral shear stress of 2.36 bars) has been applied, to the exception of the first sample (NIS2-112b) whose initial stress was 0.2 MPa for two days, after which the stress was increased to 0.5 MPa (experimental time constrain). Minimal strain rate values (s^{-1}) for a stress of 0.5 MPa (5 bars) were ranging between 1.6 10^{-9} and 3.3 10^{-9}. During the deformation of samples NIS1-59a and NIS2-72c, extra loads of 0.7 and 0.9 MPa (7 to 9 bars) have been applied (Table II). This allowed a preliminary assessment of the Glen’s law exponent.

At any stress, we obtained minimum strain rates two to four times lower than those reported for isotropic ice strained under similar conditions (Jacka, 1984). Extra load experiments allowed to assess Glen's flow exponent, which varied between 2.2 (lower stress) and 3.8 (higher stress) (Figures 27 and 28). The most important conclusion at this stage of the work is that, at conditions given here, marine ice from NIS deforms significantly slower than isotropic ice under pure shear deformation, emphasizing thereby the potential stabilizing effect of marine ice on continental flow.

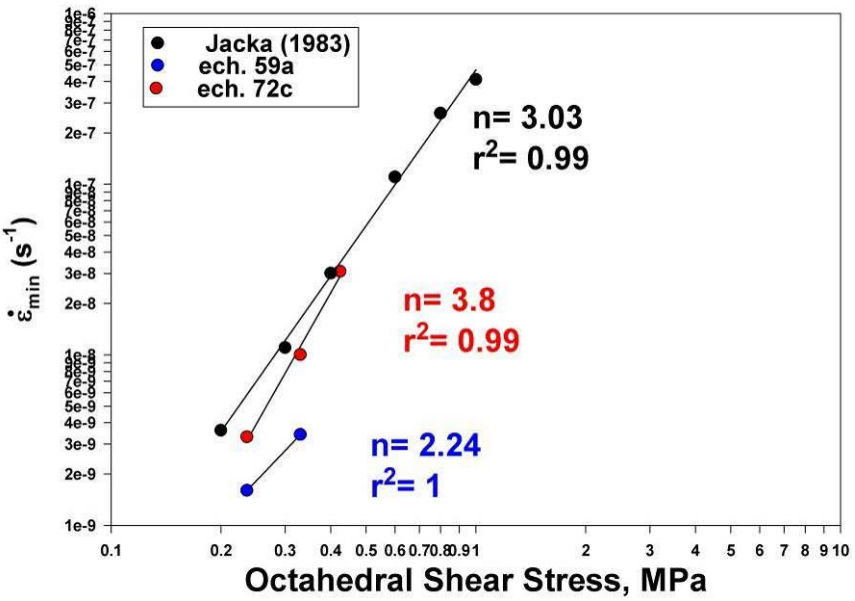

Figure 28: Results from our marine ice deformation experiments compared to those of Jacka (1983) on artificial isotropic bubbly ice

More experiments, at varying experimental conditions and with varying physico-chemical parameters will help us to refine the values given above and to gain a better understanding of the sensitivity of marine ice to changing stress configurations.

2.3. Modelling of the transition zone between ice sheet and ice shelf

Basal processes and ice shelf viscosity play an important role in marine ice sheet dynamics. A thorough understanding of this role is hampered by the difficulty of collecting data about basal processes and ice shelf viscosity. This lack of knowledge hampers the credibility of current ice-flow modelling efforts. On the other hand, for many grounding zones, there is a good spatial coverage of surface velocity, surface elevation and ice thickness. With an inverse model, we can use this data to derive information about basal processes and ice shelf viscosity. This is done by tuning the necessary input values for basal processes and ice shelf viscosity so that, when used in an ice dynamics model, the modelled surface velocity equals the observed surface velocity.

For these inversions, we developed a robust 2D time-independent isothermal higher-order flowline model (De Smedt et al., 2007). The physical model is based on Pattyn (2002) and takes into account both vertical shear and longitudinal stress gradient aspects of ice flow, which makes it suited for both valley glaciers, ice sheets and ice streams. We use a Dirichlet boundary condition at the base in the form of a basal velocity. This way, we avoid the hypothesis of a sliding law which may not hold in practice. The numerical model is based on finite elements. We use triangular elements and linear basis functions to build a piecewise linear approximation of the velocity solution. This leads to a set of equations that is very similar to a finite difference discretisation on a staggered grid. This results in a significantly better stability in the iterative solution of the physical model. The numerical solution is accurate and robust for all sets of input data, as is confirmed by ample validation experiments. Part of these validation experiments follows the ISMIP-HOM benchmarks (Pattyn et al., 2008). From these benchmark experiments, it follows that our model produces results in line with other robust higher-order models. A second improvement is a simpler and more efficient relaxation scheme for the iterative solution of the physical model. An adapted preconditioned conjugate gradient solver assures a fast solution of the ice velocity for each iteration. These virtues of our numerical model allow for a fast and robust inversion of basal parameters.

Recent satellite data shows significant changes in the dynamics of a few fast-flowing coastal glaciers. For Pine Island Glacier (PIG), that has the largest discharge of all West-Antarctic ice streams, a grounding line retreat of about 1 m a^{-1} has been observed. This retreat has been accompanied by a strong increase in surface velocity and a thinning that extends far inland. To learn more about the role of basal processes in these changes, we applied the newly developed 2D higher-order flowline model (De Smedt et al., 2007) along a 250-km-long flightline over PIG, extending from inland to the grounding line. Along this flightline, data is available on surface elevation, surface velocity and ice thickness at a resolution of 5 km (Figure 29a and b). Up to km 100 of the flightline, the observed surface velocity is approximately 100 m a^{-1}. From km 100 towards the grounding line, there is a linear increase in surface velocity up to 2000 m a^{-1}. Using the model in combination with a fixed point optimisation, we have derived the basal velocity pattern necessary to match the observed surface velocity. We performed this inversion for 2 values for the overall ice temperature: 0°C and -10°C. The actual deformation behaviour of PIG should lie between these two extremes. Since the basal ice is at pressure melting point along the whole of the profile and most of the ice deformation occurs at the bed, the 0°C scenario seems more realistic.

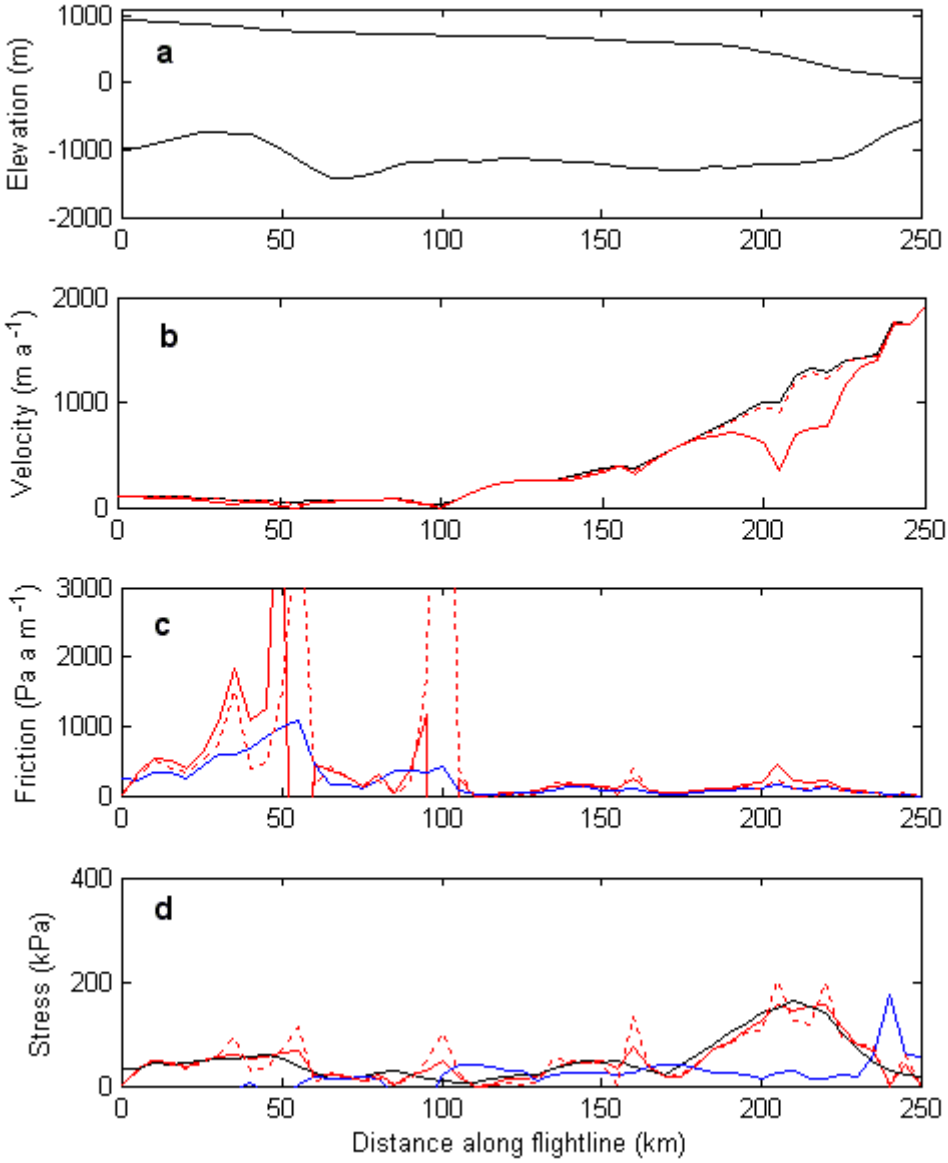

Figure 29: Observations (Vieli and Payne, 2003) and model results along a flight line over Pine Island Glacier, West-Antarctica. Model results are shown for an overall ice temperature of 0°C (solid line) and -10°C (dotted line). (a) Observed geometry. (b) Observed surface velocity (black) and derived basal velocity (red). (c) Derived friction under the assumption of a linear sliding law for this study (red) and from Vieli and Payne (2003) (blue). (d) Observed driving stress (black) and derived basal drag (red) and mean longitudinal deviatoric stress (blue).

For both inversions, the derived basal velocity equals the observed surface velocity for most of the flight line (Figure 29b). This shows that the flow of PIG is strongly dominated by basal processes. Only in 2 small zones in the inland part (around km 50 and at km 100) and a larger zone near the grounding line (km 180-230), there is a significant relative contribution of ice deformation to the horizontal velocity. The deformation spot at km 100 is caused by a local peak in basal drag (Figure 29d). The two other deformation zones are due to a steeper surface slope. The mean deformation velocity in the grounding zone should lie between 100 km a^{-1} (-10°C scenario) and 500

km a^{-1} (0°C scenario). For both scenario's, the inverted basal drag shows a distinct drop from km 100 to km 105 (Figure 29d), where we have the onset of fast flow. This drop in basal drag coincides with a strong change from compression flow to extension flow and this extension flow continues throughout the rest of the flight-line (Figure 29d). The latter is due to the steady increase of sliding velocity towards the grounding line and is responsible for the inland propagation of grounding line effects. This is supported by another modelling study on PIG (Payne et al., 2004). Payne et al. showed that a 50% drop of basal friction at the grounding line has a thinning effect extending far inland. We also find that the low basal drag zones around km 70, 110 and 170 coincide with bed depressions. This suggests a lower friction in these zones, presumably due to basal hydrology.

Under the assumption of a linear sliding law $\tau_b = \beta^2 u_b$ with τ_b the basal drag, β^2 the basal friction and u_b the basal velocity, we can derive basal friction from our model results. Just as basal drag, the resulting basal friction shows a pronounced drop around km 100 (Figure 29c). We also find a gradual rise of basal friction towards km 55, where we also have a strong drop. Throughout the rest of the profile, basal friction is very low, which is another indication of the high sensitivity of PIG to changes in the grounding zone. It is interesting to compare this friction pattern with the pattern derived by Vieli and Payne (2003), also under the assumption of a linear sliding law. In their study, Vieli and Payne use an ice-stream model, hereby assuming that vertical shearing is negligible. Our results show that this assumption is justified over most of the profile, but probably too simplistic at the inland part and the grounding zone. As a result, for these two zones, Vieli and Payne underestimate the actual friction. The general friction pattern by Vieli and Payne, however, is very similar to our reconstruction. The flow of Pine Island Glacier (PIG), West-Antarctica, is strongly dominated by basal processes. As a result, basal drag and friction are very low over most of the grounding zone. This explains the observed sensitivity of the inland flow to changes in the grounding zone. The onset of fast flow coincides with a strong drop in basal drag. Low basal drag zones coincide with bed depressions. This suggests an enhanced activity of basal processes in bed depressions. These results are in line with studies by Vieli and Payne (2003) and Payne et al. (2004).

2.4. Subglacial processes

2.4.1. Stability of subglacial lakes

More than 145 subglacial lakes have been identified underneath the Antarctic ice sheet, mainly by analyzing airborne radio-echo sounding profiles. Subglacial lakes are characterized by a strong basal reflector, constant echo strength, corroborating a smooth surface, and a flat surface compared to the surrounding with a slope which is around ten times, and in the opposite direction of, the surface slope (Siegert et al. 2005). Hence, the ice column above a subglacial lake is in hydrostatic equilibrium. Most lakes lie under a thick ice cover of >3500m and are therefore situated close to ice divides. The volume of water in known Antarctic subglacial lakes is approximately 25% of the water world-wide in surface lakes (SALE Workshop Report, 2007). This is equivalent to a uniform sheet of water 1m thick if spread out underneath the whole Antarctic ice sheet.

Subglacial lakes are supposed to be relatively closed and stable environments with long residence times and slow circulations (Kapitsa et al., 1996). Therefore, such huge amount of subglacial meltwater would pose no threat to the stability of the ice sheet if it were not moving around through a hydrological network. This view has recently been challenged through the observation of rapid subglacial lake drainage events (Gray et al., 2005; Wingham et al, 2006; Fricker et al, 2007). The observations by Wingham et al (2006) suggest the rapid transfer of subglacial lake water and periodically flushing of subglacial lakes connected with other lakes that consequently fill through a hydrological network. For the draining lake (Adventure Trench Lake), they observe a surface lowering of 4m, corresponding to a water discharge of 1.8km^3 over a period of 16 months at a rate of 50m^{3}s^{-1}. These observations stem from rapid changes at the surface from which the drainage events are inferred. At present, direct observation of such subglacial events is lacking, and therefore knowledge on the mechanisms that trigger them as well. One way, however, to investigate possible mechanisms that lead to rapid subglacial drainage is through ice-sheet modelling in which ice flow across and interactions with a subglacial lake are taken into account. We therefore developed a full Stokes numerical ice-sheet model which is coupled to the subglacial lake environment to investigate the stability of subglacial lakes and their drainage through a sensitivity analysis. A full description of the model can be found in Pattyn (2003) and Pattyn (2008). Developing a full Stokes model was necessary, as bridging effects in the force balance equations (vertical resistive stresses) cannot be neglected, especially with respect to rapid variations in lake volume. In the model, basal hydrology is represented in terms of the subglacial water flux. The water flow algorithm is invoked to check whether subglacial water captured in the lake cavity is transported outside this cavity or not and therefore serves to detect whether the hydrostatic seal is intact or broken. Full basal hydraulics, such as tunnel formation and closure and associated water discharge (Nye, 1976), are not taken into account. Besides, as small floods creating small surface depressions are considered here (not the cauldron dimensions associated with Jökulhlaups), only flotation criterion for the ice over the lake as well as grounding line migration due to lake volume variations, is considered.

Starting from the initial conditions, the model ran forward until a steady state was reached. The general characteristics of the resulting ice sheet geometry are typical for those of a slippery spot, as is a subglacial lake, i.e. a flattened surface of the ice/air

interface across the lake and the tilted lake ceiling in the opposite direction of the surface slope, due to hydrostatic equilibrium. The tilt of this surface in the direction of the ice flow will determine the stability of the lake, since the hydraulic gradient is dominated by surface slopes and therefore the flatter this air/ice surface the easier water is kept inside the lake cavity. Changes in the surface flatness will therefore be crucial in subglacial lake stability. Therefore a sensitivity analysis was carried out from which it follows that lake stability is prevalent for large lakes, shallow ice, small ice surface slope and fast ice flow. However, the most determining parameter here is general surface slope: the flatter the surrounding area the more stable lakes are, which corroborates the presence of Antarctic subglacial lakes close to ice divides.

Our hypothesis is that (partial) lake drainage is a common feature of the Antarctic subglacial lakes and that only small perturbations are necessary to lead to a sudden outburst. Therefore, three perturbation experiments were carried out, i.e. (i) an experiment where the surface of the ice sheet is slightly perturbed, (ii) one in which subglacial water is gradually added to the lake system, and a third one where 20% of the lake water volume is removed at once. The first two experiments are regarded as common gradual changes in the glacial environment that on the time scales of decades are hardly noticeable, hence forming part of the natural variability of the system. Once the drainage condition is fulfilled -- i.e. the hydrostatic seal is broken -- the lake is drained at a rate of $50 m^3 s^{-1}$ for a period of 16 months (see above). This essentially means that enough energy is released to keep the subglacial tunnel open for a while and a siphon-effect can take place. It is not clear whether this effect is only temporary or ends when the lake is completely emptied as suggested by Wingham et al. (2006). However, the drainage event of Lake Engelhardt suggests that water is still present in the lake after the event, as the surface aspect (flatness) has not changed over this period of time. Furthermore, Evatt et al. (2006) suggest that the drainage event of the Adventure Trench Lake is due to channelized flow over soft sediments at low effective pressure, rather than the emptying of a very shallow lake. Not all experiments exhibit lake drainage. Certain parameter settings, such as small ice thickness, render lakes very stable. When drainage occurs, episodic events take place, even though the initial geometric conditions are not met. These events occur at a higher frequency at the beginning, i.e. when more water is present in the lake, than later on and occur with frequencies of less than a decade. Most experiments show stable conditions after 200 years of integration, either because the drainage conditions are not fulfilled anymore, either because the cavity is devoid of water or a complete drainage has taken place. The episodic drainage results in variations in the surface elevation across the lake of rapid lowering, followed by a gradual increase until the initial level is more or less reached. This surface rise is clearly nonlinear, and the rate of uplift decreases with time. The frequency decreases with time as well as less water is present in the system, hence hampering drainage (Figure 30). Interesting to no note, however, is that the surface rise is not caused by an influx of subglacial water entering from upstream. On the contrary, less water is subsequently present in the whole subglacial system. Surface increase is due to an increased ice flux, filling up the surface depression created by the sudden lake drainage.

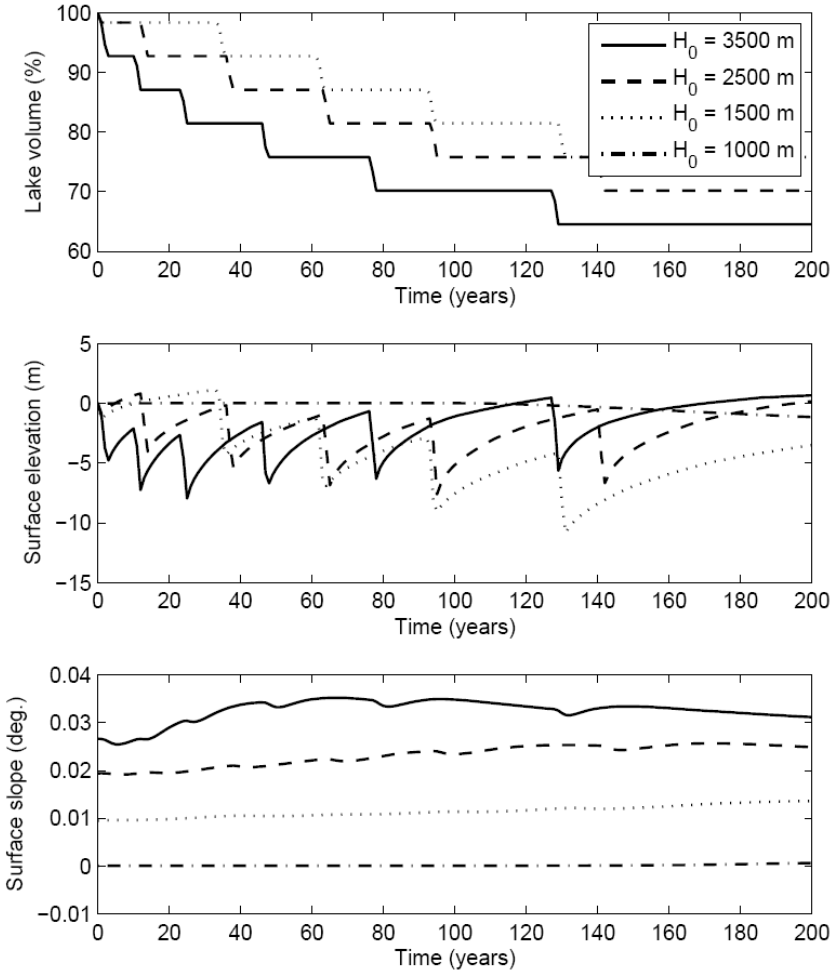

Figure 30: Time series of the perturbation experiment according to a change in surface elevation. The three panels show the time evolution of lake water volume (upper), ice surface elevation on top of the lake (middle) and ice surface slope across the lake (bottom) for the ice thickness sensitivity. No lake drainage is observed for small ice thicknesses (H_0=1000m).

Most subglacial lakes are lying close to ice divides, hence in areas of low surface slopes and high hydraulic fluid potential. Therefore, a fundamental question arises (Priscu et al., 2007): does the ice sheet control the location of subglacial lakes or does the lithospheric character necessary for lake formation, such as geothermal heat flux and the presence of basal cavities and sub-ice aquifers, constrain the evolution of these catchments? According to the model simulations, geometric effects, such as ice thickness, mean surface slope, ice viscosity (hence ice temperature), and lake size play an important role in the stability of subglacial lakes. They favour the existence of subglacial lakes near ice divides in areas of low viscosity and low surface slopes. Lake filling might therefore happen when the ice sheet is in full expansion during sustained cold periods and when surface slopes are very low, such as a glacial period. During interglacial periods, the smaller and warmer ice sheet characterized by slightly higher surface slopes in the interior facilitates lake drainage, a point that will be investigated more closer in the future and that might as well explain why underneath the Greenland ice sheet subglacial lakes are not observed.

The above described experiments have shown that the developed model is capable of exhibiting the major characteristics of drainage due to changes in ice sheet and/or subglacial lake geometry. Results demonstrate that only small changes are necessary

to provoke episodic lake drainage. These events only lead to a partial drainage of the lake, after which the ice sheet adapts to the changed conditions and ice flow `fills' the surface depression after drainage. Therefore, lake drainage on a decadal time scale can be regarded as a common feature of the subglacial hydrological system and may influence to a large extent the behaviour of large ice sheets through such jökulhlaups (Evatt et al., 2006). This has potential implications for ice stream dynamics, especially in areas that are underlain by sedimentary material. Unless this water escapes to the margin via well defined channels, it will act to increase pore-water pressures and so reduce the strength of sediments, which will increase ice velocity (Siegert et al., 2007). Finally, the experiments show that big lakes under thick ice in slow moving regions drain easy, hence a feature that should be common for subglacial Lake Vostok.

2.4.2. Coupling a Full Stokes model to a lake circulation model

As shown above, subglacial lakes in Antarctica influence the flow of the ice sheet in a significant way. The previous analysis of ice sheet/lake interaction was limited to a steady water body. However, in reality, large subglacial lakes are characterized by a water circulation. This pattern influences the mass balance at the interface between the subglacial lake and the overriding ice sheet. In collaboration with AWI, we coupled the above described full Stokes ice sheet model to a three-dimensional fluid dynamics model with eddy diffusion to simulate the basal mass balance at the ice sheet's bottom (Thoma et al, 2010). For this purpose, the ice sheet model was improved to cope with nonlinear rheology instead of Newtonian flow as shown above. Furthermore a newly developed coupler to exchange the necessary boundary conditions between the individual models was implemented. Different boundary conditions are applied over grounded ice and floating ice. This results in significantly increased temperatures within the ice on top of the lake, compared to ice at the same depth in the vicinity. Initial results demonstrate that melting at the ice's bottom increases this lateral temperature gradient. From upstream the ice flow converges towards the lake and accelerates by about 10% if basal melting at the ice-lake boundary is present. Above and downstream of the lake, where the ice flow diverges, a velocity decrease of about 10% is simulated (Thoma et al, 2010).

2.4.3. Basal properties of the Antarctic ice sheet and subglacial lake presence

Physical properties at the base of the Antarctic Ice Sheet are poorly known. The basal thermal regime is a main player in the ice sheet dynamics: if the ice is frozen to its underlying bedrock, the only velocity component will be ice deformation. But when the pressure melting point is reached at the ice base, the ice mass will start to slide over its base, reaching velocities of up to more than 1000 meters per year. Knowing whether the basal ice is melting or not is also important for the correct interpretation of paleoclimatic signals of ice cores. And it controls whether erosion and landscape modification will take place.

We used a three-dimensional thermomechanical ice sheet model (Huybrechts, 2002) to calculate the temperature distribution within the Antarctic ice sheet in an effort to help identifying regions which reach pressure melting. Two boundary conditions are needed in the temperature calculation: observed surface temperature and the basal temperature gradient. The latter is determined by basal drag, the basal sliding velocity and the geothermal heat flux from the earth.

The badly known geothermal heat flux is the largest unknown in the calculation. Some authors use a constant value, e.g. 54.6 mW/m² (Huybrechts, 1992), others prefer to divide the Antarctic continent into different geological provinces with a high geothermal heat flux in West-Antarctica, which is composed of younger oceanic crust. East-Antarctica has a lower heat flux because it consists of an old continental craton (e.g. Llubes et al., 2006). Two other approaches to calculate the geothermal heat flux for the Antarctic continent are based on extrapolation of a seismic model (Shapiro and Ritzwoller, 2004) or on the use of satellite magnetic data in combination with a model of crustal thickness to obtain a good estimate of the flux values (Fox Maule et al., 2005).

In an effort to better constrain the value of the geothermal heat flux a comprehensive calculation of Antarctic ice temperatures was made with a three-dimensional model. The solution is found from solving the thermodynamic equation under the usual assumptions, retaining the terms of vertical conduction, 3-D advection, and frictional heat dissipation from ice deformation. The model was run over the last 4 glacial cycles to obtain the transient basal temperature distribution at the present time, using the different geothermal heat flux distributions mentioned above. Subsequently, basal temperatures were compared with a map of known locations of subglacial lakes (Siegert et al., 2005). The climatic forcing was derived from the Dome C oxygen isotope record (EPICA community members, 2004). The result is shown in Figure 31.

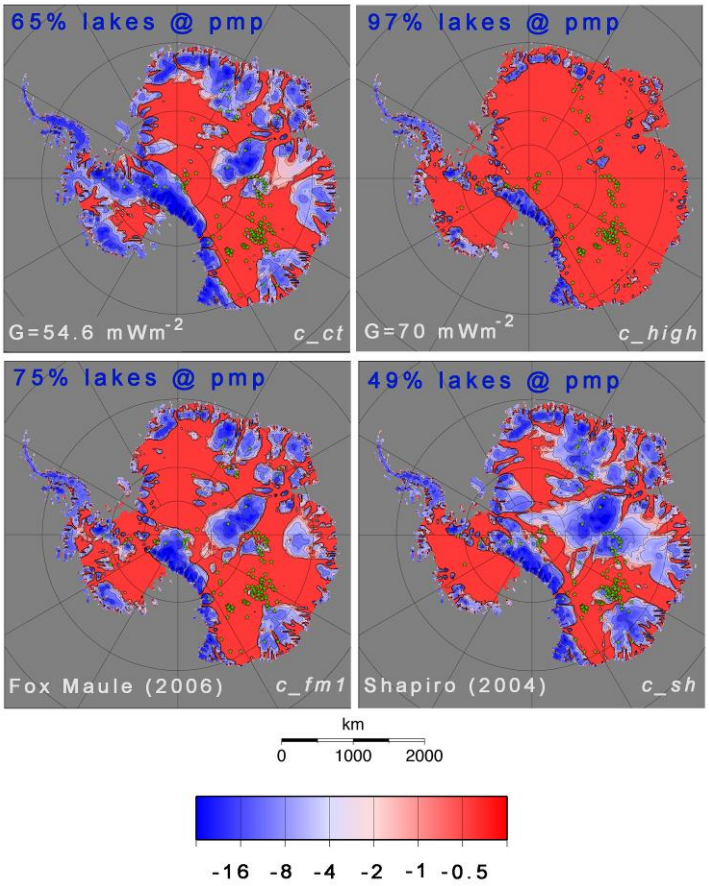

Figure 31: Modelled basal temperatures, using various representations for the geothermal heat flux. Green dots represent the location of known subglacial lakes.

Using the data of Fox Maule et al. (2005), pressure melting is reached at most of the coastal areas and in the inland regions (Figure 31). Dome C, Ridge B and Lake Vostok as well as the Siple Coast are situated in warm basal regions. Using the basal thermal regime calculated by the model, the basal melting rate can be calculated and compared with the presence of subglacial lakes (Siegert et al., 2005). In this experiment, 75 percent (108 of the 145 identified lakes) are located in a region at pressure melting point. Lakes near Dome A and Dome F are situated in cold regions whereas Lake Vostok and the lakes near Ridge B and Dome C are in pressure melting regions. The same experiments were done with values of 54.6 and 70 mW/m² and the estimate made by Shapiro and Ritzwoller (2004). The percentages of lakes that are situated in pressure melting point regions are 65.5, 96.6 and 49 percent respectively (Figure 31). Using 70 mW/m², the pressure melting point is reached almost everywhere. However, this is quite unrealistic since the East Antarctic Ice Sheet rests on an old continental craton with most likely a lower geothermal heat flux, but the experiment shows how sensitive the basal thermal regime is to the use of different values.

On the basis of these results, we favour the geothermal heat flux map Fox Maule et al. (2005). Figure 32 shows the corresponding fields of basal temperature and basal melting rate.

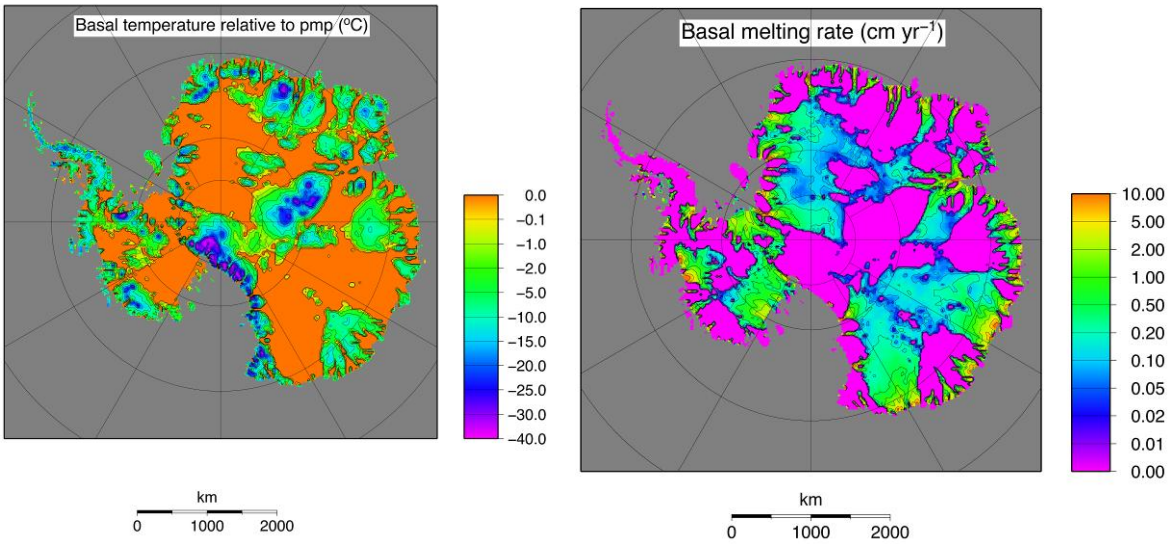

Figure 32: Modelled basal temperature (left) and basal melting rate (right), using the geothermal heat flux data from Fox Maule et al. (2005).

2.4.4. Implications for the basal ice age distribution of the Antarctic ice sheet

One of the big objectives of ice-core research is the search for ice older than 1 million years. Basal conditions are a crucial boundary condition for the potential age of basal ice in the Antarctic ice sheet. Basal melting removes the oldest ice layers from the ice sheet and this in turn is strongly controlled by the geothermal heat flux as demonstrated above. Other important conditions controlling the age of the basal ice are the ice thickness, the accumulation rate, and the strength of horizontal ice advection.

Figure 33 shows the modelled age distribution at a depth of 99% for the same experimental setup as for the basal temperature calculation using the geothermal heat flux representation of Fox Maule et al. (2005). The calculation is based on the

Eulerian approach (Rybak and Huybrechts, 2003). A second-order upwinding scheme was used for all advection terms. In the vertical, a non-uniform discretization was used with 51 layers, with thickness exponentially decreasing towards the base. The oldest ice at 99% depth with ages in excess of 1.2 million years is found in the very centre of the East Antarctic ice sheet in the vicinity of the Gamburtsev Mountains. Old ice is also modelled to occur upstream of some of the coastal mountain ranges which dam the ice flow. The pattern of old ice near to the bottom correlates very well with the coldest, slowest moving ice found in Antarctica. Large parts of East Antarctica are not suitable for drilling old ice as there is likely extensive basal melting. Old ice in the bottom layers is found to occur as an optimal combination of low accumulation rate, high ice thickness, low horizontal advection, and the absence of basal melting.

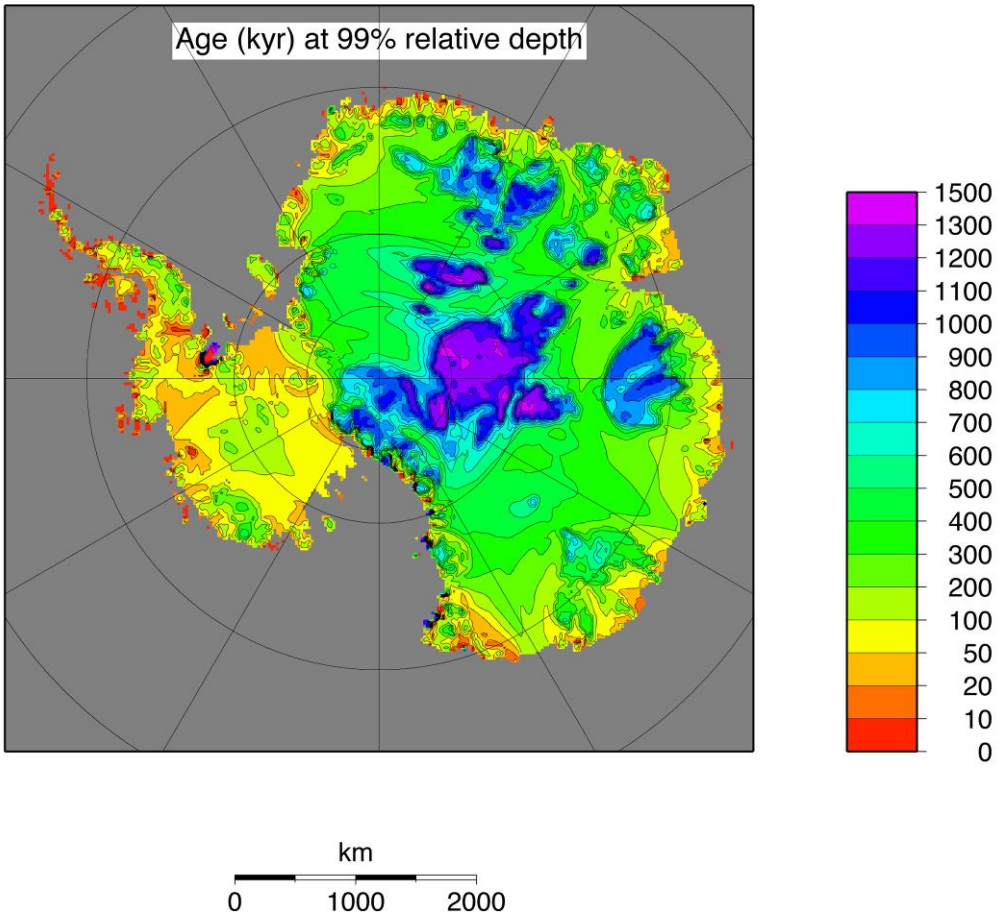

Figure 33: Modelled ice age at 99% depth in the Antarctic ice sheet using the geothermal heat flux data from Fox Maule et al. (2005).

For meaningful palaeoclimatic analyses not only the age of the ice is important, but also the thickness of the annual layers. This is demonstrated in Figure 34, which gives the predicted layer thickness of an ice layer containing 100000 years, or approximately one glacial cycle. By the layer thickness criterion, only the central ice sheet seems suitable for retrieving an ice core: here a layer containing 100 ka is predicted to be up to a 100 m thick for an ice age between 400 to 500 ka, and still 10 m or more for a layer that has an age of between 900 and 1000 ka. The bold black line is where the entire layer is above 99% depth. Below that depth there is a much larger chance for disturbances and perturbations in the layer architecture.

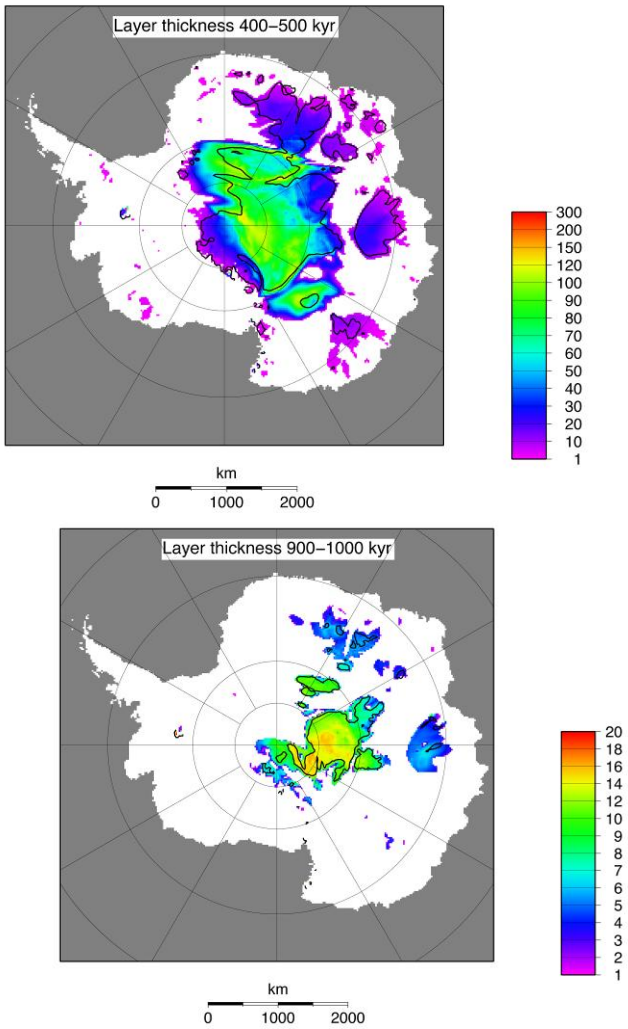

Figure 34: Predicted layer thickness (in meter) containing a sequence of 100000 years of given ice age. The bold black line delimits the area above 99% relative depth.

It should be stressed, however, that these fields should not be taken literally. It is a large-scale model estimate based on our current best knowledge of ice thickness, accumulation rate, geothermal heat flux, and ice dynamics. Although the large-scale distribution is expected to be qualitatively correct, local conditions may differ and need a thorough detailed field survey to determine the local variation of ice thickness, bed elevation, and surface accumulation.

2.4.5. Dating of the basal ice at the EDML drill site (Kohnen)

A more detailed modelling study aiming specifically at the dating and interpretation of the basal ice of the EDML ice core at Kohnen was performed in Huybrechts et al. (2007). In this study, a nested ice flow model was developed for eastern Dronning Maud Land. The model consists of a high-resolution higher-order ice dynamic flow model (Pattyn, 2003) that was nested into the 3D model of Huybrechts (2002). The large-scale model, in which all prognostic calculations take place, provides boundary conditions for the fine-scale model. The most important output of the model is the high-resolution regional velocity field. This is first obtained from a forward experiment over the last 8 glacial cycles. The result is subsequently employed in a

Lagrangian back tracing algorithm to provide particle paths back to their time and place of deposition. The procedure directly yields the depth-age distribution, surface conditions at particle origin, and a suite of relevant parameters such as initial annual layer thickness. The glaciologically derived chronology obtained in this way is shown in Figure 35. There is an excellent agreement with the EDML1 time scale for most of the profile. This proves the validity and internal consistency of the modelled velocity fields and gives confidence in our particle trajectory method.

Figure 35 only shows the dating down to 90% depth. Below that depth, for the lower 250 m, the dating increasingly depends on the value of the geothermal heat flux. This was investigated further in subsequent experiments that considered values of the geothermal heat flux to be between 2% and 30% higher than the reference value of 54.6 Wm-2. Figure 36 shows the corresponding basal temperature fields. For the reference value of the geothermal heat flux, we find that the Kohnen location is currently very close to a large area more to the south at the pressure melting point. During the glacial history the melting point was hit intermittently at Kohnen, but with only a very small amount of basal melting. For a geothermal heat flux only 5% higher, however, the Kohnen location is predicted to have been at pressure melting continuously. Consequently, basal ice was lost continuously, both at Kohnen station as along particle trajectories.

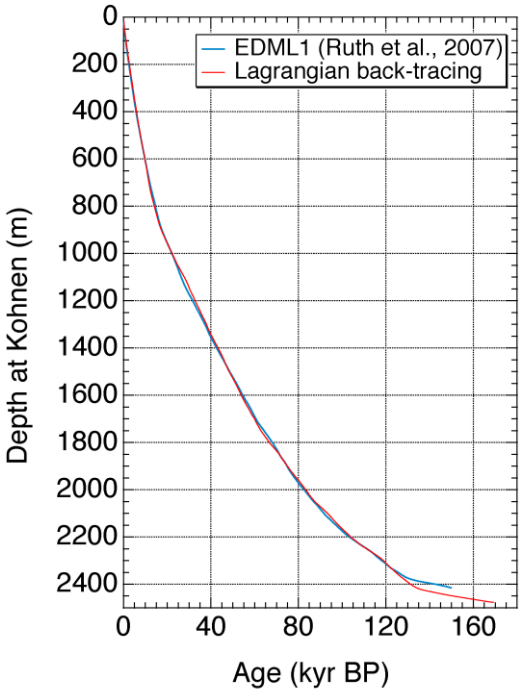

Figure 35: Model-derived depth-age distribution at Kohnen plotted as a function of real depth. For comparison, the EDML1 time scale obtained from stratigraphic matching with the EDC ice core is shown in blue (Ruth et al., 2007). Both curves agree very well, but less so for the penultimate glacial period between 125 and 150 kyr BP.

The effect on the basal ice age is enormous as basal melting gradually removes the basal ice. This only affects the ice chronology in the bottom layers and the upper 90% of depth remains largely unaffected. Actually, within the range of uncertainty on the geothermal heat flux, a basal ice age between 280000 years and more than 750000 years seems possible (Figure 37). Even though basal melting rates remain modest, only up to 1.5 mm year-1 for a geothermal heat flux 30% larger than the

reference one, this ultimately cumulates to over 1200 m of basal ice lost after 700000 years (Figure 38).
In Figure 39, the various possible options for the time scale of the basal ice of EDML is shown against the Dome C δD record. The solid colour lines are the elevation corrected δ18O values for the various values of the geothermal heat flux. Not corrected records are shown by the thin lines of the same colour. Thin black line indicates the rescaled curve of the Dome C δD record plotted against the EDC3 chronology. It is not straightforward to prefer one time scale over another. The G+15% case seems to fit best for the interglacial centred around 240000 years ago but this is not conclusive. None of the other options really seem to fit well either. Apparently, it is well possible that other processes, not taken into account in the modelling, could have perturbed the chronology of the basal layers, such as folding, ice hardness contrasts influencing thinning rates, and perhaps other processes we are not aware of.

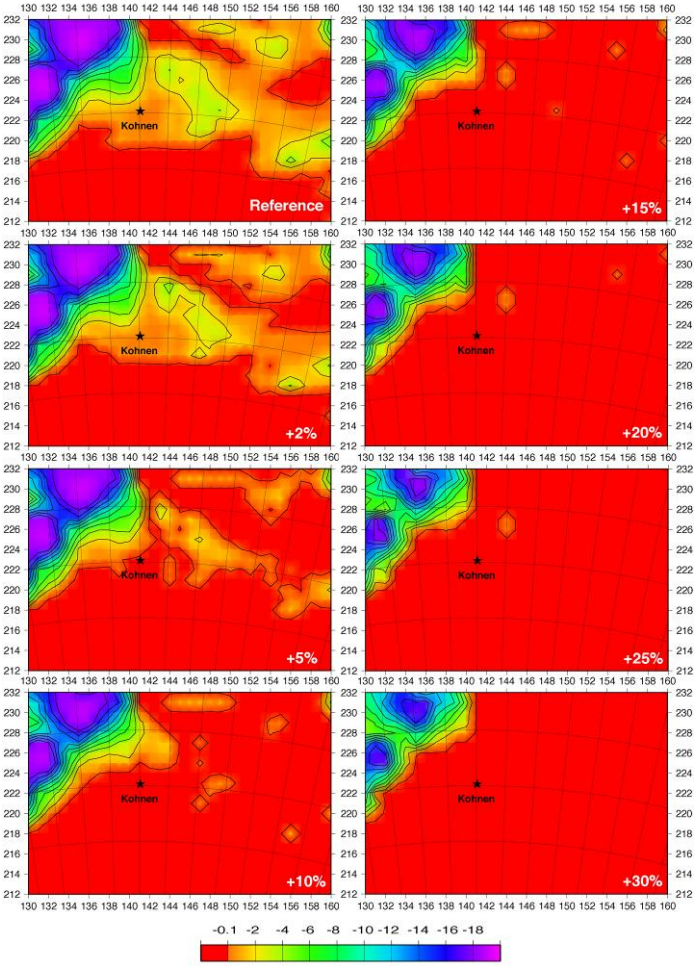

Figure 36: Basal temperature corrected for the pressure melting point in eastern Dronning Maud Land in a series of experiments with G higher between 2% and 30% than the reference value. Red areas are at the melting point. The black star denotes the location of Kohnen Station (75°00.104′ S, 0°04.07′ E).

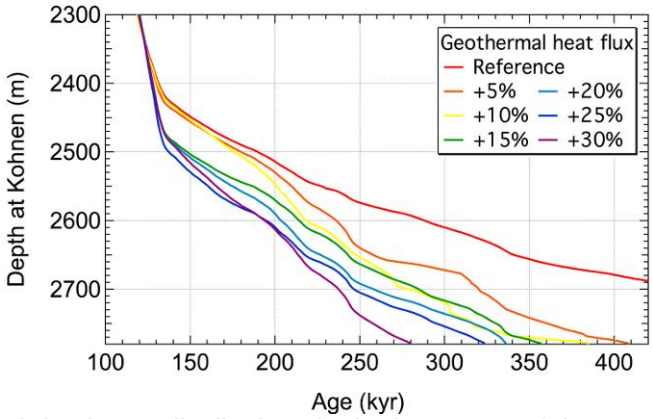

Figure 37: Model-derived depth-age distributions in the lower part of the EDML ice core plotted as a function of real depth for various values of the geothermal heat flux.

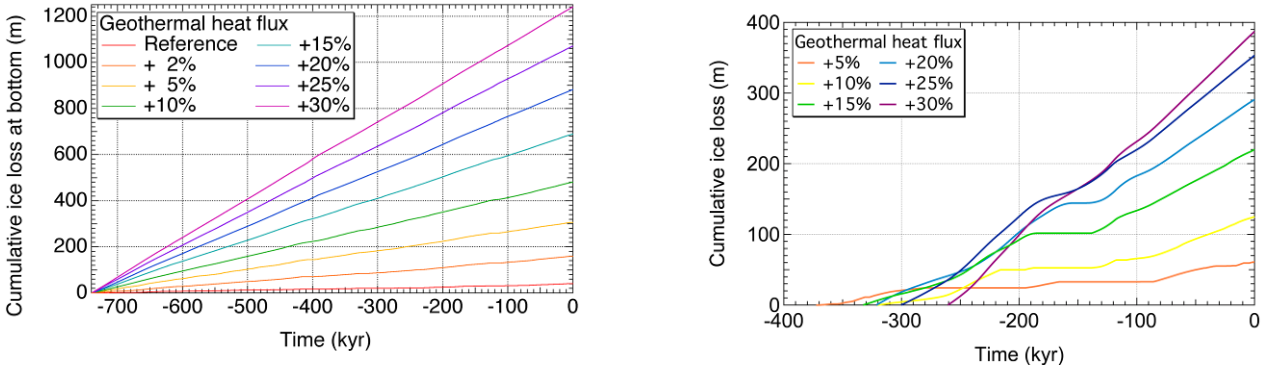

Figure 38: Cumulative ice loss at Kohnen station (left panel) and along the trajectories of 99% particle paths (right panel) for various values of the geothermal heat flux.

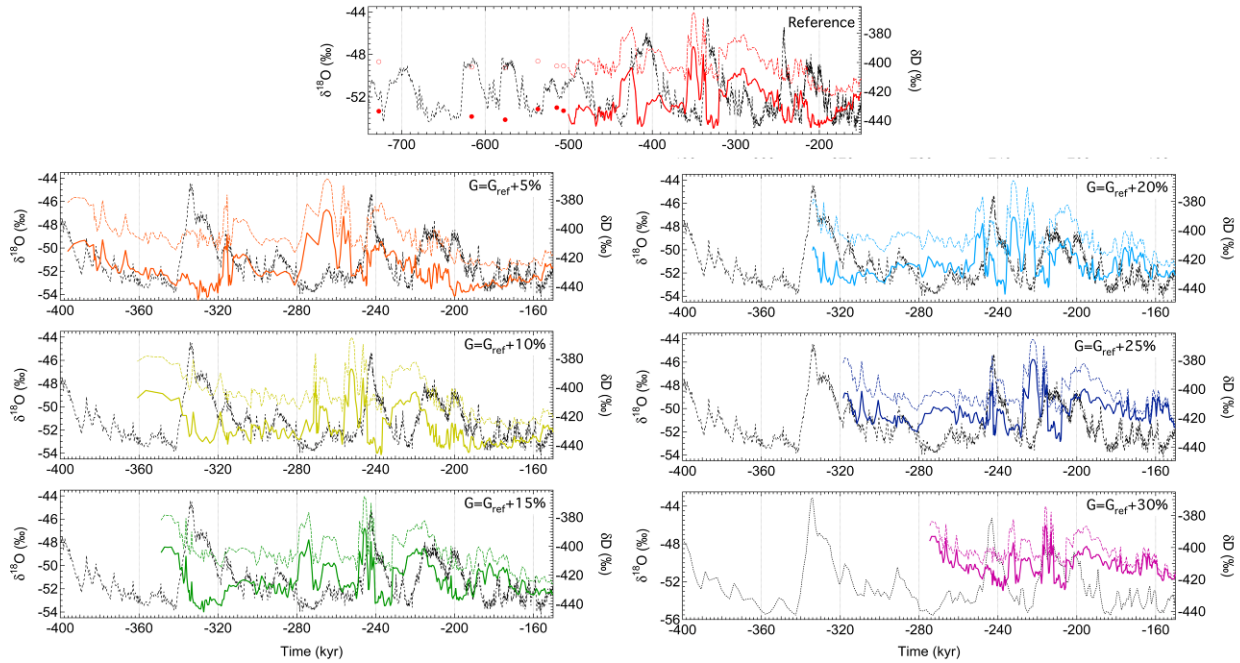

Figure 39: Selected fragments of the EDML δ18O record stretched against possible options for the time scale and compared with the Dome C δD record.

2.4.6. Basal ice properties and processes

Deep ice cores retrieved from the two present-day major ice sheets on Earth, Greenland in the North and Antarctica in the South, have delivered a wealth of unique paleoclimatic archives over the last decades. These have allowed reconstructing global climatic and environmental conditions over the last 800.000 years, including unprecedented records of cyclic changes in the composition of climatically relevant atmospheric gases (CO_2, CH_4, N_2O…). An important share of those paleoclimatic information is buried within the lowermost sections of those deep ice cores, due to the mechanical thinning of annual accumulation layers with depth. Improving our records further back in time is therefore one of the main challenges of ice core science in the near future (IPICS, 2009). A major concern in this regard is to judge how far down we can trust the paleoclimatic signals stored within the ice, since the proximity of the bedrock is likely to interfere both with the recorded temporal sequence and with the ice properties. This in turn is closely linked to the thermal regime at the bottom of the ice sheet, as has been shown previously in the literature describing basal layers of deep ice cores (e.g. Goodwin, 1993, Gow et al., 1979, Gow and Meese, 1996, Herron and Langway, 1979, Jouzel et al., 1999, Koerner and Fisher, 1979, Souchez, 1997, Souchez et al., 1998, Souchez et al., 1995a, Souchez et al., 2002a, Souchez et al., 1993a, Souchez et al., 2006, Souchez et al., 1995b, Souchez et al., 1993b, Souchez et al., 2003, Souchez et al., 2002b, Souchez et al., 2000a, Souchez et al., 1994, Souchez et al., 2000b, Tison et al., 1998, Tison et al., 1994, Weis et al., 1997). Where the ice-bedrock interface is clearly below the pressure-melting point (pmp) as, for example, at the GRIP (-9°C) or the Dye-3 (-12°C) ice coring sites in Greenland, single or multiple mixing events between the present-day ice sheet ice and local ice remnants of previous (or even initial) ice sheet configurations are encountered (Souchez, 1997, Souchez et al., 1998, Souchez et al., 1994, Souchez et al., 2000b, Verbeke, 2002). Where the ice-bedrock interface is at the pmp, the meteoric ice has the potential to melt at a rate that will depend on the heat budget at the ice-bedrock interface (geothermal heat flux, internal friction and conduction through the ice above). In some cases, where the subglacial topography allows it, like at the Antarctic Vostok site, a subglacial lake will exist. Again, depending on the heat budget but also on the subglacial lake water circulation pattern, lake ice will form at the ice-water interface in substantial amounts (e.g. Jouzel et al., 1999, Souchez et al., 2002a, Souchez et al., 2003, Souchez et al., 2000a). This ice, evidently, does not carry paleoclimatic information anymore. Furthermore, in the case of large subglacial lakes (such as Lake Vostok) where the ice column above can be considered in full hydrostatic equilibrium buoyancy, re-grounding of the ice sheet on the lee side of the lake will induce dynamical perturbations (such as folds), even in the meteoric ice above, as demonstrated for the MIS11 (Raynaud D., 2005) and for the ice just above the accreted lake ice (Souchez et al., 2002a, Souchez et al., 2003, Souchez et al., 2002b). A less documented case however, is the one where no significant water body exists at the ice-bedrock interface. If only melting occurs at the interface, with no water accumulation and no refreezing, can we then rely on the paleoclimatic information gathered in the basal layers?

2.4.6.1. Multiparametric analysis of the EPICA Dome C deep ice: can we rely on a safe paleoclimatic interpretation?

The Dome C deep ice core (EDC) is one of the two ice cores drilled in the framework of the European Project for Ice Coring in Antarctica (EPICA). It has been located at Concordia Station (Dome C - 75°06'04"S; 123°20'52" E), about 1200 km South of the French coastal station of Dumont d'Urville, and 720 km North East of the Russian Vostok Station. Detailed GPS surface topography and airborne radar surveys were conducted in 1994-1995 in order to optimize the choice for the drilling location (Rémy and Tabacco, 2000). These provided clear features of the bedrock and surface topography, showing a set of north-south-trending parallel valleys tens of meters deep in the bedrock, corresponding to smooth elongated undulations a few meters high at the surface.

A final drilling depth of 3260m was reached in December 2004, about 15 meters above the ice-bedrock interface (to prevent from eventually making contact with subglacial meltwater). The ice temperature was -3°C at 3135m and a simple extrapolation to the bottom indicates that the melting point should be reached at the interface (Lefebvre et al., 2008). The top 3200m of the EDC ice core have already been extensively studied and provided a full suite of climatic and environmental data over the last 8 climatic cycles (e.g. Delmonte et al., 2008, Durand et al., 2008, EPICA Community Members, 2004, Jouzel et al., 2007, Lambert et al., 2008, Loulergue et al., 2008, Lüthi et al., 2008, Wolff et al., 2006). Raisbeck et al. (2006) have confirmed the old age of the deep EDC ice by presenting evidence for enhanced ^{10}Be deposition in the ice at 3160-3170m (corresponding to the 775-786 kyr interval in the EDC2 time scale) consistent with the age and duration of the Matuyama-Brunhes geomagnetic reversal. A coherent interpretation of CO_2 and CH_4 profiles (Loulergue et al., 2008, Lüthi et al., 2008) has also established the presence of Marine Ice Stages (MIS) 18 (ca. 740-750 kyr BP) and 19 (ca. 780-790 kyr BP). However, a detailed study of the isotopic composition of O_2 and its relationship to daily northern hemisphere summer insolation and comparison to marine sediment records has shown potentially anomalous flow in the lower bottom 500m of the core with associated distortion of the EDC2 time scale by a factor of up to 2. This has led to the construction of the new, currently used, EDC3 timescale.

The last 12 meters of the available core show visible solid inclusions (Figure 40e), which are traditionally interpreted as a sign of interactions with the bedrock and usually qualified as "basal ice". We will therefore use that terminology here below, and reserve the term "deep ice" for the upper part of the bottom 60 meters which are the focus of this study. Solid inclusions within the basal ice are spherical in shape, brownish to reddish in colour, and generally increase both in size and density with increasing depth. Between 3248.30 m (first occurrence of inclusion visible by eye) and 3252.15m they are only sparse (0 to 10 inclusions per 50 cm ice core length) and less than 1mm in diameter. In the lower 8 meters, inclusions get bigger (up to 3 mm in the last 50 cm sample) and reach more than 20 individual inclusions per 50 cm ice core length. In several cases, especially for the bigger inclusions, these are "enclosed" in a whitish ovoid bubble-like feature (e.g. upper left corner of Figure 40e). Careful visual examination of the texture of each individual inclusion suggests that these are not made of single particles, but more likely consist of aggregates of a

large number of smaller inclusions. In most cases, these inclusions appear to occur at crystals boundaries. A detailed study of the morphology, mineralogy and chemistry of some of these individual inclusions is described in a companion paper (de Angelis et al., in prep.). Finally, it should be kept in mind that these characteristics are valid for ice collected some 15 meters above the actual ice-bedrock interface. We do not, unfortunately, have any information on the properties of the ice below.

The basal ice of the EDC core shows a relatively low debris content, if compared to the other deep ice coring sites described in previous studies (Camp Century, GRIP, Dye-3, Vostok…), and could be processed using "standard" procedures. It has thus been decided, for practical reasons and uniformity, to analyze the bottom ice in continuity with the cutting scheme used for the ice above. The multiparametric data set discussed in this paper has therefore been obtained applying analytical techniques described in full in previous studies focusing on single parameters. These are therefore not described in this report.

Figure 40a and b plot the full δD profile of the EPICA ice core, vs. depth and age respectively. The age time scale is a combination of EDC3 for the ice above 3200 meters and EDC2 for the ice below. As stated above, we will use the "basal ice" terminology for the lower 12 meters (red open triangles) and qualify the 48 meters above as "deep ice" (blue open squares). "Bottom ice" will refer to the whole 60 meters sequence. A combined Vostok-EDC $\delta^{18}O_{atm}$ profile (isotopic composition of atmospheric oxygen in ice) vs. EDC3 time scale is shown in Figure 40d (adapted from Dreyfus et al., 2007, Petit et al., 1999 for the ice above 3200m). The $\delta^{18}0$ benthic record stack of Lisiecki and Raymo (2005) is also plotted as a reference in Figure 40c. The co-isotopic properties of the EPICA Dome C bottom ice (open squares for deep ice, open triangles for basal ice) are described in Figure 41a (δD vs. $\delta^{18}O$) and 45b (d_{excess} vs. δD) and compared to those of the ice above 3200 m.

Figure 42 summarizes the available low resolution gas and dust concentrations data. Total gas content (black dots in Figure 42a) is only available for the deep ice section, while CH_4 and CO_2 are covered for both the deep (open squares in Figure 42a) and basal (open triangles in Figure 42a) sections. The full concentrations ranges observed for CH_4 and CO_2 during the preceding climatic cycles are also shown for reference, as white and black vertical bars respectively. A limited number of dust concentration measurements are shown in Figure 42b (same symbols as above) and also compared to the full glacial (excluding transitions) range during the previous climatic cycles (black vertical bar).

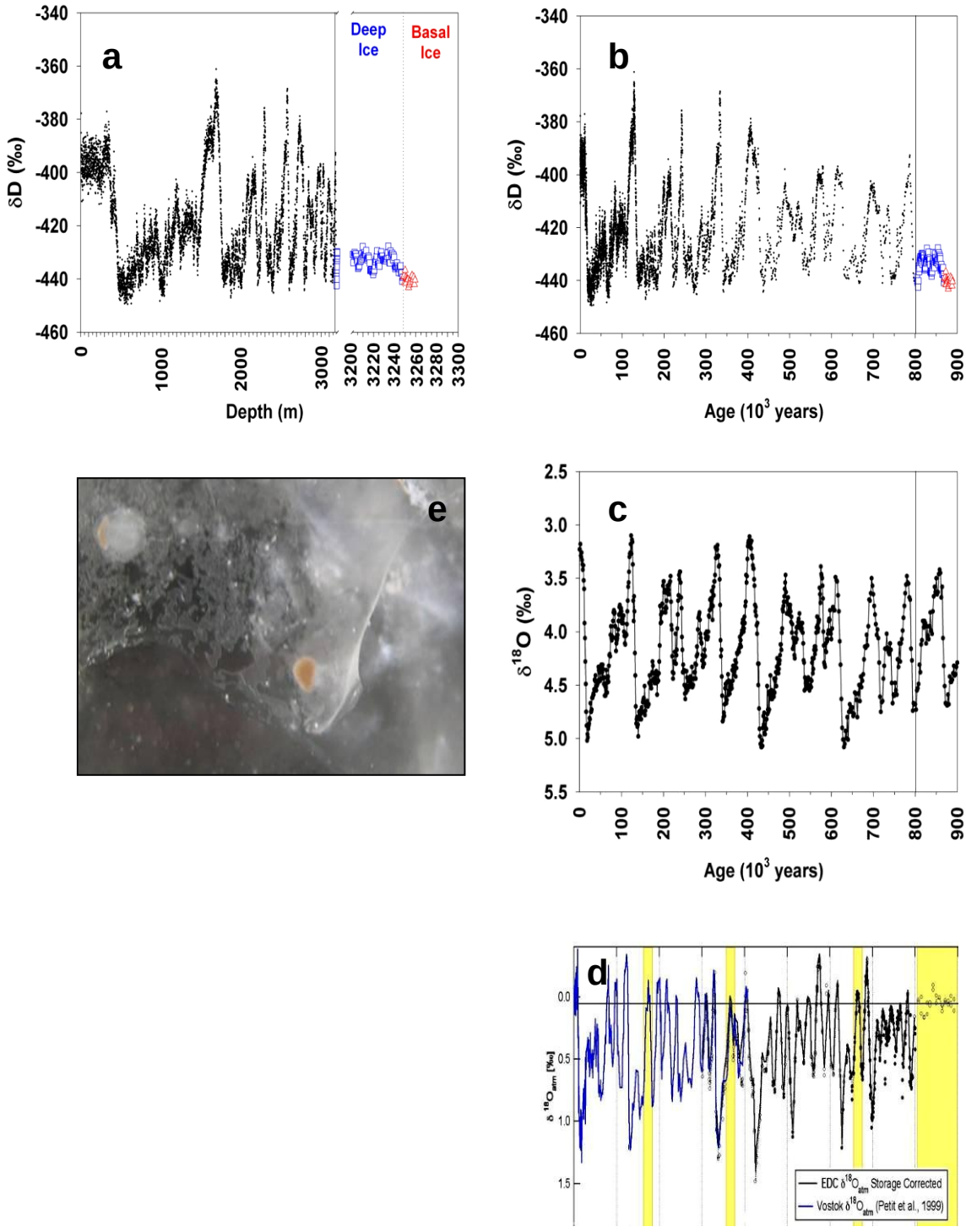

Figure 40: a) EDC δD_{ice} vs. depth, b) EDC δD_{ice} vs. age (EDC3 time scale for the first 800 ky - black dots - and EDC 2 time scale for the deep and basal ice), c) $\delta^{18}O$ vs. age for the benthic record stack of Lisiecki and Raimo (2005), d) Combined Vostok and EDC $\delta^{18}O_{atm}$ vs. age (adapted from Dreyfus et al., 2007*) and e) visual appearance of the EDC basal ice in the lower meters of the core (photo: D. Dahl-Jensen). For reasons described in the text, ice below 3200m depth is referred to as « deep ice » (blue squares) and « basal ice » (red triangles) describes the ice below 3248.30m, where solid inclusions are visible.

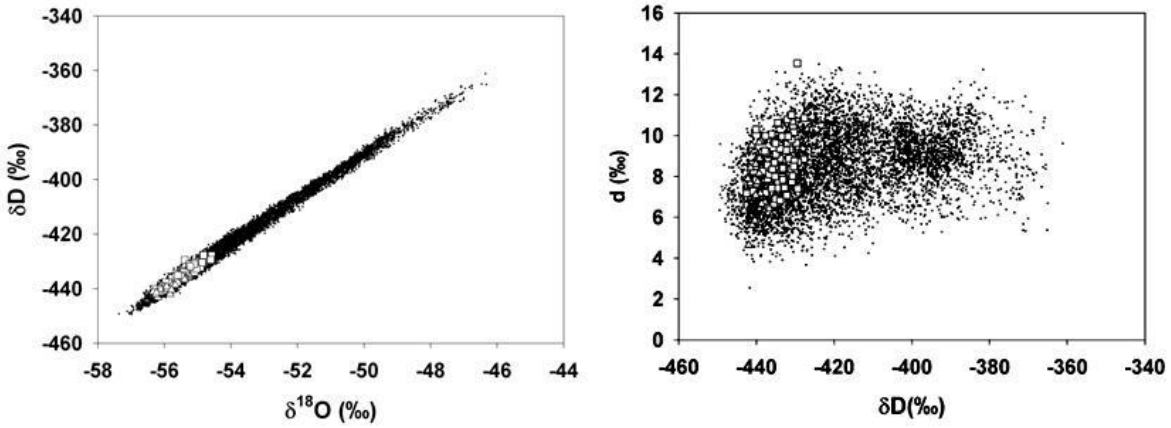

Figure 41: a) δD_{ice} (‰) vs. $\delta^{18}O_{ice}$ (‰) and b) d (deuterium excess ‰) vs. δD_{ice} (‰) for the deep (open squares) and basal (open triangles) ice at EPICA Dome C, as compared to the ice above 3200m (black dots). See text for details.

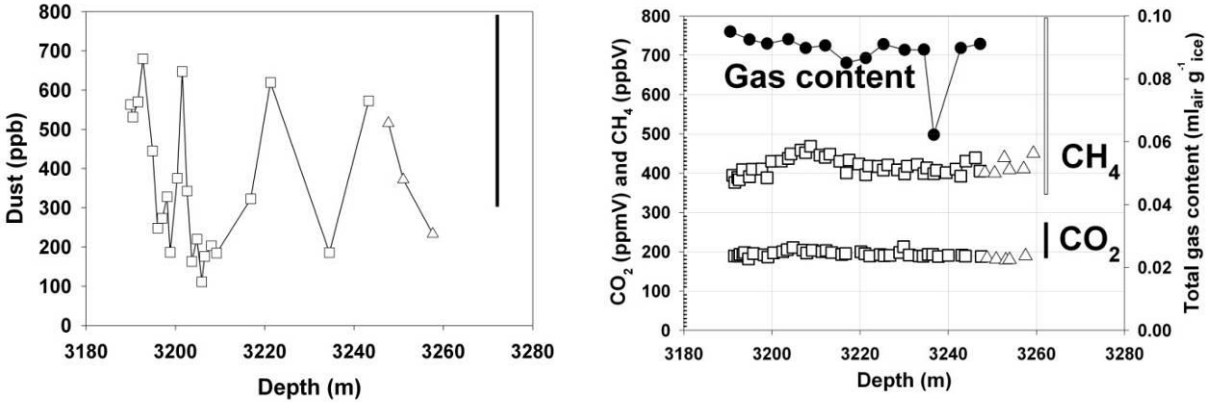

Figure 42: Gas and dust properties of the deep (open squares) and basal (open triangles) ice at EPICA Dome C: a) total gas content ($ml_{air}g_{ice}^{-1}$, black dots), methane (ppbV) and carbon dioxide (ppmV) - white and black vertical bars cover the full concentrations range observed respectively for CH_4 and CO_2 during the preceding climatic cycles, b) dust concentrations (ppb) -black vertical bar covers the full glacial range during the previous climatic cycles.

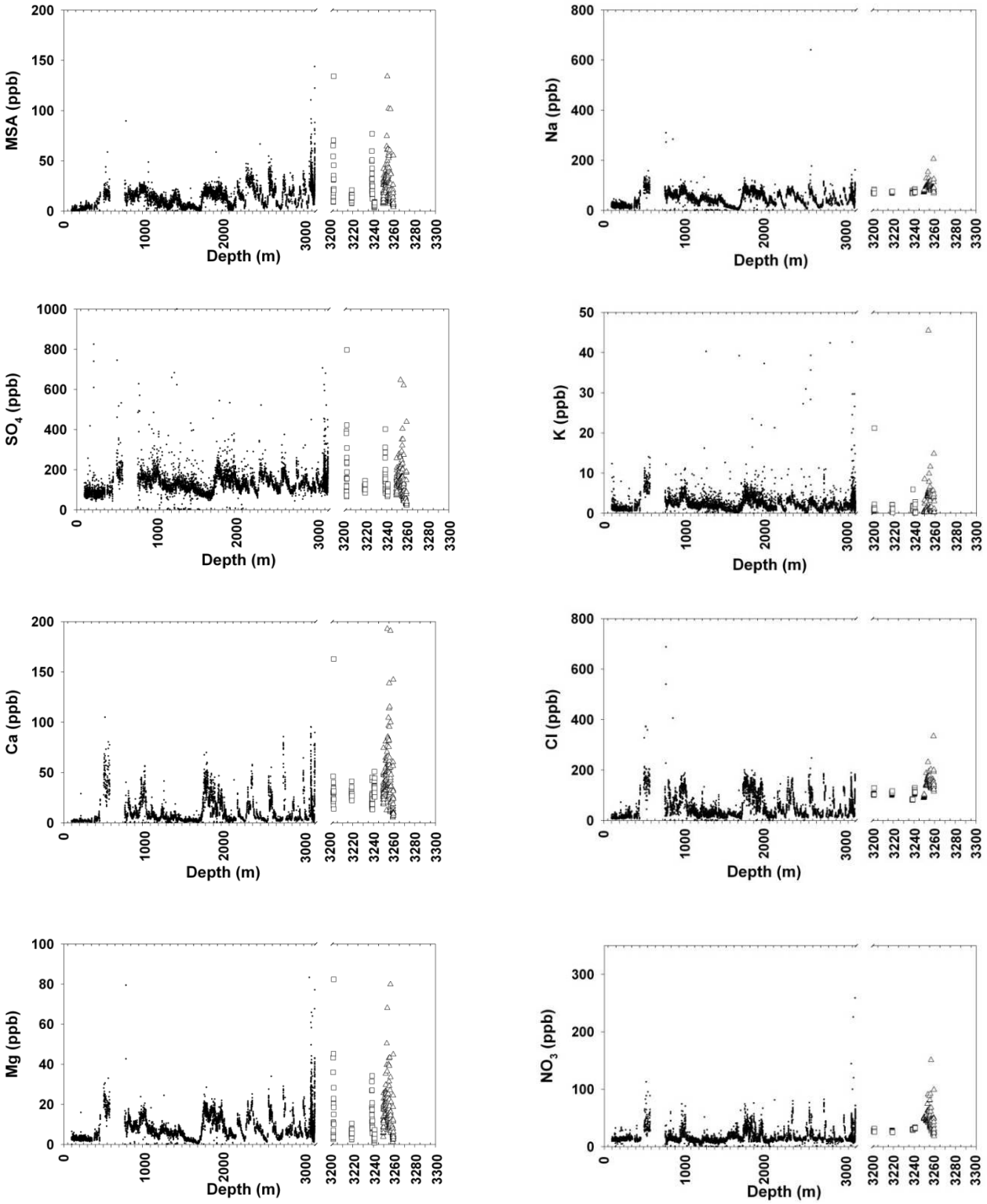

Figure 43: Concentrations (in ppb or ngg^{-1}) of selected chemical species in the deep (open squares) and basal (open triangles) ice of the EPICA Dome C core, as compared to those of the preceding climatic cycles (black dots, courtesy of the EPICA chemical consortium). Resolution is between 5 and 8 cm above 3200m depth and between 1.5 and 5 cm in the deep and basal ice below 3200 m. Note the change of depth scale below 3200m

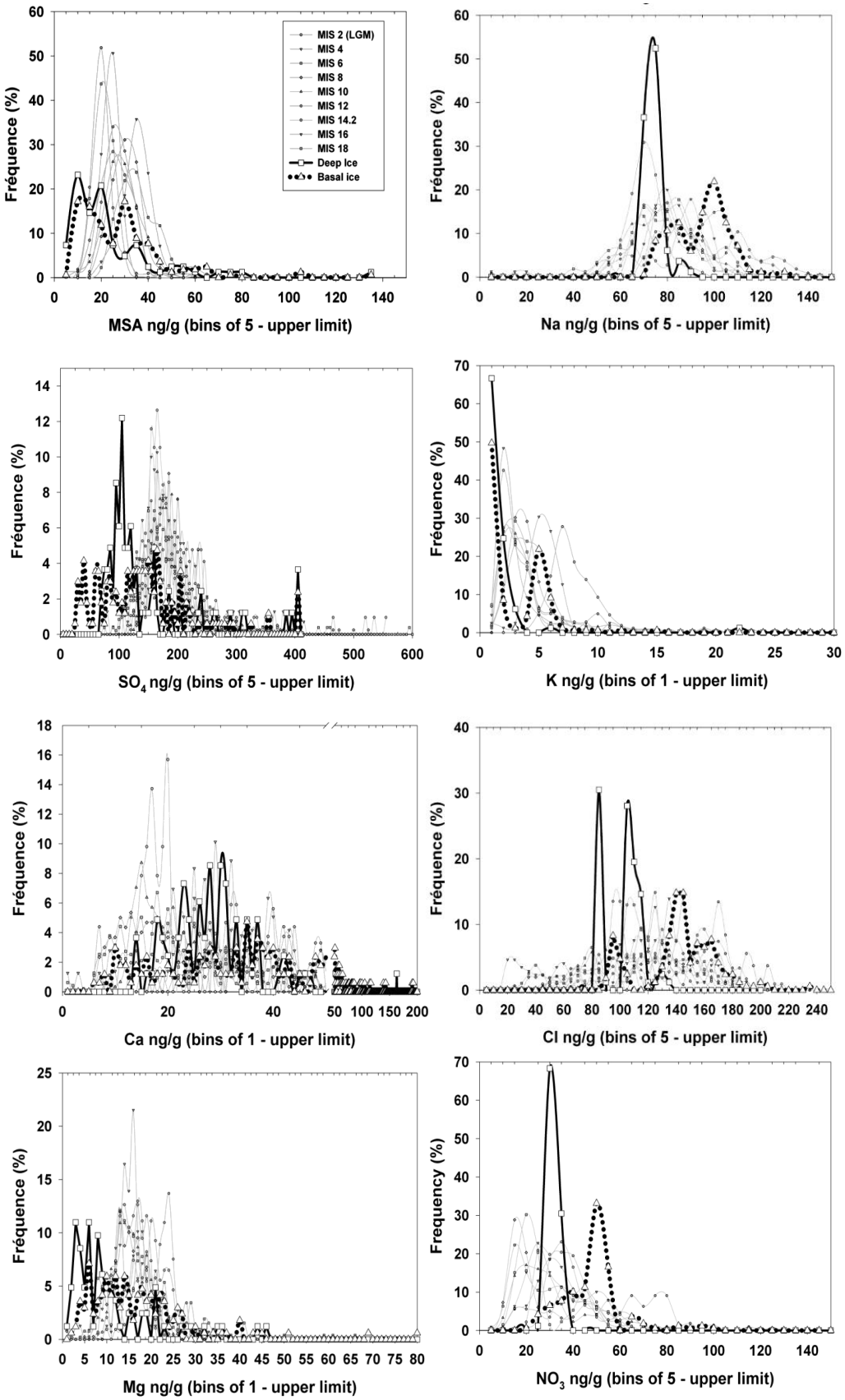

Figure 44: Frequency distribution of concentrations (in bins of 1 or 5 ngg^{-1} or ppb) of selected chemical species in the deep (open squares - thick black solid line) and basal (open triangles - thick black dotted line) ice of the EPICA Dome C core, as compared to those for the preceding full glacial periods (incremented symbols and thin grey lines - courtesy of EPICA Chemistry Consortium). See text for definition of « full glacials ».

Deep and basal ice concentrations of selected chemical species (MSA, SO_4, Ca, Mg, Na, K, Cl, NO_3) are presented in two complementary ways, respectively in Figures 43 and 44. In Figure 44 high-resolution (1.5 to 5 cm) profiles of discrete sections in the deep (open squares) and basal (open triangles) ice are shown, along with the 5-8 cm resolution profile in the ice above 3200m (black dots, courtesy of the EPICA Chemistry Consortium). In Figure 44 the same data set has been re-arranged as a simple frequency distribution within bins of 5 or 1 ngg^{-1} depending on the species. Deep ice is plotted as open squares on thick solid line and basal ice as open triangles on thick dotted line. All data from preceding "full glacial" intervals (i.e. excluding transitions) are plotted as a background in thin grey lines with incremented symbols (see caption in upper left graph for MSA). Table 1 summarizes the data set used in Figure 44 in terms of concentration means and 1σ-values, with the depth and isotopic ranges associated to each time interval chosen. Finally, Figure 45 plots the mean equivalent crystal radii for the deep and basal ice (symbols as above), as obtained from preliminary measurements in the field, and compare those to both measurements using Automatic Ice Texture Analyzers and modelling results described in Durand et al. (2008).

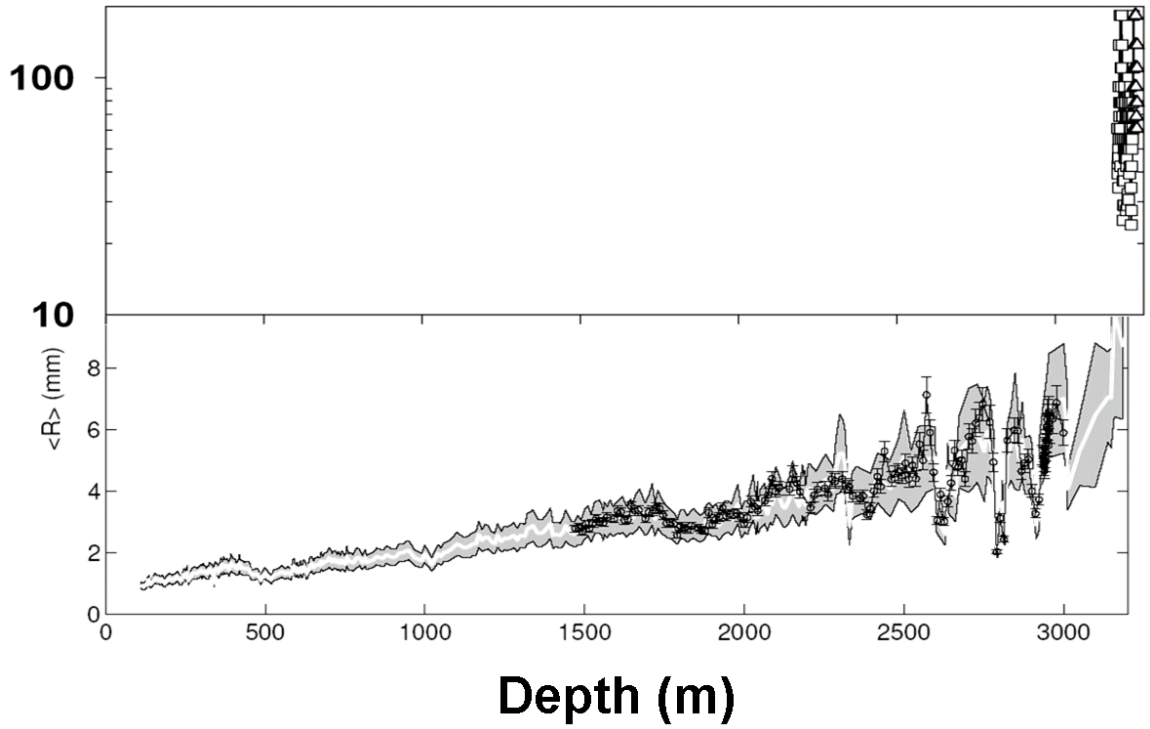

Figure 45: Mean equivalent crystals radii in the deep (open squares) and basal (open triangles) ice layers of the EPICA Dome C ice core, as compared to measurements (crosses) and modelling range (white line and grey shaded area) in ice above 3200m depth from Durand et al. (2007). Deep and basal ice measurements are preliminary results obtained using the linear intercept technique « on site» while the data from above 3200m were obtained using Automatic Ice Texture Analyzers (AITAs - Wang and Azuma, 1999; Russell-Head and Wilson, 2001; Wilen et al., 2003). Note the difference in scale between the lower (linear) and upper (logarithmic) panels.

Glacial	Depth range (m)		Isotopic range (δD ‰)		MSA (ngg^{-1})		SO_4 (ngg^{-1})		Ca (ngg^{-1})		Mg (ngg^{-1})	
			min	max	mean	σ	mean	σ	mean	σ	mean	σ
MIS 2	507.72	583.46	-449.3	-432.8	**18.24**	*7*	**213.78**	*85.15*	**43.27**	*14.89*	**19.31**	*4.08*
MIS 4	1007.63	1042.22	-446.4	-430.5	**20.94**	*4*	**194.8**	*52.52*	**30.85**	*10.96*	**14.28**	*3.84*
MIS 6	1801.83	1997.02	-447.1	-419.8	**18.6**	*5*	**170.01**	*51.73*	**23.6**	*12.25*	**13.54**	*4.04*
MIS 8	2320.04	2398.55	-444.5	-421.5	**27.9**	*6.13*	**192.05**	*50.92*	**23.37**	*12.98*	**14.92**	*4.28*
MIS 10	2599.91	2649.96	-445	-425.1	**26.77**	*7.88*	**183.55**	*43.56*	**22.92**	*9.84*	**14.92**	*3.86*
MIS 12	2783.21	2794.94	-440.9	-422.5	**23.44**	*5.04*	**187.36**	*45.54*	**43.47**	*19.09*	**19.82**	*5.5*
MIS 14.2	2915.73	2919.88	-436.4	-429.3	**23.75**	*6.37*	**162.06**	*21.72*	**20.46**	*6.19*	**15.8**	*2.75*
MIS 16	3037.57	3039.77	-441	-412.3	**32.61**	*6.95*	**167.86**	*39.55*	**36.09**	*17.21*	**16.37**	*5.84*
MIS 18	3137.83	3153.12	-441.4	-423.7	**36.4**	*23.47*	**195.35**	*139.18*	**31.26**	*19.76*	**20.03**	*25.47*
Deep Ice	3201	3248	-442.5	-427.7	**21.5**	*20.32*	**150.39**	*107.98*	**29.53**	*16.87*	**11.49**	*12.48*
Bottom Ice	3248	3259.3	-443.2	-436.7	**25.27**	*18.43*	**139.58**	*91.46*	**42.1**	*29.44*	**16.25**	*11.23*

Glacial	Depth range (m)		Isotopic range (δD ‰)		Na (ngg^{-1})		Cl (ngg^{-1})		NO_3 (ngg^{-1})		K (ngg^{-1})	
			min	max	mean	σ	mean	σ	mean	σ	mean	σ
MIS 2	507.72	583.46	-449.3	-432.8	**97.37**	*17.54*	**160.68**	*48.64*	**40.93**	*16.01*	**7.45**	*1.89*
MIS 4	1007.63	1042.22	-446.4	-430.5	**79.81**	*17.75*	**129.89**	*25.25*	**29.38**	*12.41*	**4.91**	*2.34*
MIS 6	1801.83	1997.02	-447.1	-419.8	**71.57**	*16.65*	**107.56**	*40.45*	**24.72**	*12.63*	**3.74**	*2.36*
MIS 8	2320.04	2398.55	-444.5	-421.5	**76.76**	*35*	**112.06**	*38.05*	**26.24**	*17.2*	**3.84**	*5.24*
MIS 10	2599.91	2649.96	-445	-425.1	**77.8**	*32.3*	**112.76**	*61.56*	**30.21**	*19.92*	**5.77**	*9.76*
MIS 12	2783.21	2794.94	-440.9	-422.5	**72.7**	*19.82*	**138.46**	*34.04*	**48.69**	*22.43*	**3.93**	*3.32*
MIS 14.2	2915.73	2919.88	-436.4	-429.3	**70.88**	*15.13*	**110.46**	*21.66*	**34.33**	*17.31*	**3.16**	*5.7*
MIS 16	3037.57	3039.77	-441	-412.3	**78.23**	*12.32*	**111.67**	*21.46*	**32.89**	*11.94*	**3.07**	*4.96*
MIS 18	3137.83	3153.12	-441.4	-423.7	**80.44**	*13.94*	**114.44**	*31.38*	**26.28**	*13.95*	**3.26**	*3.98*
Deep Ice	3201	3248	-442.5	-427.7	**71.78**	*3.79*	**99.91**	*13.39*	**29.03**	*2.42*	**1.94**	*2.4*
Bottom Ice	3248	3259.3	-443.2	-436.7	**93.16**	*15.43*	**141.68**	*30.42*	**46.26**	*15.37*	**2.68**	*4.17*

Table III: Mean concentration and 1□ values (ngg^{-1} or ppb) for selected chemical species in the Deep and Basal ice of the EPICA Dome C ice core, as compared to those of the preceding full glacial periods. Depth (meters) and □D (‰) ranges are given for each time interval considered.

In this first section of the discussion, we will demonstrate that some of the deep and basal ice properties appear coherent with an unmodified climatic signature. As shown in Figure 42a,b both the deep and basal ice display δD values typical of a mild to cold glacial period, with respective ranges of -427.7 to -442.5‰ and -436.7 to -443.2‰ (Table III), as would be expected for MIS 20. In the co-isotopic δD-δ^{18}O diagram of Figure 44a, all samples align well with those from the previous climatic cycles, with a slope of 8.48, close to the value of 8.19 for the samples above 3200m, i.e. in accordance with a Meteoric Water Line. This is very different from the Vostok case, where the refrozen lake ice samples were shown to be clearly located on a freezing slope of 4.88, only slightly higher than the theoretical one calculated from the estimated lake water isotopic value (Souchez et al., 2002a). Also, the d_{excess} values shown in Figure 44b are within the range of those observed in the previous glacials, while refreezing processes are known to lower the deuterium excess values (Souchez et al., 2002a, Souchez and Lorrain, 1991). These are first arguments to preclude large scale refreezing as a plausible process for our bottom ice formation.
The gas properties of the bottom ice are probably even more convincing of a true climatic signature (Figure 42a). The total gas content, to the exception of a single suspicious value, is very stable with a mean value at 0.088 $ml_{air}g^{-1}_{ice}$, which happens to be identical to the one obtained for the whole 0-400 ky interval further up in the core (Raynaud et al., 2007). Methane and Carbon dioxide signatures are also extremely stable and typical of full glacial conditions (mean values of respectively 417 ppbV and 193 ppmV). Although they show much larger variations, most of dust concentrations also typically lie within the boundaries of a full glacial range (Figure 42b).

Table 1 gives the mean concentration values of the considered suite of chemical species. A systematic comparison of the deep ice and bottom ice mean values to those of each of the previous full glacial episodes (with similar δD ranges) shows very good compatibility, further suggesting that the mean paleoclimatic signal has not been modified in the vicinity of the ice-bedrock interface. Indeed, any large-scale regelation process of meteoric ice meltwater would induce significant departure of the chemical composition (both in terms of total impurity content and of chemical speciation) of the refrozen ice from the initial values present in the meteoric ice. de Angelis et al. (2005, 2004) have shown that, in the case of refreezing of the Lake Vostok water, away from any sediment source (ice type 2), the concentrations were significantly lower than those in meteoric ice, in accordance with the efficient rejection of impurities during freezing at very low rates. Conversely, the upper part of the Vostok lake ice, that is thought to have accreted in a shallow bay upstream of Vostok (ice type 1), shows a total ionic content 5 to 50 times higher than meteoric ice, with a specific signature suggesting contamination from salts originating from deeper sedimentary strata, close to evaporites in composition.

Clues for a “disturbed” paleoclimatic record

There are however some features of the bottom ice that raise questions about its paleoclimatic significance. As stated above, the presence of visible solid inclusions aggregates in the lower 12 meters could be the result of incorporation processes of sedimentary material at the ice-bedrock interface (Boulton, 1979, , 1996, Cuffey et al., 2000, Gow et al., 1979, Gow and Meese, 1996, Herron and Langway, 1979,

Holdsworth, 1974, Iverson, 1993, Iverson and Semmens, 1995, Knight, 1997, Koerner and Fisher, 1979, Souchez et al., 1988, Souchez et al., 2000b, Tison and Lorrain, 1987, Tison et al., 1993, Tison et al., 1989). Comparison of Figure 43b with 43c reveals a strong discrepancy between the EDC δD record and the benthic record stack of Lisiecki and Raimo (2005) prior to 800 ky, without showing MIS21 in the EDC profile which, instead, displays an unusually long glacial period. Furthermore, the $\delta^{18}O_{atm}$ profile of Figure 43d is also somewhat peculiar, in two ways: first it is extremely stable despite known large fluctuations in the precession and ice volume at the time, to which the $\delta^{18}O_{atm}$ has been shown to be very sensitive (Bender, 2002, Dreyfus et al., 2007, Jouzel et al., 2007), and, second, it displays values close to 0‰, which are generally typical of full interglacial rather than full glacial.

Finally, although generally coherent with the previous climatic cycles in terms of mean concentration values, individual chemical species can be regrouped in two pools with specific and contrasted chemical dispersion behaviour (Figure 43 and 44, Table III). MSA, SO_4, Ca and Mg, on the one hand, clearly show increased variability, both in the deep and basal ice (see left column of Figure 43 and 1σ values in Table III), a trend that seems to initiate in MIS18 already. The frequency distributions in Figure 44 confirm this variability as compared to previous glacials, with a tendency of skewing towards lower values for MSA, SO_4 and Mg, especially in the deep ice. On the other hand, Na, K, Cl, and NO_3 behave noticeably differently in the deep ice and in the basal ice (right column in Figure 43). The deep ice shows very low variability and narrow frequency peaks in the graphs of Figure 44, while the basal ice behaves similarly to the previous glacial, but with a tendency of skewing towards the higher range of concentrations.

Mechanisms for dissolved and solid impurities distribution and relocation within ice cores

Ohno et al. (2005) recently discussed the location and chemical forms of water-soluble impurities in ice cores. Initially entrapped in-between the snow grains that will evolve into firn and then ice under increasing metamorphism, these could therefore be found either within the ice crystals themselves, or within the unfrozen liquid that separates the grain boundaries as a result of “premelting” (Rempel et al., 2001, Rempel et al., 2002, Wettlaufer, 1999), be it veins, nodes or triple junctions. A common view amongst glaciologists is that because those impurities produce strain-energy within ice grains and because trace acids must exist as acid solutions given their very low eutectic point, they will progressively be forced into grain boundaries as grain growth and recrystallization occur (Glen et al., 1977, Rempel, 2003, Rempel et al., 2001, Rempel et al., 2002, Wettlaufer, 1999). Although this has been confirmed for sulfur atoms at triple junctions of grain boundaries in the early days of scanning electron measurements in ice (Mulvaney et al., 1988), there has been growing evidence that e.g. sulfates also exist as salts trapped as inclusions within grains (e.g. Baker and Cullen, 2003). Ohno et al. (2005), using micro-Raman spectroscopy, underline that even at shallow depth (185m) in the Dome Fuji ice core, the fraction of SO_4^{2-} existing as salts within the micro-inclusions exceeded 50% of the total SO_4^{2-}. Similar fraction values between 30% and 60% were found for Na^+, Ca^{2+} and Mg^{2+} in discrete samples spanning the 5.6 to 87.8 ky BP interval.

Relocation of impurities under increasing recrystallization is likely to become important in the deeper part of ice cores, where the ice temperature gets closer to the pmp and the temperature gradient generally increases. One of those relocation processes, that has been intensively discussed in the recent years, is the mechanism often referred to as “anomalous diffusion” (Rempel, 2003, Rempel et al., 2001, Rempel et al., 2002). In this process, it is surmised that, as grains slowly grow and recrystallize within ice sheets, most of the impurity molecules are preferentially excluded from the solid grains and enriched in the melt. As the polycrystalline mixture of ice and premelt liquid solution flows downwards under gravity at a velocity “v”, it encounters gradual variations in temperature leading to gradients in intergranular concentrations which, in turn, drive molecular diffusion of solutes relative to the porous ice matrix. The net result is that the bulk impurity profile will move downwards at a rate that differs by a finite “anomalous velocity” v_c from the downwards velocity “v” of the ice itself. A typical modelling case study for the conditions at the location of the GRIP ice core predicts separation of the bulk-impurity profile from the contemporaneous ice by a maximum amount of about 90 cm in the bottom layers (3028m). Note that, as underlined by Ohno et al. (2005), this theory relies on the postulate that all impurities are located at grain boundaries. If, as discussed above, a fair share of these are distributed within the crystal itself, then the process is likely to be considerably hampered (Rempel, 2003). Another important feature of this migration process is that the amplitude of the concentration changes should not be altered, even in the case of asynchronous initial deposition of different species with contrasted concentration levels (Rempel, 2003) . It is therefore difficult to invoke anomalous diffusion to explain the contrasts in species concentration variability observed in our bottom ice at EPICA Dome C.

Another interesting process discussed by Rempel (2005), is the one in which the density difference between interstitial premelt water and ice produces a hydraulic gradient that drives a downwards liquid flow. When the temperature rises towards the glacier bed, the associated permeability increase leads to more rapid fluid transport, internal melting supplying the changing flow. Although the author shows that, in the specific case where the lower region of the glacier floats on a subglacial reservoir, a reduction in the hydraulic gradient results from surface energy effects and causes a decreasing transport rate in the lower few tens of centimetres, this process provides a potential mechanism for downwards migration of the chemical compounds accumulated in the premelt layer as recrystallization at high temperature proceeds. It could therefore be invoked to explain why, for some of the species (Na, K, Cl and NO_3, right columns in Figures 43 and 44) involved in this study, the deep ice shows concentrations in the low range of the glacial spectrum while the basal ice is generally bi-modal and skewed towards the higher concentration values.

Finally, it is also worth looking at the few detailed studies on impurity distribution within the accreted lake ice of Lake Vostok (de Angelis et al., 2005, de Angelis et al., 2004). Although the form (solid vs. dissolved) and origin of these impurities might differ from those found in meteoric ice above, both ice types (bottom meteoric ice at EDC and accreted ice at Vostok) have been submitted to intense recrystallization (strong 10-fold increase of grain size in the EDC bottom ice - Figure 45, and huge - several tens of cm in size- crystals at Vostok, (Montagnat et al., 2001)) at high temperatures (>-5°C), potentially involving impurity relocation. It is interesting to note that their high-resolution spatial distribution presents striking similarities. Indeed, fine-

scale (1 cm) analyses of accreted ice samples at Vostok (e.g. Fig. 5 in de Angelis et al., 2004) show that Cl, Na, F and NO_3 have a uniform distribution throughout the samples, while SO_4, Ca and Mg are much more heterogeneous. This is clearly the behavior we have underlined in our EDC bottom ice (Figures 43 and 44): much higher variability in the bottom ice than in the meteoric ice above, and much higher variability for SO_4, Ca, Mg and MSA than for Na, K, Cl and NO_3 in both the deep and basal ice layers. In the case of the Vostok accreted ice, de Angelis et al. (2005) suggest that Cl, Na and K are incorporated within the ice as brine micro-pockets, while SO_4, Ca and Mg are present in the form of insoluble material (initially suspended in the lake water),all impurities being originally randomly distributed within the unconsolidated frazil ice lattice. These authors then surmise that, as consolidation, grain growth and recrystallization occur at high temperature (-3°C), ice-soluble ionic species like Cl^-, Na^+ or NO_3^- become more efficiently distributed throughout the ice lattice, evolving towards homogeneity, while the other ions or very fine sulfate salt particles, which are not in equilibrium with the ice lattice, are excluded and gathered in inclusions of increasing sizes, leading to a greater heterogeneity. Although SO_4 and associated species clearly could not initially exist as a suspension in lake water in the EDC case (where refreezing of a water body is inconsistent with the isotopic and gas data sets), a similar relocation process under recrystallization could have been at work, as illustrated below.

A scenario for the evolution of the EPICA deep and basal ice

We have seen in the previous sections that some of the properties of the EDC bottom ice are consistent with a pristine paleoclimatic record, while others raise some suspicion. We have also demonstrated that significant net refreezing of a water body at the bottom of the ice sheet can be discarded. Another set of processes that have been shown to alter the basal ice properties is mixing or folding under enhanced deformation close to the ice-bedrock interface (Souchez, 1997, Souchez et al., 1998, Souchez et al., 2002a, Souchez et al., 1995b, Souchez et al., 2003, Souchez et al., 2002b, Souchez et al., 2000b). Among the anomalies in EDC bottom ice properties, the stability of the δD profile for an unusual period of time, if we trust the EDC time scale and compare our data to the Lisiecki and Raimo benthic record (Figure 40) is probably the most prominent. Homogenization through mixing is a process that has been invoked by Souchez et al. (2002a, 2002b) to explain the isotopic properties of the 3400-3538m Vostok depth interval, just above the meteoric-lake ice interface. They indeed show that the δD values are there bracketed in a tight range corresponding to mean values between glacial and interglacial, and that the deuterium excess variability is also strongly reduced. If this was the case for the EDC bottom ice, we should expect, from the comparison of Figures 40b and 40c, that the bottom ice shows mean isotopic values between those of MIS20 and MIS21 in Figure 41b, which it does not, being truly of glacial signature. Also, samples from the deep and bottom ice span the whole glacial deuterium excess range. Mixing with a local end-term inherited from a previous or initial ice sheet configuration is also unlikely. It has only been described for basal ice condition largely below the pmp and generally shows contrasted properties between the present-day ice sheet ice and the local end-term, with a whole range of intermediate values in the mixing zone.

If mixing is therefore improbable at EDC, another mechanical way of explaining the abnormal length of MIS20 is relative vertical stretching under changing stress

conditions, i.e. alteration of the stratigraphic time scale. Although, given the location chosen for the EPICA Dome C drilling, stress conditions should be (and are) essentially those of vertical uniaxial compression, Durand et al. (2008) indicate that the fabrics in layers of larger mean crystal sizes (about 6 mm) below 2850 meters show signs of dispersion of the strong single maximum (which is the rule below 1500m depth) along a weak vertical girdle. These changes might be the sign of evolving stress conditions near the bottom of the ice sheet, and were recently interpreted so, to explain anomalous flow below 2700m (Dreyfus et al., 2007) and reworking of sulphate spikes below 2800m under increased recrystallization (Traversi et al., 2006).

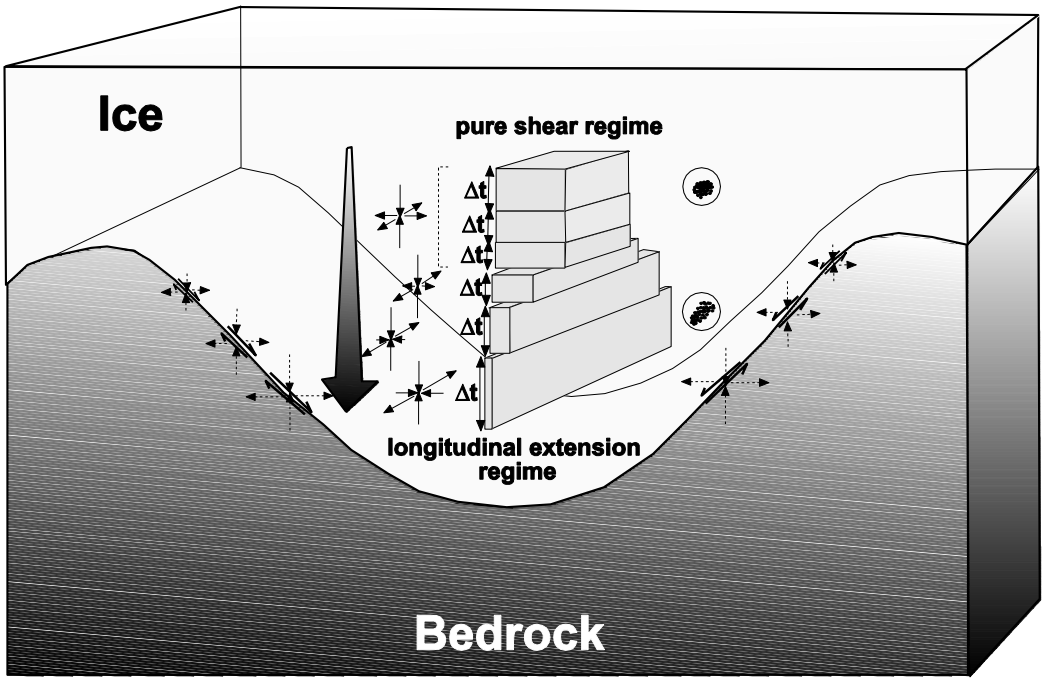

Figure 46: Schematic of the hypothesized impact of the confining bedrock topography (elongated valleys typically several tens of meters deep - Remy and Tabacco, 2000) on the stress regime, layer thickness and ice fabric patterns in the bottom ice of EPICA Dome C.

In Figure 46, we schematically show what might be the impact of a confining bedrock topography consisting of elongated valleys tens of meters deep (Rémy and Tabacco, 2000) on the stress field and the ice fabric in the bottom ice of EPICA DC. As the ice moves passed the crests of the subglacial valleys, simple shear associated with the friction on the lateral sides of the valley will progressively combine with the uniaxial vertical compression. The resulting stress field, will therefore transition form uniaxial vertical compression to longitudinal extension, as illustrated by the 3D-arrows in the central part of the drawing of Figure 46. The associated change in fabrics will be from a vertical single maximum to a vertical girdle fabric, in a plane parallel to the subglacial valley sides. This new pattern might be the one already suggested in the discretely changing fabrics described by Durand et al. (2008) below 2800 meters. Because the principal stress transverse to the subglacial valley slowly shifts from extensional to compressive, the result could be a *relative* vertical stretching of individual accumulation layers, depending on the intensity of the principal extension along the valley axis.

In that context, we can now propose a plausible scenario for the evolution of the properties of our deep and basal ice at EPICA Dome C, as illustrated in Figure 47. A changing stress field and the high temperatures, close to the pmp, will trigger sustained migration recrystallization within the bottom layers. Mean crystal size values (up to more than 10 cm) plotted in Figure 45 are undisputable proof that recrystallization is indeed very active there. This process will tend to relocate the impurities at grain boundaries. Increasing water content in the premelt layer will also slowly initiate downwards density-driven migration of the water and of the associated impurities. The latter will behave differently, depending on the species. Detailed SEM and XRF micro-probe elemental analyses of individual aggregates inside the EDC basal ice are described in a companion paper (de Angelis et al., in prep.). They reveal that $CaCO_3$ and $CaSO_4$ are common within these aggregates. These compounds could then be either newly precipitated salts (as observed concentrations are compatible with saturation for e.g. $CaSO_4$ given estimated vein sizes at those ambient temperatures) or pre-existing solid inclusions, eventually initially present inside the crystals (Ohno et al., 2005). SO_4, Ca, Mg and MSA (which can also be associated with salts, Ohno et al., 2005) mean concentrations in the deep ice and the basal ice will therefore remain within the range of other glacials, but their spatial distribution at the high-resolution scale of sampling, will show much greater variability than meteoric ice above (Figures 43, 44 and 8-right column). The other group of species (Na, Cl, K, NO_3) will remain in the dissolved state within the premelt layer, and partly and more easily migrate downwards. A remaining fraction of these ice-soluble ionic species will however be redistributed homogeneously within the recrystallized grains. We therefore observe a narrow frequency distribution for these species (Figure 44), and mean concentration values that are on the low side of glacial ranges in the deep ice (Figure 43, Table III). This left skewing of the concentration frequency distribution in the deep ice is also somewhat the case for MSA, SO_4 and Mg. As expected from the premelt migration process, concentration frequency distributions for Na, K, Cl and NO_3 in the basal ice are bimodal (in crystals vs. in premelt) and skewed towards the high side of the range observed in the other glacials.

The large inclusions visible in the bottom 12 meters of basal ice are principally located at grain boundaries. Theoretical considerations from Alley et al. (1986, eq. 21) should lead to a high velocity ice grain boundary migration regime, with decoupling of the grain boundaries from the particle aggregates, because of their relatively large sizes and very low volume fraction. However, as underlined by these authors, this is probably no more valid for the “warm” (EDC bottom) ice, in a full migration recrystallization process, where the increased water content in the vein network will favour Ostwald ripening as the temperature of the ice-impurity system rises above the melting point of the impure grain boundaries. Another feature to consider here is that the particle aggregates might also behave very differently from single particles in terms of drag force on the grain boundaries.

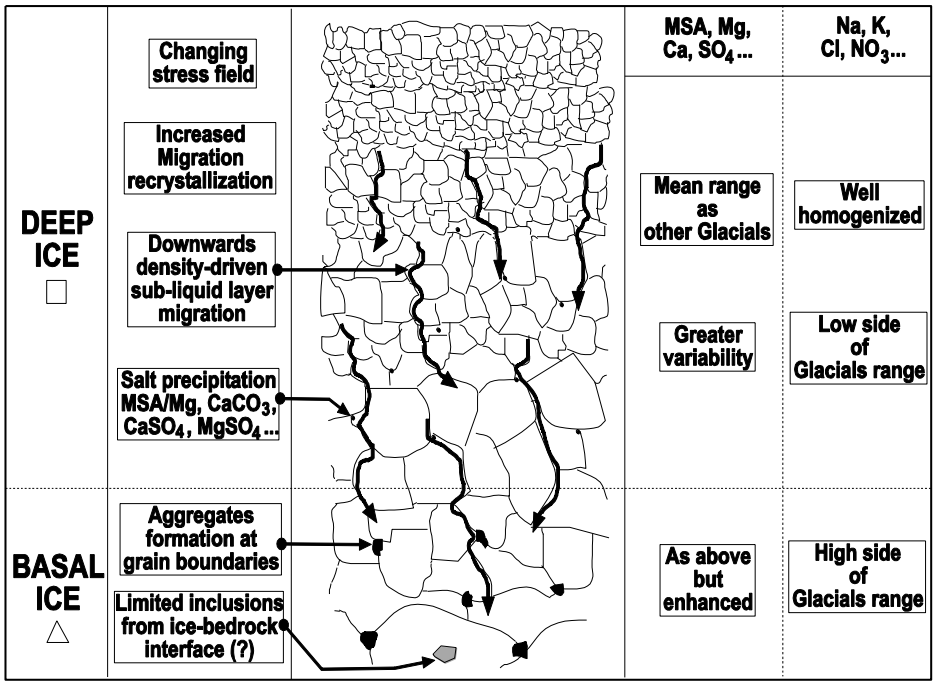

Figure 47: Sketch of potential chemical sorting effects during enhanced migration recrystallization processes under a changing stress field, close to the pressure melting point, in the deep and basal ice of EPICA Dome C (see text for details).

We have until now focused on a plausible explanation for the peculiarities of the chemical signature of our deep and basal ice at EDC. How do the gas and dust properties fit into the proposed mechanism? Why would the relocation process invoked for the chemical impurities not alter the total air content or the CH_4 and CO_2 concentrations? First of all, it should be noted that the resolution of our gas data sets is much lower than the one we achieved for the chemical species. Also, one should remember that the gas molecules are exclusively present as clathrates at these elevated depths and little is known on the behaviour of those during small-scale phase changes under large overburden pressures. If the glacial MIS20 "stretching" hypothesis is valid, it is not surprising to observe a stable $\delta^{18}O_{atm}$ signal. More puzzling is the fact that the values are more typically interglacial in nature (close to 0‰, Figure 40d). However, careful comparison of the $\delta^{18}O_{atm}$ and δD curves for Vostok and EDC (e.g. in Figure 40, Dreyfus et al., 2007and Figure 40b,d of this report) shows that in every glacial there is at least one time period when $\delta^{18}O_{atm}$ is close to 0‰ and δD values are similar to those observed in our EDC bottom ice (-427 to -443 ‰). These intervals would correspond to episodes where precession favours warm northern hemisphere summers and would therefore represent glacial conditions with a strong (East) Asian monsoon. Unfortunately, the resolution of the dust record in our bottom ice does not allow us to appropriately discuss potential contradictions with the proposed mechanisms discussed above, but at least the large variability of the data within the glacial range would fit into our increased relocation scheme.

Conclusions

We have used a multiparametric approach to discuss the plausibility of recovering an unaltered paleoclimatic signature from the deep and basal ice of the EPICA Dome C ice core. We have shown that some of the data (δD values, total air content, gas

composition, dust content, mean chemical species concentrations) suggest a pristine meteoric glacial signature while others (length of the glacial, $\delta^{18}0_{atm}$, visible inclusions, variability of the chemical species distribution) betray mechanical and compositional alteration of the bottom ice. Ice stable isotopes and total air content rule out large scale refreezing processes of a water reservoir as the origin for the bottom ice. Mixing, be it internally (as in Vostok MIS11) or with a local ice remnant of previous or initial ice sheet configuration (as in GRIP and Dye-3) can be equally discarded.

Using a new high resolution data set for selected chemical species in the deep and basal EDC ice and remote sensing information on the general setting of the Dome C area, we propose a mechanism in which the confining bedrock topography contributes to a downwards change in the stress field from uniaxial vertical compression to longitudinal extension along the valley axis. This stress configuration change results in a potential vertical stretching of the ice layers, which explains the abnormal length of MIS20. Combined with an ice temperature close to the pressure melting point it also favours rapid migration recrystallization, as witnessed by the large increase in grain size. This, in turn, induces relocation of dissolved and solid impurities, with accumulation of newly formed salts and already existing solid inclusions in the premelt layer, forming aggregates. Those become visible about 12 meters above the bottom of the core and increase in size and number downwards. The basal inclusions thus mainly consist of reworked existing material, rather than representing incorporation of allochthonous material from the ice-bedrock interface. Only a few potential candidates for the latter (large, single, non-spherical inclusions) were detected in the lowermost layer (de Angelis, in prep.). Although the mean concentration values were not significantly different from those observed in the previous full glacial periods, some chemical sorting is apparent, especially for those species that are not involved in salt formation. We suggest this results from a slow process of downwards migration of the premelt layer under the hydraulic gradient resulting from the density difference between ice and interstitial water. The ice isotopic, gas and dust properties are apparently not affected by these small scale processes that however only become detectable at high-resolution sampling (sub-crystal size). The apparent discrepancy in the $\delta^{18}O_{atm}$ signal is resolved if one considers potential stretching of a glacial time span during which precession favors warm northern hemisphere summers, as has happened temporarily in each of the previous glacial isotopic stages.

We conclude that the paleoclimatic signal is only marginally affected in terms of global ice properties at the bottom of EPICA Dome C, but that the time scale has been considerably distorted by mechanical stretching due to the increasing influence of the subglacial topography. It is interesting to note that MIS18 already shows signs of chemical relocation and increased variability for the species involved in salt formation (MSA, SO_4, Mg and, in a lesser extent Ca), before the timescale (EDC3) got significantly distorted. Along the same line the anomalous flow detected below 2700m, that led to the change from the EDC2 to the EDC3 time scale, might already find its roots in this subglacial topography distortion. Future work on the EPICA DC bottom ice will involve high resolution gas measurements in selected areas and an in-depth analysis of the crystallographic properties below 3200 meters. Hopefully, these will allow us to validate and refine the general mechanism discussed here.

2.4.6.2: Gas properties of basal ice from the Berkner Island ice core: alteration of the paleoclimatic signal goes well above the debris-rich basal ice layer

The Berkner Island ice core drilling project took place in 2004-2005 and was led by the British Antarctic Survey under a UK-France collaborative effort (Mulvaney et al., 2007). Berkner Island, the largest Antarctic Island, lies to the South of the Weddell Sea, embedded between the Ronne and the Filchner Ice Shelves (79°32.9'S, 45°40.7'W). The altitude at the drilling site is 890 m a.s.l. and the ice thickness 947 ± 1m. The basal temperature has been estimated at -11.6°C. It is therefore cold based. The motivation for the drilling was multiple and encompasses a) documentation of the ice thickness and volume in the Weddell Sea during the LGM, b) documentation of the phasing between Greenland Dansgaard-Oeschger events and Antarctic warm events in a coastal site and c) documentation of the AABW production under the Filchner-Ronne Ice Shelf during the LGM. The drilling reached a final depth of 948 meters, the bottom 0.5 meters of which being loaded with a uniform matrix of fine sand sediments in moderate concentration. Occasional larger particles conglomerate were also seen in this bottom section (Figure 48).

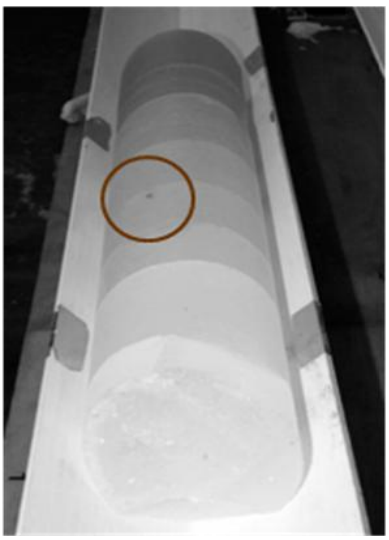

Figure 48: view of the basal section of the Berkner Island ice core bottom 0.5 m section on retrieval. The red circle shows larger inclusions.

We have been invited to investigate the gas composition of this cold bottom ice. Figure 49 shows the high resolution profiles of total gas content, gas composition and O_2/N_2 ratio in the bottom 110 cm of the core. A first striking observation is that none of the gas concentrations are atmospheric. The total gas content shows no significant trend, apart from a decrease within the bottom 20 cm. Some of the values are compatible with measured values at equivalent altitude (1000 m, 0.12) during the Dome Summit-Cape Folger traverse (Law Dome, Martinerie, PhD Thesis, unpublished); there is a slight loss in other places (0.10).

The bottom 20 cm also show a clear enrichment in methane and carbon dioxide, although in moderate amounts as compared to what has been measured at other cold based deep ice locations such as GRIP or Dye-3 in Greenland. This reflects a clear interaction with biogenic gases produced at the ice-bedrock interface. The

impact is not restricted to the bottom 20 cm, since both CO_2 and CH_4 show values above atmospheric in the whole profile. Another interesting feature in common with the GRIP and Dye-3 ice cores is the steady decrease of the O_2 concentration downwards, which cannot result from in-situ respiration, given the very moderate increase of carbon dioxide at equivalent levels. Argon is slightly depleted downwards suggesting moderate reworking in the presence of a water phase. The global regularity of the profiles is in strong contrast with what was describes at the bottom of the larger (and probably older) ice sheets, where large synchronous fluctuations of all the variables in the basal layers indicated active mixing processes between a local end term and the overriding ice sheet (see references p. 46). Here, the shape of the profiles is more suggesting a regular diffusion process between the soil at the interface and the overlying ice, maybe in the initial warmer stages of deposition where diffusion processes would have been facilitated during the firnification process. Obviously, in this case, the alteration of the paleoclimatic signal goes well above the debris-bearing bottom ice, and further investigations on the ice higher up will be required to get the complete picture.

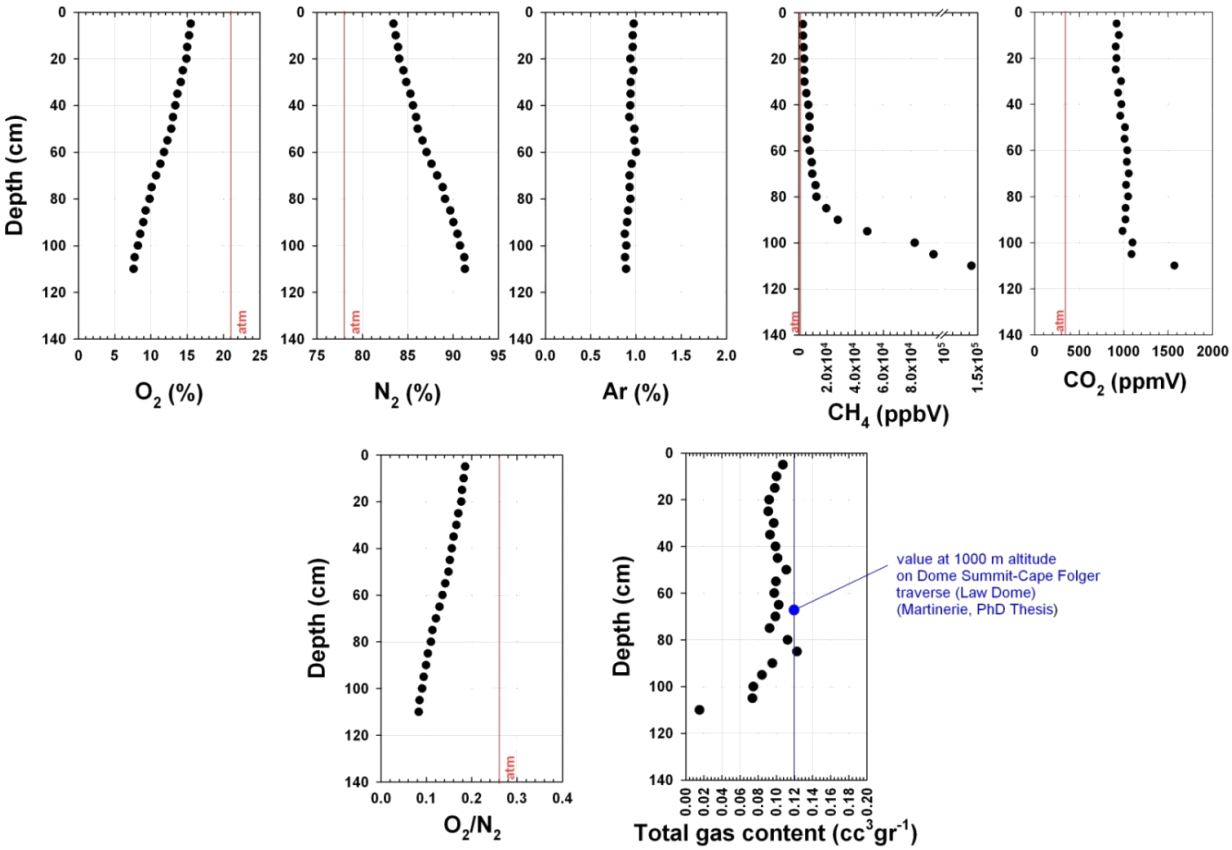

Figure 49: Gas properties of the bottom meter of the Berkner Island ice core.

2.4.6.3. Gas properties of the basal refrozen water from the EPICA DML ice core: a mixed signature of drilling contamination and subglacial processes at work

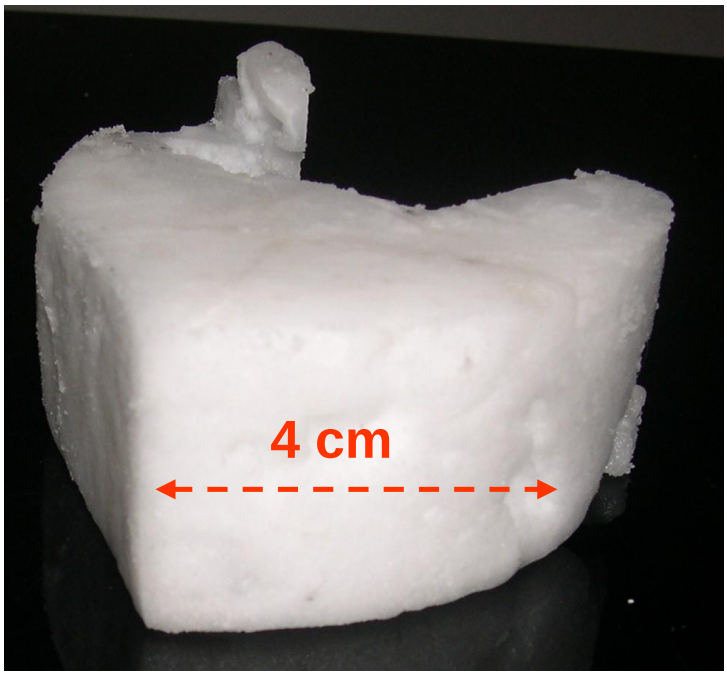

Figure 50:EPICA Dronning Maud Land basal refrozen water sample. Note the similarity to Chlathrate ice.

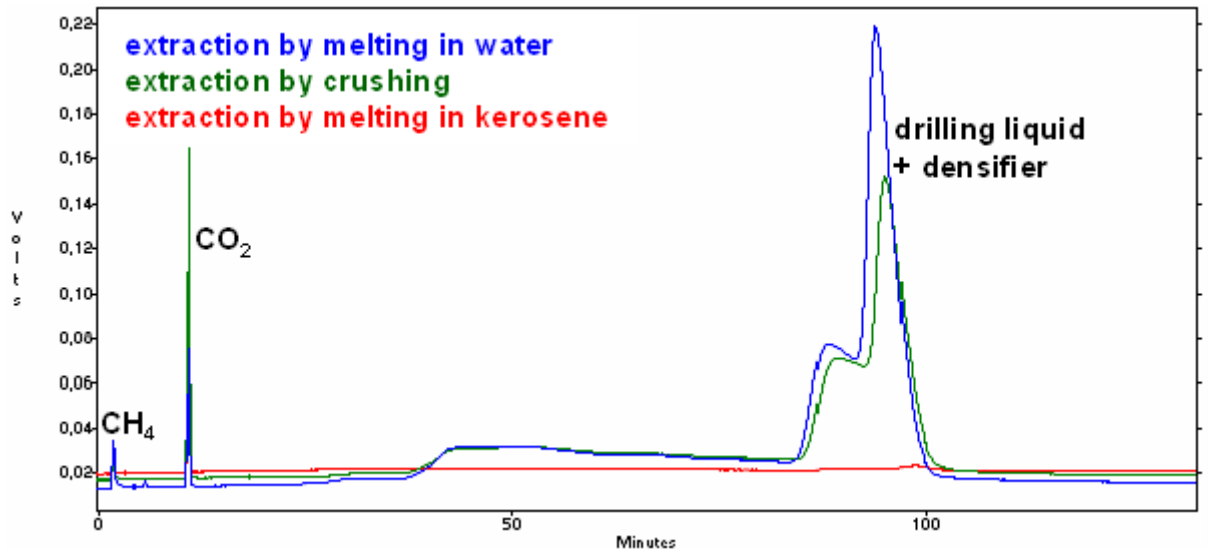

Figure 51: Combined chromatograph for the elution of three samples of gas extracted from the EDML refrozen water using three different techniques. The drilling liquid and densifier peak is clearly seen for the samples extracted by melting under water and crushing. It is however absent from the extraction method using melting in kerosene. This is explained by the fact that the density of the densifier and drilling liquid is higher than that of kerosene. These compounds therefore remain at the bottom of the melting.

We have been solicited by our colleagues of the Alfred Wegener Institute (S. Kipfstuhl) to contribute to the study of the basal refrozen water that has been collected in the EPICA Dronning Maud Land (EDML) drill hole, after unplanned infiltration of the subglacial water in the bottommost part of the ice sheet at that location. At the end of this deep drilling (2774.15 m), liquid water of subglacial origin swept and refroze into the bottom of the drill hole, in contact with the drilling liquid (Foran + D40) and the densifier (HCFC-141b). The refrozen bottom water clearly differs from ice of meteoric origin and it is rather similar to clathrate ice (Figure 50). It is "light" and appears very white and opaque. X-ray and Raman spectroscopy analyses (University of Gottingen) show that it is made of 48%±8% of hexagonal ice, 48%±8% of hydrate type II and 4% n-pentane. The latter comes from the drilling fluid and is too big to produce hydrate type II. Atmospheric gases (N_2, O_2, Ar, CO_2, CH_4) can only produce hydrate type I (Davidson, 1973, Miller, 1973). This leaves us with the densifier as a potential candidate for the clathrates, and, indeed, its molecular structure (CH_3CCl_2F) is very close to a known clathrate II compound: CH_3CClF_2. Further, chromatographic elution of the gas extracted from the ice (Figure 51) clearly shows a peak associated with elution of pure densifier vapour. Clearly, the ice that formed at the time of subglacial water infiltration, did incorporate portions of the densifier and of the drilling fluid (emulsion).

We are however mainly interested in the "atmospheric" component of the ice, to see if we can learn something from it, in terms of subglacial water sources and properties. To collect this fraction of the gas content we tried various techniques that proved to be more or less successful. Our usual technique to extract the total amount of gases from the ice, using a Toepler pump system with ice melted and refrozen in an evacuated vessel did not work. It simply continuously evaporated the densifier which has a very high partial vapour pressure (40x water value!), resulting in the collection of ridiculously large amounts of gas. We therefore opted for the old method used by Langway (1958), where the ice block is melted at room temperature in a liquid (water or kerosene), under an inverted funnel connected to a burette filled with the liquid. As the ice melts, the gases collect at the top of the graduated burette, where the total gas content is read at the end of the experiment. Further corrections need to be applied to subtract the vapour partial pressure contribution of water, kerosene, drilling liquid and densifier, in order to obtain the actual contribution of the atmospheric gases to the total.

Gas composition (O_2, N_2, CO_2, CH_4) was obtained using the traditional ice crushing extraction technique at low temperature and under vacuum, with Gas Chromatography measurements on the same sample, using an Interscience Trace GC. Table IV here below summarizes the total gas content and gas composition measurements we have made on several samples of refrozen water (about 20), the stratigraphy of which however remaining uncertain.

	Total Gas ($l\ kg^{-1}$)		O_2 (%)		N_2 (%)		CO_2 (ppmV)		CH_4 (ppmV)		O_2/N_2	
	Min	Max	Min	Max	Min	Max	Min	Max	Min	Max	Min	Max
samples	0.38	4.07	21.26	30.65	69.04	78.38	1100	3600	2.7	11	0.27	0.46
Air bubbles in ice	0.09		20.95		78.08		200-370		0.6		0.27	
Solubility in water at0°C and under 2700 m of ice	6.26		37.8		62.19		22400		117.54		0.59	

Table IV: Atmospheric gas composition in the samples of refrozen water from the EDML drill hole

A first obvious feature is the large range of total gas content in the ice samples analyzed (380 ml to 4 litres per kg of ice). Another striking feature is that this is, in all cases, much higher than the usual mean value of about 90 ml per kg of ice normally encountered in deep ice cores. It should be noted also that the maximum value is however still below the expected saturation value for water at about 245 bars, i.e. below 2700 meters of ice (around 6 litres per kg of ice). Gas compositions also indicate that the ice was globally under-saturated as compared to water solubility, at least for carbon dioxide, methane and oxygen. O_2 to N_2 ratios range between the atmospheric value (characteristic of the bubbles in the ice) and the saturation solubility value in fresh water. These characteristics give us some hints on the processes occurring at the ice-bedrock interface. If, as one might hypothesize, the only input of gases to the melted pure crystals of ice at the ice-bedrock interface, are those initially occluded in the bubbles at the surface (closed system), and if no fractionation occurs on melting, then the dissolved gases in the subglacial waters should display an O_2/N_2 ratio close to atmospheric, until saturation occurs for the less soluble gases when freezing occurs in the drill hole. However, if the hypothesis is true that the only source of gases are the bubbles in the ice, it is impossible to understand total gas content values of up to 4 litres per kg of refrozen ice, when the mean value in meteoric ice is only 0.09. We have therefore to think of potential processes that could be responsible for the gas enrichment in the subglacial water. Until now we can think of three possible mechanisms depicted in Figure 52.

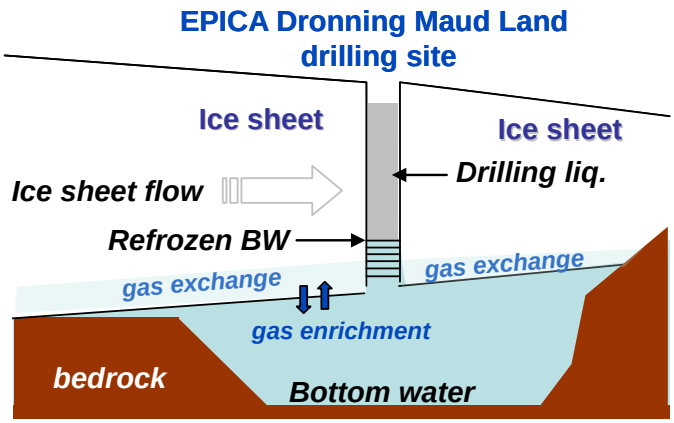

Figure 52a: An ice sheet moves over a water body of constant volume, with **small scale** melting-refreezing processes affecting the intercrystalline sub-liquid layer during recrystallization close to the pressure melting point within the bottom layers. This process has been identified under ice shelves at the meteoric ice - marine ice interface (J.-L. Tison, pers. com.), and proven to be physically possible at the metric scale by Rempel et al. (2001). This should then result in the gas impoverishment of the bottom meteoric ice. Preliminary results indeed show very low conductivity and total gas content in the basal few meters of ice at EDML (S. Kipfstuhl, pers. com.).

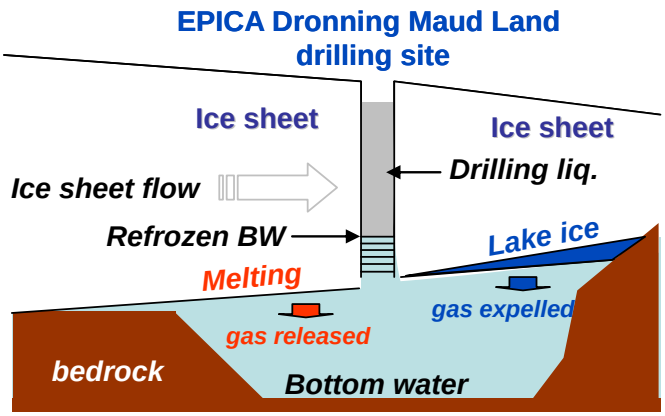

Figure 52b: An ice sheet moves over a water body of constant volume with **large scale** melting-refreezing: the Vostok case. The gas enrichment results here from both the melting of meteoric ice and refreezing of lake ice (in a general cell of thermohaline circulation), which occurs with a near total expulsion of gases in the remaining liquid. However, no large body of water appears to exist in the vicinity of EDML.

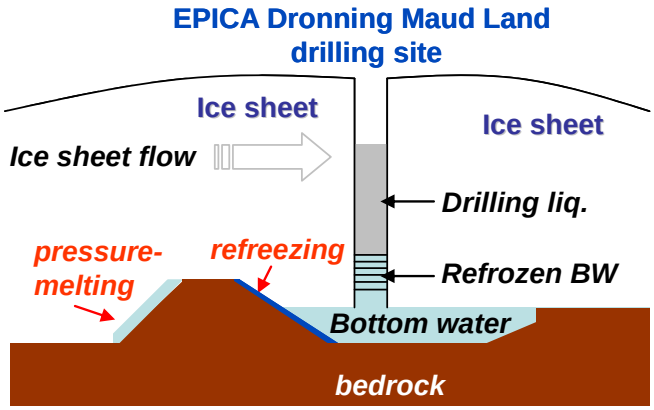

Figure 52c: An ice sheet moves around bedrock obstacles, with bottom ice at the pressure-melting point, and with a potential water film or layer at the interface. Melting on stoss side of bedrock bumps delivers air bubbles to the interface water, and refreezing on the lee side rejects and concentrates gases in the solution.

Note that all three processes could involve selective diffusion of gases ahead of the freezing interface, which would favour the faster diffusing oxygen and increase the O_2/N_2 ratio in the subglacial water. It should be emphasized, however, that part of the interpretation of this data set is depending on unknown processes of gas exchanges and nucleation occurring at the time of solidification of the infiltrating subglacial water within the drill hole. A large range of consolidation rates is plausible, which probably - at least partly - explains the wide range of total gas content values observed in the different samples.

2.4.6.4. Crystallographic investigations in basal ice at subfreezing temperature (Taylor Glacier, Dry Valleys, Antarctica)

In an attempt to formalize basal ice processes at subfreezing temperature and to assess the potential role played by debris during recrystallization, crystallographic and structural analyses have been conducted in cold basal ice from the snout of Taylor Glacier, Antarctica (Samyn et al., 2007). Fabric analysis shows a clear increase in grain boundary and nucleation kinetics at the interface between debris-rich and debris-free ice layers of the basal ice sequence, which denotes strain localization at these interfaces during basal ice genesis. Analogies with bottom ice from deep polar ice sheets where temperature is currently higher than at the studied site are highlighted and recrystallization scenarios are proposed for the development of the fabrics observed. It is shown that by controlling the repartition of stress and strain energy within basal ice, the rheology of debris-rich ice layers plays a decisive role in recrystallization dynamics at structural interfaces, which in turn controls the dynamics of the whole ice body. It is also shown that the same recrystallization regimes may occur in cold glaciers and temperate ice sheets, provided that strain accumulation has been high enough in the former. This challenges the common belief that migration fabrics observed in bottom ice from deep ice-sheets are exclusive to stagnant, annealed ice.

3. POLICY SUPPORT

The ASPI project allowed three Belgian teams to further develop and improve their experimental and modelling tools to study Antarctic ice cores and the dynamics of the Antarctic ice sheet, with a particular focus on transition zones. This has enabled the ASPI teams to contribute to on-going national and international scientific and policy-relevant efforts.

A better understanding of paleoclimates as can be inferred from ice cores is important to better understand crucial interactions in the climate system and better validate model predictions of future climate change. Work performed within ASPI has contributed significantly to the success of EPICA (European Project for Ice Coring in Antarctica). The basal ice is an especially rich source to reconstruct the climates of the past as it contains the oldest ice sequences. These have however been exposed longest to the sometimes disturbing effects of ice dynamics. Especially important are the effects of the basal heat input on basal melting rates and ice sliding velocities. Results obtained within this project have aided the international effort to further explore potentially suitable locations to find the oldest ice and better understand physical processes operating at the ice sheet base (contribution to IPICS, the International Partnerships in Ice Core Sciences).

The ice flow models that were further developed and improved within the ASPI project are unique worldwide. These models have allowed ASPI teams to better investigate crucial zones important for the stability of the Antarctic ice sheet as well as to study the behaviour of the Antarctic ice sheet as a whole, both in past and future climates. The 3D Antarctic ice sheet model has been solicited in the past three IPCC assessment reports to project the contribution of the Antarctic ice sheet to sea-level change. The ice dynamic tools at hand and the leading role played by ASPI members in international model intercomparison exercises lets us expect that our research will also be included in the next IPCC AR5.

Finally, the ASPI project has allowed Belgian teams to keep a glaciological research potential operational to be able to perform scientific work out of the Princess Elisabeth Station, and this also contributes to the objectives of Belgian science policy.

4. DISSEMINATION AND VALORISATION

Members of the ASPI team participated in many of the most important national and international conferences to present the results of their work and to act as session convenors. Over the lifetime of the project, more than 150 communications (talks as well as posters) were presented. A non-exhaustive list of the meetings attended by ASPI members included all of the annual meetings of the European Geosciences Union (EGU), most of the fall meetings of the American Geophysical Union (AGU), most of the international symposia organised by the International Glaciological Society (IGS), many of the meetings organised by the Scientific Committee of Antarctic Research (SCAR) and by the International Association of Cryospheric Sciences (IASC), amongst several others. Some members of the ASPI team were also heavily involved in the IPCC.

At the national level, members of the ASPI team were interviewed more than 100 times for radio, newspapers, and television. On a regular basis, invitations were accepted for talks for a wider audience in schools, organisations and as part of the outreach programmes of our universities.

In addition, the main research results of the ASPI team were published in 15 peer-reviewed papers resulting directly from the project, often co-authored by members of different ASPI groups. Together with non peer-reviewed and ASPI-related work, more than 60 publications arose from the project.

5. PUBLICATIONS

5.1. ASPI publications

5.1.1. Peer reviewed

Fitzsimmons, S., Webb, N., Mager, S., MacDonnell, S., Lorrain, R., Samyn, D. (2008) : Mechanisms of basal ice formation in polar glaciers: An evaluation of the apron entrainment model, Journal of Geophysical Research, Vol. 113, F02010, doi:10.1029/2006JF000698

Huybrechts, P. (2009): Westside story of Antarctic ice, Nature, 458, 295-296.

Huybrechts, P., O. Rybak, F. Pattyn, U. Ruth, and D. Steinhage (2007) : Ice thinning, upstream advection, and non-climatic biases for the upper 89% of the EDML ice core from a nested model of the Antarctic ice sheet. Climate of the Past 3(4): 577-590.

Huybrechts, P., O. Rybak, D Steinhage and F Pattyn (2009) : Past and present accumulation rate reconstruction along the Dome Fuji-Kohnen radio echo sounding profile, Dronning Maud Land, East Antarctica. Annals of Glaciology 50(51). 112-120.

Mager, S., Fitzsimmons, S., Frew, R., Samyn, D., Lorrain, R. (2009): Composition and origin of amber ice and its influence on the behaviour of cold glaciers in the McMurdo Dry Valleys, Antarctica, Journal of Glaciology, Vol. 55, No. 190,, 363-372

Pattyn, F. (2008): Investigating the stability of subglacial lakes with a full Stokes model. Journal of Glaciology. 54(185): 353-361.

Pattyn, F., A. Huyghe, S. De Brabander, and B. De Smedt (2006) : The role of transition zones in marine ice sheet dynamics. Journal of Geophysical Research (Earth Surface). 111 (F2): No. F02004, doi:10.1029/2005JF000394.

Pattyn, F., L. Perichon, A. Aschwanden, B. Breuer, B. de Smedt, O. Gagliardini, G. H. Gudmundsson, R. Hindmarsh, A. Hubbard, J. V. Johnson, T. Kleiner, Y. Konovalov, C. Martin, A. J. Payne, D. Pollard, S. Price, M. Rueckamp, F. Saito, O. Soucek, S. Sugiyama, and T. Zwinger (2008) : Benchmark experiments for higher-order and full-Stokes ice sheet models (ISMIP-HOM). The Cryosphere 2(3), 95-108.

Rybak, O,.O., P. Huybrechts, F. Pattyn, and D. Steinhage (2007): Regionalnaya model' dinamiki l'da. Chast' 2. Post-eksperimentalnaya obrabotka dannykh (in Russian: Regional ice-dynamic model. Part 2. Post-experimental processing of data), Materialy Glatsiologicheskikh issledovanii (Data of glaciological studies), 103, 3-10.

Rybak, O.O., and P. Huybrechts (2007): Lagranzhev metod rascheta vozrasta i izotopnogo sostava lda v trekhmernoy modeli Antarkticheskogo ledovogo shita (in Russian), A Lagrangian method of calculation of age and isotopic composition of ice in a 3-D model of the Antarctic ice sheet. Kryosfera Zemli, 11(4), 70-79.

Rybak, O.O., and P. Huybrechts (2008): Sensitivity of the EDML ice core chronology to the geothermal heat flux, Materialy Glatsiologicheskikh issledovanii (Data of glaciological studies), 105, in press.

Rybak, O.O., P. Huybrechts, F. Pattyn, and D. Steinhage (2007): Regionalnaya model' dinamiki l'da. Chast'1. Opisaniye modeli, postanovka chislennykh eksperimentov i sovremennaya dinamika potoka v oksrestnostiakh stantsii Konen (in Russian; Regional ice-dynamic model. Part 1. Model description, performance of numerical experiments, and present-day ice-flow dynamics around Kohnen station), Materialy Glatsiologicheskikh issledovanii (Data of glaciological studies), 102, 3-11.

Samyn, D., Svensson, A., Fitzsimmons, S.J. (2008) : Dynamic implications of discontinuous recrystallization in cold basal ice: Taylor Glacier, Antarctica. Journal of Geophysical Research, 113, F03S90, doi: 10.1029/2006 JF000600.

Samyn, D., Fitzsimmons, S., Lorrain, R. (2009) : Rotating micro-structures in Antarctic cold basal ice: implications for glacier flow and its interpretation, International Journal of Earth Sciences, DOI 10.1007/s00531-009-0478-5.

Schaefer, M., O. Gagliardini, F. Pattyn and E. Le Meur (2008) : Applicability of the Shallow Ice Approximation inferred from model inter-comparison using various glacier geometries. The Cryosphere Discuss. 2: 557-599.

5.1.2. Submitted to co-authors (peer reviewed)

Tison, J.-L., de Angelis, M., Littot, G., Wolff, E., Samyn, D., Jouzel, J., Stenni, B., Johnsen, S., Lipenkov, V., Loulergue, L., Barnola, J.-M., Petit, J.-R., Delmonte, B., Dreyfus, G., Dahl-Jensen, D., Lüthi, D ., Schilt, A., Lorrain, R. and Souchez, R. (2009) : Can we retrieve a clear paleoclimatic signal from the deeper part of the EPICA Dome C ice core?, for submission to Earth and Planetary Sciences Letters.

5.1.4. Others (non peer reviewed)

De Smedt, B.; de Groen, P.; Pattyn, F. (2006) Inverse modelling of basal friction using a 2D higher-order ice-flow model. Geophysical Research Abstracts 8: EGU06-A-06420.

Huyghe, A.; Pattyn, F.; Huybrechts, P. (2006) Testing numerical techniques to solve the mass continuity equation in a coupled ice-sheet / ice-shelf model. Geophysical Research Abstracts 8: EGU06-A-05520.

Huybrechts, P., O. Rybak, F. Pattyn, and D. Steinhage (2006): Non-climatic biases and chronology of the EDML ice core derived from a nested Antarctic ice sheet model, Geophysical Research Abstracts 8, EGU06-A-09803.

De Smedt, B.; de Groen, P.; Pattyn, F. (2007) A robust 2D higher-order ice-flow model for inverse applications. Geophysical Research Abstracts 9: EGU2007-A-00834.

De Smedt, B.; Pattyn, F.; de Groen, P.; Nolan, M. (2007) Inverse modelling of basal velocity using a 2D higher-order ice-flow model. Geophysical Research Abstracts 9: EGU2007-A-00846.

Rybak, O.; Huybrechts, P.; Pattyn, F.; Steinhage, D. (2007) Model-derived ice core chronology and non-climatic biases in the lower part of the EDML ice core. Geophysical Research Abstracts 9: EGU2007-A-02203.

Calov, R.; Greve, R.; Huybrechts, P.; Bueler, E.; Pollard, D.; Pattyn, F.; Tarasov, L. (2007) First Results of the ISMIP-HEINO Model Intercomparison Project. : EGU2007-A-02910.

Pattyn, F.; ISMIP-HOM participants (2007) ISMIP-HOM: Results of the Higher-Order Ice Sheet Model Intercomparison exercise. Geophysical Research Abstracts 9: EGU2007-A-01351.

5.2. ASPI-related publications

5.2.1. Peer-reviewed

Alley, R., P.U. Clark, P. Huybrechts, and I. Joughin (2005) : Ice sheets and sea-level change, Science, 310, 456-460 (authors are listed alphabetically and contributed equally).

Bassett, S.E., G.A. Milne, M.J. Bentley and P. Huybrechts (2007): Modeling Antarctic Sea-Level Data to Explore the Possibility of a Dominant Antarctic Contribution to Meltwater Pulse IA, Quaternary Science Reviews, 26, 17-18, 2113-2127.

EPICA Community Members (incl.. P. Huybrechts, O. Rybak, J.-L. Tison) (2006): One-to-one interhemispheric coupling of millennial polar climate variability during the last glacial, Nature, 444, 195-198, doi:10.1038/nature05301.

Gregory, J., and P. Huybrechts (2006): Ice-sheet contributions to future sea-level change, Philosophical Transactions of the Royal Society of London A, 364, 1709-1731, doi: 10.1098/rsta.2006.1796.

Huybrechts, P. (2006): Numerical modeling of ice sheets through time, in: Knight, P.G. (ed.): Glacier Science and Environmental Change, Blackwell Publishing (Oxford), 406-412.

Huybrechts, P. (2007): Ice sheet modeling, in B. Riffenburgh (ed): Encyclopedia of the Antarctic, Routledge, New York, 514-517.

Huybrechts, P. (2009): Cryosphere, in Gornitz, V. (ed.): Encyclopedia of paleoclimatology and ancient environments, Encyclopaedia of Earth Science Series, Springer Verlag (Berlin, Heidelberg, New York), 221-226.

Jouzel, J. and 31 others (incl. J.-L. Tison and Souchez, R.) (2007): Orbital and millennial Antarctic climate variability over the last 800.000 years, Science, DOI: 10.1126/science.1141038.

Ruth, U., J.-M. Barnola J.-M., J. Beer, M. Bigler, T. Blunier, E. Castellano, H. Fischer, F. Fundel, P. Huybrechts, P. Kaufmann, S. Kipfstuhl, A. Lambrecht, A. Morganti, F. Parrenin, O. Rybak, M. Severi, R. Udisti, F. Wilhelms, and E. Wolff (2007): "EDML1": A chronology for the EDML ice core, Antarctica, over the last 150 000 years. Climate of the Past, 3, 475-48.

Severi, M, S. Becagli, E. Castellano, A. Morganti, R. Traversi, R. Udisti, U. Ruth, H. Fischer, P. Huybrechts, E. Wolff, F. Parrenin, P. Kaufmann, F. Lambert, and J.P. Steffensen (2007): Synchronisation of the EDML and EDC ice cores for the last 52 kyr by volcanic signature matching, Climate of the Past, 3, 367-374.

Steffen, K., R. Thomas, E. Rignot, G. Cogley, M. Dyurgerov, S. Raper, P. Huybrechts, E. Hanna (2009): Cryospheric Contributions to Sea-level Rise and Variability, in: J. Church, P. Woodworth, T. Aarup, and S. Wilson (eds.): Understanding Sea-level Rise and Variability, Blackwell Publishing, in press.

Wen, J., K.C. Jezek, A.J. Monaghan, B. Sun, J. Ren, P. Huybrechts (2006): Accumulation variability and mass budgets of the Lambert Glacier-Amery Ice Shelf system at high elevations, Annals of Glaciology, 43, 351-360.

Wen, J., K.C. Jezek, H.A. Fricker, B.M. Csatho, U.C. Herzfeld, K.L. Farness, P. Huybrechts (2007): Mass budget of the Lambert, Mellor and Fischer Glaciers and basal fluxes beneath their flowbands on Amery Ice Shelf, Science in China Series D Earth Sciences, 50, 11, 1693-1706, doi: 10.1007/s11430-007-0120-y.

Wen, J., Y. Wang, J. Liu, K.C. Jezek, P. Huybrechts, B.M. Csatho, K.L. Farness, and B. Sun (2008): Mass budget of the grounded ice in Lambert Glacier-Amery Ice Shelf system, Annals of Glaciology 48, 193-197.

6. ACKNOWLEDGEMENTS

Part of the work discussed in this report was performed as a contribution to the European Project for Ice Coring in Antarctica (EPICA), a joint European Science Foundation/European Commission scientific programme, funded by the EU (EPICA-MIS) and by national contributions from Belgium, Denmark, France, Germany, Italy, the Netherlands, Norway, Sweden, Switzerland and the United Kingdom. The main logistic support was provided by IPEV and PNRA (at Dome C) and AWI (at Dronning Maud Land). We thank Hans Oerter and Hanno Meyer (Alfred-Wegener-Institut) for access to the unpublished $d^{18}O$ data in the lower 10% of the EDML ice core drilled at Kohnen.

Acknowledgements for support with the experimental ice-core research are furthermore due to P. Duval, M. Montagnat, G. Durand, and D. Raynaud at the Laboratoire de Glaciologie et de Géophysique de l'Environnement (LGGE), G. Orombelli, M. Frezzotti, M. Meneghel, and A. Bondesan at the Progetto Nazionale di Ricerce in Antartide (PNRA), B. Stenni at the Laboratorio di Geochimica Isotopica, Universita di Trieste, A. Khazendar at the Jet Propulsion Laboratory (JPL, USA), A. Jenkins, R. Mulvaney at the British Antarctic Survey (BAS, UK), Antarctica New Zealand, S. Fitzsimmons at the University of Dunedin, New Zealand, and S. Kipfstuhl (Alfred Wegener Insititut, Bremerhaven).

7. REFERENCES

Alley, R.B., Perepezko, J.H.Bentley, C.R., 1986. Grain growth in polar ice : I. Theory,. J. Glaciol. 32, 415-424.

Baker, I.Cullen, D., 2003. SEM/EDS observations of impurities in polar ice: artefacts or not? Journal of Glaciology 49, 184-190.

Bender, M.L., 2002. Orbital tuning chronology for the Vostok climate record supported by trapped gas composition. Earth and Planetary Science Letters 204, 275-289.

Boulton, G.S., 1979. Processes of erosion on different substrata. J. Glaciol. 23, 15-38.

Boulton, G.S., 1996. Theory of glacial erosion, transport and deposition as consequence of subglacial sediment deformation. J. Glaciol. 42, 43-62.

Cuffey, K., Conway, H., Gades, A., Hallet, B., Lorrain, R., Severinghaus, J.P., Steig, E., Vaughn, B.White, J., 2000. Entrainment at cold glacier beds. Geology 28, 351-354.

Davidson, D. W. (1973): Clathrate hydrates. In 'Water: a comprehensive treatise. Vol. 5', London.

de Angelis, M., Morel-Fourcade, M.-C.B., J.-M., Susini, J.Duval, P., 2005. Brine micro-droplets and solid inclusions in accreted ice from Lake Vostok (East Antarctica). Geophysical Research Letters 32, doi: 10.1029/2005GL022460.

de Angelis, M., Petit, J.-R., Savarino, J., Souchez, R.Thiemens, M.H., 2004. Contributions of an ancient evaporitic-type reservoir to subglacial Lake Vostok chemistry. Earth and Planetary Sciences Letters 222, 751-765.

De Smedt, B., P. de Groen and F. Pattyn. (2007): A robust 2D higher-order ice-flow model for inverse applications. Geophysical Research Abstracts 9: EGU2007-A-0083.

Delmonte, B., Andersson, P.S., Haqnsson, M., Schöberg, H., Petit, J.-R., Basile-Doelsch, I.Maggi, V., 2008. Aeolian dust in East Antarctica (EPICA-Dome C and Vostok): Provenance during glacial ages over the last 800 kyr. Geophysical Research Letters 35, doi:10.1029/2008GRL033382.

Dreyfus, G.G., Parrenin, F., Lemieux-Dudon, B., Durand, G., Masson-Delmotte, V., Jouzel, J., Barnola, J.-M., Panno, L., Spahni, R., Tisserand, A., Siegenthaler, U.Leuenberger, M., 2007. Anomalous flow below 2700m in the EPICA Dome C ice core detected using $d^{18}O$ of atmospheric oxygen measurements. Climate of the Past 3, 341-353.

Durand, G., Svensson, A., Persson, A., Gagliardini, O., Gillet-Chaulet, F., Sjolte, J., Montagnat, M.Dahl-Jensen, D., 2008. Evolution of the texture along the EPICA Dome C ice core. Proceedings of the 2nd International Workshop on Physics of Ice Core records (PICR-2), Hokkaido University, Sapporo, Japan, Institute of Low Temperature Science,

Duval P. (1976): Lois du fluage transitoire de la glace polycristalline pour divers états de contrainte. Ann. Geophys., 32, (4), 335-350.

Eicken, H., 1992. Salinity profiles of Antarctic sea ice: field data and model results. Journal of Geophysical Research 97, 15545-15557.

Eicken, H., 1998. Deriving modes and rates of ice growth in the Weddell Sea from microstructural, salinity and stable-isotope data. Antarctic sea ice : physical processes, interactions and variability 74, 89-122.

Eicken, H., Oerter, H., Miller, H., Graf, W., Kipfstuhl, J., 1994. Textural characteristics and impurity content of meteoric and marine ice in the Ronne Ice Shelf, Antarctica. J. Glaciol. 40, 386-398.

EPICA Community members, 2004. Eight glacial cycles from an Antarctic ice core. Nature 429, 623-628.

Evatt, G., A. Fowler, C. Clark, N. Hulton (2006): Subglacial floods beneath ice sheets, Phil. Trans. R. Soc. A., 364, 1769-1794.

Fox Maule, C., M. E. Purucker, N. Olsen, K. Mosegaard (2005): Heat flux anomalies in Antarctica revealed by satellite magnetic data, Science 309, 464–467.

Fricker, H., T. Scambos, R. Bindschadler, L. Padman (2007): An active subglacial water system in West Antarctica mapped from space, Science 315 (1544).

Glen, J.W., Homer, D.R.Paren, J.G., 1977. Water at grain boundaries: its role in the purification of temperate glacier ice. International Association of Hydrological Sciences Publications 118, 263-271.

Goldberg, D., D. Holland (2007): Grounding line movement and ice-shelf buttressing in marine ice sheets: an adaptive approach, Ice Modeling Workshop, LANL Institute of Geophysics and Planetary Physics, Aug 18, 2007.

Goodwin, I.D., 1993. Basal ice accretion and debris entrainment within the coastal ice margin, Law Dome, Antarctica. J. Glaciol. 39, 157-166.

Gow, A.J., Epstein, S.Sheehy, W., 1979. On the origin of stratified debris in ice cores from the bottom of the Antarctic Ice Sheet. J. Glaciol. 23, 185-192.

Gow, A.J.Meese, D.A., 1996. Nature of basal debris in the GISP2 and Byrd ice cores and its relevance to bed processes. Ann. Glaciol. 22, 134-140.

Gray, L., I. Joughin, S. Tulaczyk, V. Spikes, R. Bindschadler, K. Jezek (2005): Evidence for subglacial water transport in the West Antarctic ice sheet through three-dimensional satellite radar interferometry. Geophysical Research Letters 32 (L035001).

Herron, S.Langway, C., 1979. The debris-laden ice at the bottom of the Greenland ice-sheet. J. Glaciol. 23, 193-207.

Herterich, K. (1987): On the flow within the transition zone between ice sheet and ice shelf, in: C. J. Van der Veen and J. Oerlemans (eds.): Dynamics of the West Antarctic Ice Sheet, D. Reidel, Dordrecht, 185-202.

Hindmarsh, R. (1993): Qualitative dynamics of marine ice sheets, in Ice in the Climate System, W. Peltier (Ed.), NATO ASI Series I (12), 67-99, Berlin, Springer-Verlag.

Hindmarsh, R. (2004): A numerical comparison of approximations to the Stokes equations used in ice sheet and glacier modeling, J. Geophys. Res. 109 (F01012), doi:10.1029/2003JF000065.

Hindmarsh, R. C. A. (1996): Stability of ice rises and uncoupled marine ice sheets, Ann. Glaciol., 23, 105-115.

Hindmarsh, R., C., A., Le Meur, E. (2001): Dynamical processes involved in the retreat of marine ice sheets, J. Glaciol., 47, 271-282.

Hindmarsh, R.C.A. (2006): The role of membrane-like stresses in determining the stability and sensitivity of the Antarctic ice sheet: back pressure and grounding line motion, Phil. Trans. R. Soc. A, 364, 1733-1767, doi:10.1098/rsta.2006.1797.

Holdsworth, G., 1974. Meserve Glacier, Wright Valley, Antarctica, part I. Basal processes. n° 37, Institute of Polar Studies, The Ohio State University Research Foundation, Columbus

Huybrechts, P. (1992): The Antarctic ice sheet and environmental change: a three-dimensional modelling study, Berichte zur Polarforschung, 99.

Huybrechts, P. (2002): Sea-level changes at the LGM from ice-dynamic reconstructions of the Greenland and Antarctic ice sheets during the glacial cycles. Quaternary Science Reviews, 21, 1-3, 203-231.

Huybrechts, P., A. Payne and the EISMINT Intercomparison Group (1996): The EISMINT benchmarks for testing ice-sheet models. Ann. Glaciol. 23, 1-12.

Huybrechts, P., Abe Ouchi, A., Marsiat, I., Pattyn, F., Payne, T., Ritz, C., Rommelaere, V. (1998): Report of the Third EISMINT Workshop on Model Intercomparison, European Science Foundation, Strasbourg, 120 p.

Huybrechts, P., De Wolde, J. (1999): The dynamic response of the Greenland and Antarctic ice sheet to multiple-century climatic warming, J. Clim., 12, 2169-2188.

Huybrechts, P., O. Rybak, F. Pattyn, U. Ruth, and D. Steinhage (2007): Ice thinning, upstream advection, and non-climatic biases for the upper 89% of the EDML ice core from a nested model of the Antarctic ice sheet, Climate of the Past, 3, 693-727.

International Partnerships in Ice Core Sciences, 2009. IPICS White papers. www.pages-igbp.org/ipics/whitepapers.html

Iverson, N.R., 1993. Regelation of ice through debris at glacier beds: Implications for sediment transport. Geology 21, 559-562.

Iverson, N.R.Semmens, D., 1995. Intrusion of ice into porous media by regelation: A mechanism of sediment entrainment by glaciers. J. Geophys. Res. 100, 10219-10230.

Jacka, T.H. (1984): The time and strain required for development minimum strain rates in ice. Cold Regions Science and Technology, 8, 261-268.

Jouzel, J. and 31 others (2007): Orbital and Millennial Antarctic Climate Variability over the Past 800,000 Years. Science, 1141038 DOI: 10.1126.

Jouzel, J., Masson-Delmotte, V., Cattani, O., Dreyfus, G., Falourd, S., Hoffmann, G., Minster, B., Nouet, J., Barnola, J.M., Chappelaz, J., Fischer, H., Gallet, J.C., Johnsen, S., Leuenberger, M., Loulergue, L., Luethi, D., Oerter, H., Parrenin, F., Raisbeck, G., Raynaud, D., Schilt, A., Schwander, J., Selmo, E., Souchez, R., Spahni, R., Stauffer, B., Steffensen, J.-P., Stenni, B., Stocker, T.F., Tison, J.-L., Werner, M.Wolff, E.W., 2007. Orbital and Millennial Antarctic Climate Variability over the Past 800,000 Years. Science 317, DOI: 10.1126/science.1141038.

Jouzel, J., Petit, J.R., Souchez, R., Barkov, N., Lipenkov, V., Raynaud, D., Stievenard, M., Vassiliev, N., Verbeke, V.Vimeux, F., 1999. More than 200 meters of lake ice above subglacial lake Vostok, Antarctica. Science 286, 2138-2141.

Kapitsa, A, J. Ridley, G. Robin, M. Siegert and I. Zotikov (1996): A large deep freshwater lake beneath the ice of central East Antarctica, Nature 381, 684-686.

Khazendar A. (2000): Marine ice formation in rifts of Antarctic ice shelves – A combined laboratory study and modeling approach, Univ. Libre de Bruxelles, Ph.D. Thesis, 153 pp., unpublished.

Khazendar A., Tison J.-L., Stenni B., Dini M., Bondesan A. (2001): Significant marine-ice accumulation in the ablation zone beneath an Antarctic ice shelf. J. Glac., 47 (158), 359-367.

Khazendar, A., Tison, J.-L., Stenni, B., Dini, M.Bondesan, A., 2001. Significant marine ice accumulation in the ablation zone beneath an Antarctic ice shelf. Journal of Glaciology 47, 359-368.

Knight, P.G., 1997. The basal ice layer of glaciers and ice sheets. Quaternary Science Reviews 16, 975-993.

Koerner, R.M.Fisher, D.A., 1979. Discontinuous flow, ice texture, and dirt content in the basal layers of the Devon Island Ice Cap. J. Glaciol. 23, 209-221.

Lambert, F., Delmonte, B., Petit, J.-R., Bigler, M., Kaufmann, P.R., Hutterli, M.A., Stocker, T.F., Ruth, U., Steffensen, J.P.Maggi, V., 2008. Dust-Climate couplings over the past 800,000years from the EPICA Dome C ice core. Nature 452, doi:10.1038/nature06763.

Langway, C. C. J. (1958): Bubbles pressures in Greenland glacier ice. In 'Inter. Union Geodesy Geophys. Symposium of Chamonix', 336-349.

Lefebvre, E., Ritz, C., Legrésy, B.Possenti, P., 2008. New temperature profile measurement in the EPICA Dome C borehole. Geophysical Research Abstracts, EGU General Assembly 2008, 13-18 April 2008, European Geophysical Union.

Lipscomb, W.H., E. Bueler, D. Holland J. Johnson, S. Price (2008): Building a Next-Generation Community Ice Sheet Model, Report on a Workshop, Los Alamos National Laboratory, 18-20 August 2008.

Lisiecki, L.E.Raymo, M.E., 2005. A Pliocene-Pleistocene stack of 57 globally distributed benthic $d^{18}O$ records. Paleoceanography 20, doi:10.1029/2004PA001071.

Little, C.M. and 19 others, (2007): Towards a new generation of ice sheet models, EOS Trans. Amer. Geophys. U., 88(52), 578-579, doi:10.1029/2007EO520002.

Llubes, F. R. M., C. Lanseau (2006): Relations between basal condition, subglacial hydrological networks and geothermal flux in Antarctica, Earth and Plan. Sci. Lett. 241, 655–662.

Loulergue, L., Schilt, A., Spahni, R., Masson-Delmonte, V., Blunier, T., Lemieux, B., Barnola, J.-M., Raynaud, D., Stocker, T.F.Chappelaz, J., 2008. Orbital and millennial-scale features of atmospheric CH_4 over the past 800,000 years. Nature 453, doi:10.1038/nature06950.

Lüthi, D., Le Floch, M., Bereiter, B., Blunier, T., Barnola, J.-M., Siegenthaler, U., Raynaud, D., Jouzel, J., Fischer, H., Kawamura, K.Stocker, T.F., 2008. High-resolution carbon

dioxide concentration record 650,000-800,000 years before present. Nature 453, doi:10.1038/nature06949.

Mayer, C., Huybrechts, P. (1999): Ice-dynamic conditions across the grounding zone, Ekströmisen, East Antarctica, J. Glaciol., 45, 384-398.

Miller, S. L. (1973): The Clathrate Hydrates - Their Nature and Occurrence. Physics and Chemistry of Ice. Royal Society of Canada, 42-50.

Montagnat, M., Duval, P., Bastie, P., Hamelin, B., de Angelis, M., Petit, J.R.Lipenkov, V.Y., 2001. High crystalline quality of large single crystals of subglacial ice above Lake Vostok (Antarctica) revealed by hard X-ray diffraction. C.R. Acad. Sc. Paris, Série IIa Sciences de la Terre et des Planètes 333, 419-425.

Moore, J.C., Reid, A.P.Kipfstuhl, J., 1994. Microstructure and electrical properties of marine ice and its relationship to meteoric ice and sea ice. J. Geophys. Res. 99, 5171-5180.

Mulvaney, R., Allemany, O. And Possenti, P., 2007. The Berkner Island (Antarctica) ice-core drilling project. Annals of Glaciology, 47, 115-124.

Mulvaney, R., Wolff, E.W.Oates, K., 1988. Sulphuric acid at grain boundaries in Antarctic ice. Nature 331, 247-249.

Nye, J. (1976): Water flow in glaciers: jökulhlaups, tunnels and veins, J. Glaciol 17(76), 181-207.

Ohno, H., Igarashi, M.Hondoh, T., 2005. Salt inclusions in polar ice cores: Location and chemical form of water-soluble impurities. Earth and Planetary Science Letters 232, 171-178.

Paterson, W.S.B., 1994. The physics of Glaciers, 3rd edition, Oxford, Butterworth-Heinemann, 481 pp.

Pattyn, F. (2002): Transient glacier response with a higher-order numerical ice-flow model. Journal of GLaciology, 48(162), 467-477.

Pattyn, F. (2003): A new three-dimensional higher-order thermomechanical ice-sheet model: basic sensitivity, ice-stream development and ice flow across subglacial lakes. Journal of Geophysical Research (Solid Earth), 108 (B8), 2382, doi:10.1029/2002JB002329.

Pattyn, F. (2008) Investigating the stability of subglacial lakes with a full Stokes ice sheet model. J. Glaciol. 54(185): 353-361.

Pattyn, F., A. Huyghe, S. De Brabander, and B. De Smedt (2006): The role of transition zones in marine ice sheet dynamics. J. Geoph. Res. (Earth Surface). 111 (F2): No. F02004, doi:10.1029/2005JF000394.

Pattyn, F., Huyghe, A., De Brabander, S., De Smedt, B. (2006): Role of transition zones in marine ice sheet dynamics, J. Geophys. Res., 111, F02004, doi 10.1029/2005JF000394.

Pattyn, F., L. Perichon, A. Aschwanden, B. Breuer, B. de Smedt, O. Gagliardini, G. H. Gudmundsson, R. Hindmarsh, A. Hubbard, J. V. Johnson, T. Kleiner, Y. Konovalov, C. Martin, A. J. Payne, D. Pollard, S. Price, M. Rueckamp, F. Saito, O. Soucek, S. Sugiyama, and T. Zwinger (2008) Benchmark experiments for higher-order and full-Stokes ice sheet models (ISMIP-HOM). The Cryosphere 2(3), 95-108.

Payne, A.J., A. Vieli, A.P.. Shepherd, D.J. Wingham and E. Rignot. (2004): Recent dramatic thinning of largest West Antarctic ice stream triggered by oceans. Geophysical Research Letters 31, L23401, doi: 10.1029/2004GL021284.

Petit, J., Jouzel, J., Raynaud, D., Barkov, N., Barnola, J.M., Basile, I., Bender, M., Chappellaz, J., Davis, M., Delaygue, G., Delmotte, M., Kotlyakov, V., Legrand, M., Lipenkov, V., Lorius, C., Pépin, L., Ritz, C., Saltzman, E.Stievenard, M., 1999. Climate and atmospheric history of the past 420,000 years from the Vostok ice core, Antarctica. Nature 399, 429-436.

Pollard, D., and R.M. DeConto (2007): Grounding line behavior in a heuristically coupled ice sheet-shelf model, Geophysical Research Abstracts, EGU2007-A-03103.

Pollard, D., R. DeConto (2009). Modeling West Antarctic Ice Sheet growth and collapse through the last 5 million years, Nature, 458, 329-332, doi:10.1038/nature07809.

Priscu, J., S. Tulaczyk, M. Studinger, M. Kennicutt, B. Christner, C. Forman (2007): Antarctic subglacial water: origin, evolution and microbial ecology. In Vincent W. and J. Laybourn-Parry (eds.) Polar Limnology, Oxford University Press, UK, in press.

Raisbeck, G.M., Yiou, F., Cattani, O.Jouzel, J., 2006. ^{10}Be evidence for the Matuyama-Brunhes geomagnetic reversal in the EPICA Dome C ice core. Nature 444, doi:10.1038/nature05266.

Raynaud D., B.J.M., R. Souchez, R. Lorrain, Petit J.-R., Duval P., Lipenkov V., 2005. The record for marine isotopic stage 11. Nature 436, 30-40.

Raynaud, D., Lipenkov, V., Lemieux-Dudon, B., Duval, P., Loutre, M.-F.Lhomme, N., 2007. The local insulation signature of air content in Antarctic ice. A new step toward an absolute dating of ice records. Earth and Planetary Science Letters 261, 337-349.

Rempel, A. W., Waddington, E. D., Wettlaufer, J. S. and Worster, M. G. (2001): Possible displacement of the climate signal in ancient ice by premelting and anomalous diffusion. Nature 411, 568–571.

Rempel, A., 2005. Englacial phase changes and intergranular flow above subglacial lakes. Annals of Glaciology 40, 191-194.

Rempel, A.W., 2003. Segregation, transport and interaction of climate proxies in polycrystalline ice. Canadian Journal of Physics 81, 89-97.

Rempel, A.W., Waddington, E.D., Wettlaufer, J.S.Worster, M.G., 2001. Possible displacement of the climate signal in ancient ice by premelting and anomalous diffusion. Nature 411, 568-571.

Rempel, A.W., Wettlaufer, J.S.Waddington, E.D., 2002. Anomalous diffusion of multiple impurity species: predicted implications for the ice core climate record. Journal of Geophysical Research 107,

Rémy, F.Tabacco, I.E., 2000. Bedrock features and ice flow near the EPICA ice core site (Dome C, Antarctica). Geophysical Research Letters 27, 405-408.

Ritz, C., Rommelaere, V., Dumas, C. (2001): Modeling the evolution of Antarctic ice sheet over the last 420,000 years: Implications for altitude changes in the Vostok region, J. Geophys. Res., 106, 31,943-31,964.

Ruth, U., J.-M. Barnola J.-M., J. Beer, M. Bigler, T. Blunier, E. Castellano, H. Fischer, F. Fundel, P. Huybrechts, P. Kaufmann, S. Kipfstuhl, A. Lambrecht, A. Morganti, F. Parrenin, O. Rybak, M. Severi, R. Udisti, F. Wilhelms, and E. Wolff (2007): "EDML1": A chronology for the EDML ice core, Antarctica, over the last 150 000 years. Climate of the Past, 3, 475-48.

Rybak, O., and P. Huybrechts (2003). A comparison of Eulerian and Lagrangian methods for dating in numerical ice sheet models. Annals of Glaciology 37, 150-158.

SALE Workshop Report (2007): Subglacial Antarctic Lake Environments (SALE) in the International Polar Year 2007-08, Advanced Science and Technology Planning Workshop, 24-26 April 2006, Grenoble, France.

Samyn, D., Svensson, A and Fitzsimons, S. (2007): Discontinuous recrystallization in cold basal ice from an Antarctic glacier: dynamic implications. J. Geophys. Res. (Earth Surface), under review.

Schoof, C. (2006): A variational approach to ice stream flow, J. Fluid. Mech., 556, 227-251, doi: 10.1017/S0022112006009591.

Schoof, C. (2007a): Marine ice-sheet dynamics. Part1. The case of rapid sliding, J. Fluid. Mech., 573, 27-55.

Schoof, C. (2007b): Ice sheet grounding line dynamics: steady states, stability and hysteresis, J. Geophys. Res., 112, F03S28, doi: 10.1029/2006JF000664.

Shapiro, N., M. Ritzwoller (2004): Inferring surface heat flux distributuions guided by a local seismic model: particular application to Antarctica, Earth and Planet.Sci. Lett. 223, 213–234.

Shepherd, A., And D. Wingham (2007): Recent sea-level contributions of the Antarctic and Greenland ice sheets, Science 315, 1529-1532.

Shepherd, A., D. Wingham, and E. Rignot (2004): Warm ocean is eroding West Antarctic Ice Sheet, Geophys. Res. Letters, 31 (L23402), doi:10.1029/2004GL021106.

Siegert, M;, A. Le Brock and A. Payne (2007): Hydrological connections between Antarctic subglacial lakes: The flow of Water beneath the East Antarctic ice sheet and implications of sedimentary processes, Glacial Sedimentary Processes and Products. In press.

Siegert, M., S. Carter, I. Tobacco, S. Popov, D. Blankenship (2005): A revised inventory of Antarctic subglacial lakes, Ant. Sci. 17 (3) 453–460.

Souchez, R., 1997. The build up of the ice sheet in Central Greenland, Journal of Geophysical Research. J. Geophys. Res. 102, 26317-26323.

Souchez, R., Bouzette, A., Clausen, H., Johnsen, S.Jouzel, J., 1998. A stacked mixing sequence at the base of the Dye 3 core, Greenland. Geophysical Research Letters 25, 1943-1946.

Souchez, R., Janssens, L., Lemmens, M.Stauffer, B., 1995a. Very low oxygen concentration in basal ice from Summit, Central Greenland. Geophys. Res. Lett. 22, 2001-2004.

Souchez, R., Jean-Baptiste, R., Petit, J.R., Lipenkov, V.Jouzel, J., 2002a. What is the deepest part of the Vostok ice core telling us ? Earth Science Review 60, 131-146.

Souchez, R., Jouzel, J., Landais, A., Chapellaz, J., Lorrain, R.Tison, J.-L., 2006. Gas isotopes in ice reveal a vegetated central Greenland during ice sheet invasion. Geophysical Research Letters 33 L24503.

Souchez, R., Jouzel, J.Johnsen, S., 1993a. Ice formed at the edge of the Greenland Ice Sheet prior to 250 ky preserved at Summit ; environmental implications. EOS, Transactions of the American Geophysical Union 85.

Souchez, R., Lemmens, M., Tison, J.-L., Lorrain, R.Janssens, L., 1993b. Reconstruction of basal boundary conditions at the Greenland Ice Sheet margin from gas composition in the ice. Earth Planet. Sci. Lett. 118, 327-333.

Souchez, R., Lemmens, M.Chappellaz, J., 1995b. Flow-induced mixing in the GRIP basal ice deduced from the CO_2 and CH_4 records. Geophysical Research Letters 22 41-44

Souchez, R., Lorrain, R., Tison, J.-L.Jouzel, J., 1988. Co-isotopic signature of two mechanisms of basal-ice formation in Arctic outlet glaciers. Ann. Glaciol. 10, 163-166.

Souchez, R., Petit, J.-R., Jouzel, J., de Angelis, M.Tison, J.L., 2003. Reassessing Lake Vostok's behaviour from existing and new ice core data. Earth and Planetary Science Letters 217, 163-170.

Souchez, R., Petit, J.R., Jouzel, J., Simões, J., de Angelis, M., Barkov, N., Stievenard, M., Vimeux, F., Sleewaegen, S.Lorrain, R., 2002b. Highly deformed basal ice in the Vostok core, Antarctica. Geophys. Res. Lett. 29, 40.41-40.44.

Souchez, R., Petit, J.R., Tison, J.L., Jouzel, J.Verbeke, V., 2000a. Ice formation in subglacial Lake Vostok, Central Antarctica. Earth and Planetary Science Letters 181, 529-538.

Souchez, R., Tison, J.L., Lorrain, R., Janssens, L., Stievenard, M., Jouzel, J., Sveinbjörnsdottir, A.Johnsen, S.J., 1994. Stable isotopes in the basal silty ice preserved in the Greenland Ice Sheet at Summit; Environmental implications. Geophys. Res. Lett. 21, 693-696.

Souchez, R., Vandenschrick, G., Lorrain, R.Tison, J.-L., 2000b. Basal ice formation and deformation in Central Greenland : a review of existing and new ice core data. In: A. J. Maltman, Hubbard, B., Hambrey, M. (Eds.), Deformation of Glacial Materials, Special Publication n°176, 13-22.

Souchez, R.Lorrain, R., 1991. Ice composition and glacier dynamics, 207 pp. Heidelberg, Springer-Verlag, 0 387 52521 1

Thoma, M., K. Grosfeld, C. Mayer, and F. Pattyn (2010) Interaction between ice sheet dynamics and subglacial lake circulation: a coupled modelling approach, The Cryosphere 4(1): 1-12.

Tison J.-L., Khazendar A., Roulin E., 2001. A two-phase approach to the simulation of the combined isotope/salinity signal of marine ice, Journal of Geophysical Research, 106 (C12), 31387-31401.

Tison, J.-L., 2002. Ice-ocean interactions in Antarctica: The marine ice perspective. Thèse d'Agrégation, 253 pp., Université Libre de Bruxelles, unpublished

Tison, J.-L., Khazendar, A.Roulin, E., 2001. A two-phase approach to the simulation of the combined isotope/salinity signal of marine ice. Journal of Geophysical Research 106, 31387-31401.

Tison, J.-L., Lorrain, R.D., Bouzette, A., Dini, M., Bondesan, A.Stiévenard, M., 1998. Linking landfast sea ice variability to marine ice accretion at Hells Gate Ice Shelf, Ross Sea. In: M. O. Jeffries (Eds.), Antarctic sea ice : physical processes, interactions and variability, 74, 375-407.

Tison, J.-L., Petit, J.R., Barnola, J.M.Mahaney, W.C., 1993. Debris entrainment at the ice-bedrock interface in sub-freezing temperature conditions (Adélie Land, Antarctica). J. Glaciol. 39, 303-315.

Tison, J.-L., Ronveaux, D.Lorrain, R., 1993. Low salinity frazil ice generation at the base of a small antarctic ice shelf. Antarctic Science 5, 309-322.

Tison, J.-L., Souchez, R., Wolff, E.W., Moore, J.C., Legrand, M.R.de Angelis, M., 1998. Is a periglacial biota responsible for enhanced dielectric response in basal ice from the Greenland Ice Core Project ice core ? Journal of Geophysical Research, 1998 103, 18885-18894.

Tison, J.-L., Souchez, R.Lorrain, R., 1989. On the incorporation of unconsolidated sediments in basal ice : present-day examples. Zeitschrift für Geomorphologie 72, 173-183.

Tison, J.-L., Thorsteinsson, T., Lorrain, R.Kipfstuhl, J., 1994. Origin and development of textures and fabrics in basal ice at Summit, Central Greenland. Earth Planet. Sci. Lett. 125, 421-437.

Tison, J.-L.Lorrain, R., 1987. A mechanism of basal ice layer formation involving major ice-fabrics changes. J. Glaciol. 33, 47-50.

Traversi, R., Becagli, S., Castellano, E., Marino, F., Severi, M., Udisti, R., Kaufmann, P., Lambert, F., Stauffer, B., Hansson, M., Petit, J.R., Ruth, U., Raisbeck, G.Wolff, E.W., 2006. Chemical characterization of peculiar ice layers at the bottom of the EPICA-DC ice core. Geophysical Research Abstracts, 8, 07199. European Geosciences Union General Assembly 2006, 02-07 April 2006, EGU.

Van der Veen, C., J. (1999): Fundamentals of Glacier Dynamics, A. A. Balkema, Rotterdam/ Brookfield, 459 p.

Vaughan, D. and R. Arthern (2007): Why is it hard to predict the future of ice sheets?, Science 315, 1503-1504.

Verbeke, V., R. Lorrain, Johnsen S.J., J.-L. Tison, 2002. A multiple-step deformation history of basal ice from the Dye3 (Greenland) core : new insights from the CO_2 and CH_4 content. Annals of Glaciology 35, 231-236.

Vieli, A. and A.J. Payne (2003): Application of control methods for modelling the flow of Pine Island Glacier, West Antarctica. Annals of Glaciology, 36, 197-204.

Vieli, A. and A.J. Payne (2005): Assessing the ability of numerical ice sheet models to simulate grounding line migration, J. Geophys. Res., 110 (F01003), doi:10.1029/2004JF000202.

Walker R.T., T.K. Dupont, B.R. Parizek, R.B. Alley (2008): Effects of basal-melting distribution on the retreat of an ice shelf, Geophys. Res. Letters, 35, L17503, doi:10.1029/2008GL034947.

Weeks, W.F.Ackley, S.F., 1986. The growth, structure and properties of sea ice. In: N. Untersteiner (Eds.), The geophysics of sea ice, 146, 9-164.

Weertman (1974): Stability of a junction of an ice sheet and ice shelf, J. Glaciol., 13, 3-11.

Weis, D., Demaiffe, D., Souchez, R., Gow, A.J.Meese, D.A., 1997. Nd, Sr and Pb isotopic compositions of basal material in Central Greenland : inferences for ice sheet development. Earth and Planetary Science Letters 150, 161-169.

Wettlaufer, J.S., 1999. Impurity effects in the Premelting of ice. Physical Review Letters 82, 2516-2519.

Wingham, D., M. Siegert, A. Shepherd, A. Muir (2006): Rapid discharge connects Antarctic subglacial lakes, Nature 440, 1033-1036.

Wolff E.H. et al. (2006) Southern Ocean sea-ice extent, productivity and iron flux over the past eight glacial cycles. Nature 440, 491-496 doi:10.1038/nature04614.